

ESCOLA POLITÉCNICA
PROGRAMA DE PÓS-GRADUAÇÃO EM CIÊNCIA DA COMPUTAÇÃO
MESTRADO EM CIÊNCIA DA COMPUTAÇÃO

ELISA GARCIA PEREIRA

EXPLORING SOFT ERROR SUSCEPTIBILITY IN FET DEVICES VIA GEANT4 SIMULATION

Porto Alegre
2024

PÓS-GRADUAÇÃO - *STRICTO SENSU*



Pontifícia Universidade Católica
do Rio Grande do Sul

**PONTIFICAL CATHOLIC UNIVERSITY OF RIO GRANDE DO SUL
SCHOOL OF TECHNOLOGY
COMPUTER SCIENCE GRADUATE PROGRAM**

**EXPLORING SOFT ERROR
SUSCEPTIBILITY IN FET
DEVICES VIA GEANT4
SIMULATION**

ELISA GARCIA PEREIRA

Master Thesis submitted to the Pontifical Catholic University of Rio Grande do Sul in partial fulfillment of the requirements for the degree of Master in Computer Science.

Advisor: Prof. Dr. Fernando Gehm Moraes

**Porto Alegre
2024**

Ficha Catalográfica

Elaborada pelo Sistema de Geração Automática de Ficha Catalográfica da PUCRS
com os dados fornecidos pelo(a) autor(a).
Bibliotecária responsável: Clarissa Jesinska Selbach CRB-10/2051

ELISA GARCIA PEREIRA

EXPLORING SOFT ERROR SUSCEPTIBILITY IN FET DEVICES VIA GEANT4 SIMULATION

This Master Thesis has been submitted in partial fulfillment of the requirements for the degree of Master in Computer Science, of the Computer Science Graduate Program, School of Technology of the Pontifical Catholic University of Rio Grande do Sul

Sanctioned on August xx, 2024.

COMMITTEE MEMBERS:

Prof. Dr. Tiago Roberto Balen (PGMICRO/UFRGS)

Prof. Dr. César Augusto Missio Marcon (PPGCC/PUCRS)

Prof. Dr. Fernando Gehm Moraes (PPGCC/PUCRS - Advisor)

AGRADECIMENTOS

Gostaria de expressar minha sincera gratidão à minha família: meus pais, Luis Gustavo e Neiva, minhas avós, Francelina e Aguilar, ao meu companheiro Hermes, e também à Eliane e ao Pedro, pelo apoio e incentivo incondicionais nessa jornada e em minhas decisões acadêmicas.

Desejo estender meus sinceros agradecimentos ao meu orientador, Fernando Moraes, cuja orientação e expertise foram fundamentais para a realização desta dissertação. Agradeço também a Ney Calazans, Rafael Garibotti e Luciano Ost, cujas contribuições foram essenciais para a concretização desta pesquisa. Sou igualmente grata pelas discussões enriquecedoras com Marcos Deros, Henri Boudinov, Henrique Trombine e Gabriela Hoff, que contribuíram significativamente para o desenvolvimento deste trabalho.

Um agradecimento especial ao Juninho, por ter me apresentado ao grupo de pesquisa, o que me abriu as portas para à ciência da computação e aos meus colegas do grupo que muito me ajudaram a aprender sobre o mundo da microeletrônica. Por fim, agradeço às minhas amigas, que me acompanham desde a escola, Carol, Ju e Teca, pelo apoio e incentivo.

Agradeço à PUCRS pela bolsa PRO-Stricto e também à CAPES/PROEX pelo auxílio financeiro dado durante o mestrado.

EXPLORANDO A SUSCEPTIBILIDADE A SOFT ERROR EM DISPOSITIVOS FET POR MEIO DE SIMULAÇÃO COM GEANT4

RESUMO

Nos últimos anos, houve um avanço significativo na tecnologia de dispositivos eletrônicos. No entanto, esses dispositivos são suscetíveis a Efeitos de Evento Único (SEEs), devido à interação de raios cósmicos com regiões sensíveis de circuitos, o que pode produzir erros de processamento. Portanto, é relevante conduzir estudos visando correlacionar eventos de raios cósmicos com potenciais erros de processamento causados por estes, especialmente no que diz respeito a interações entre a área sensível de um circuito e partículas específicas. Este trabalho apresenta um estudo de simulação usando o *toolkit* Geant4 para entender a interação de raios cósmicos com diversos nodos tecnológicos eletrônicos, bem como possíveis efeitos. As simulações conduzidas foram realizadas utilizando prótons, partículas alfa, píons positivos, píons negativos, múons positivos e múons negativos. Estas partículas foram incididas com energias variando de 0,5 MeV a 100 TeV e em vários ângulos de incidência. Os resultados revelaram que partículas alfa geram o maior número de elétrons, o que é particularmente relevante nas proximidades do espaço exterior, enquanto prótons, que constituem a maior parte dos raios cósmicos, têm um impacto significativo não apenas no espaço exterior mas também sobre em órbitas baixas da Terra. Embora os múons positivos e píons tenham efeitos menores, eles são mais proeminentes em altitudes inferiores, incluindo o nível do solo. O ângulo de incidência demonstra ser importante na avaliação de SEEs, com tecnologias planares demonstrando maiores ocorrências de elétrons, enquanto FinFETs mostram potencial para a geração de corrente de inversão de bits, apesar de gerarem menos elétrons.

Palavras-Chave: Erros Soft, Raios Cósmicos, MOSFET, FinFET, Geant4.

EXPLORING SOFT ERROR SUSCEPTIBILITY IN FET DEVICES VIA GEANT4 SIMULATION

ABSTRACT

In recent years, there have been significant advancements in electronic device technology. However, these devices are susceptible to Single-Event Effects (SEEs) due to the interaction of cosmic rays with sensitive regions, which can lead to processing errors. Therefore, it is necessary to conduct a study to correlate cosmic ray events with the potential for processing errors, particularly concerning interactions between the sensitive area of the device and specific particles. In this work, we present a simulation study using Geant4 to understand the interaction of cosmic rays with technology and their possible effects. Our simulations used incident particles such as protons, alpha particles, positive pions, negative pions, positive muons, and negative muons. These particles were incident with energies ranging from 0.5 MeV to 100 TeV and at various angles of incidence. The simulations showed that alpha particles generate the most electrons, which is particularly relevant near outer space, while protons, which constitute the majority of cosmic rays, have a significant impact not only in outer space on low earth orbit SEEs, although positive muons and pions have less effects, they are more prominent in lower levels, including ground level. Angular incidence is critical in SEE evaluation, with planar technologies demonstrating higher occurrences of electrons, and FinFETs showing potential for bit-flip current generation despite fewer electrons.

Keywords: Soft Errors, Cosmic Rays, MOSFET, FinFET, Geant4.

LIST OF FIGURES

Figure 2.1 – Air shower generated from cosmic rays [192].....	16
Figure 2.2 – Planar and FinFET transistors (Source: https://www.synopsys.com/glossary/what-is-a-finfil.html).	18
Figure 3.1 – Number of publications per year.....	24
Figure 3.2 – Publication per journals – TNS : IEEE Transactions on Nuclear Science, MR : Microelectronics Reliability, Elect : Electronics (Switzerland), TCASI : IEEE Transactions on Circuits and Systems I, SST : Semiconductor Science and Technology.	25
Figure 3.3 – Heat map indicating the number of publications by countries.	25
Figure 3.4 – Heat map of heavy ion experiments (obtained using the Periodic Trend Plotter Tool [162])......	28
Figure 4.1 – Coordinates used to characterize planar and FinFET transistors (Source: https://www.synopsys.com/glossary/what-is-a-finfil.html - modified).	35
Figure 4.2 – Planar channel and effective channel (Source: [176]).	35
Figure 4.3 – Planar and FinFET architecture design.	36
Figure 4.4 – FET architectures design detailed segmentation.	36
Figure 4.5 – Geant4-based simulation for 65nm and 22nm technology nodes, removing the substrate area, bringing the chosen four distinct angular measurement groups.	43
Figure 5.1 – Particle (x-axis) versus Average Number of Electrons (y-axis). This graph shows the average number of electrons measured for each particle. The average is calculated over the angle of incidence and energies.	48
Figure 5.2 – Energy versus Average Number of Electrons per Particle.	49
Figure 5.3 – Circuitry for the memory cell, with the read and write circuits.	50
Figure 5.4 – Simulation of a memory cell in 65nm technology, with 4 write and 4 read operations. The differential lines, BL and BLB, are pre-charged when the <i>clk</i> signal is equal to '0'.	51
Figure 5.5 – Simulation of a memory cell in 65nm technology, with 4 write and 4 read operations. Note the two source currents on 'Q' and 'nQ' signals inducing bitflips.	52
Figure 5.6 – Simulation of bitflips on 65nm, 28nm, and 7nm. The simulation highlights the current inducing the bitflips for each technology.	52

Figure 5.7 – Current per incidence angle for different particles. Gold line: minimum current needed to cause a bitflip obtained from electrical simulation. Violet line: minimum current calculated by replacing I_{ON} with I_{dsat} in Equation 4.15.	54
Figure 5.8 – Radar chart showing the number of electrons, comparing different technologies and angles normalized by particles.	55
Figure 5.9 – Radar chart showing the current, comparing different technologies and angles normalized by particles.	56

LIST OF TABLES

Table 3.1 – Relationship between facilities and publications originating from these in the years 2018-2022.	26
Table 3.2 – An account of particles and the frequency with which survey papers mention their use.	27
Table 4.1 – 65nm Technology Details.	37
Table 4.2 – 32nm Technology Details.	38
Table 4.3 – 22nm Technology Details.	39
Table 4.4 – 14nm Technology Details.	40
Table 4.5 – 7nm Technology Details.	41
Table 4.6 – Summary of experimental parameters and conditions.	43
Table 5.1 – Current, in μA , to induce a bitflip for different technology nodes. We consider the smallest current to induce a bitflip.	53
Table 5.2 – Number of electrons (N) across different technologies and angles. I: current (μA). Complete table with other particles in GitHUB [151].	53
Table 5.3 – Simulation and Saturation Current Values for Different Technologies. The I_{ON} saturation values are from references [174–177, 214].	54

CONTENTS

1	INTRODUCTION	12
1.1	MOTIVATION	13
1.2	OBJECTIVES	13
1.3	CONTRIBUTION	13
1.4	DOCUMENT ORGANIZATION	14
2	BACKGROUND KNOWLEDGE	15
2.1	COSMIC RAYS IN ATMOSPHERE	15
2.1.1	PROTONS	16
2.1.2	NEUTRONS	16
2.1.3	ALPHA PARTICLE	17
2.1.4	PIONS	17
2.1.5	MUONS	17
2.2	PLANAR AND FINFET TRANSISTORS	17
2.3	GEANT4	19
2.3.1	RELATED WORK USING GEANT4 IN FET DEVICES	20
3	LITERATURE REVIEW	22
3.1	SURVEY METHODOLOGY	22
3.2	PUBLICATIONS BY YEAR	24
3.3	JOURNALS TARGETED BY ARTICLES	24
3.4	RADIATION FACILITIES AND COUNTRY LOCATIONS	25
3.5	PARTICLES	27
3.6	PARTICLES AND COUNTRIES	29
3.7	IMPACTS FROM CIRCUIT TECHNOLOGY	30
3.8	TRENDS	32
4	METHODOLOGY	34
4.1	GEANT4: BASIC INFORMATION	34
4.2	TECHNOLOGY PARAMETERS	34
4.3	SIMULATION PARAMETERS	42
4.4	SIMULATION RESULTS DATA MANIPULATION	44
4.5	CURRENT CALCULUS	44

5	RESULTS	47
5.1	PARTICLE VERSUS AVERAGE NUMBER OF ELECTRONS	47
5.2	ENERGY VERSUS AVERAGE NUMBER OF ELECTRONS	48
5.3	CELL MEMORY SIMULATION	50
5.4	ANGLE OF INCIDENCE VERSUS CURRENT	53
5.5	QUALITATIVE COMPARISON BETWEEN TECHNOLOGY, ANGLE OF INCIDENCE, AND INCIDENT PARTICLES	55
5.6	FINAL REMARKS	57
6	CONCLUSION	58
6.1	PUBLICATIONS DURING THE MSC PROGRAM	59
	REFERENCES	60

1. INTRODUCTION

Cosmic rays consist of high-energy particles, mostly protons, alpha particles, and heavy ions atomic nuclei [73], that continuously enter Earth's atmosphere. Upon entering the atmosphere, they interact with it, creating a cascade of many secondary particles such as muons, protons, neutrons, and pions, leading to the formation of an extensive air shower [182]. The particles from this shower interact with materials in the atmosphere and on Earth's surface. This interaction can lead to various consequences, including specific effects on electronic devices as high electric charge doses [71] and atoms ionization [93].

When cosmic rays particles strike electronic devices, they can cause harmful effects, categorized under phenomena collectively known as Single Event Effects (SEEs) [111]. SEEs occur when a single ionizing particle hits a sensitive region within an electronic device, generating a current surge. If this surge occurs near the drain of a transistor in its off-state mode within sequential logic, it holds the potential to modify the value stored in memory cells without the occurrence of a specific write operation. This is called Single Event Upset (SEU), also known as a soft error. On the other hand, if the surge affects combinational logic, it can propagate through the circuit, resulting in a Single Event Transient (SET) that may impact connected circuits [20].

The susceptibility of an integrated circuit to SEEs can vary depending on the electronic device. Several works have explored the impact of radiation-induced errors in electronic devices, ranging from cryptography hardware implementations on SRAM-based FPGAs [18, 76] to the execution of modern machine learning algorithms [131, 190, 191]. For instance, Zhang and Li [230] suggest that smaller devices or those operating under reduced voltage supply are more susceptible to radiation-induced errors.

In addressing the aforementioned problem, it is essential to study the key parameters contributing to Single Event Effects and how these effects manifest. To address this issue, we propose a computational simulation study aimed to model the impact of particles known to belong to cosmic cascades - such as protons, neutrons, muons, pions, alpha particles, and others. The focus will be on simulating the ionization process that produces electrons in structures similar to MOSFET and FinFET transistors. Our study is divided into multiple phases, beginning with a literature review of the current state of experimental research on soft errors. This review involves identifying the facilities, particles, and hardware devices under investigation over the past five years. Our research provided information that allowed us to structure the parameters of interest for the computational simulation. As a result, we developed a research plan outlining how each particle interacts with different technology nodes, considering their specific characteristics. The objective is to gain a comprehensive understanding of the relationship between particles, technology, and soft errors.

1.1 Motivation

The influence of cosmic rays on electronic devices is a significant concern in the field of microelectronics [152]. This research was initially inspired by Takashi *et al.*'s paper [100], which discussed the occurrence of Multiple Cell Upset (MCU) events in 20nm planar SRAMs when exposed to positive muons. In contrast, earlier studies by the same authors on 65nm and 28nm planar SRAMs did not observe significant MCU events [122, 133]. Although the original study focused solely on positive muons, it is important to broaden the investigation to include the effects of other incident particles. This consideration led us to explore the impact of cosmic ray-induced phenomena on various technology nodes. Existing literature indicates that protons can cause soft errors in technologies of 32nm and beyond. This raises the question of whether other cosmic ray particles, such as muons from the cosmic ray cascade, might have similar effects on even smaller technologies, a possibility suggested by Takashi's work [100]. Following a thorough literature review, we observed that most research has concentrated on heavy ions, protons, and neutrons. Motivated by these findings, we propose a more extensive study using computational simulations to model the interaction of diverse particles with different devices, aiming to achieve a deeper understanding of the impact of cosmic ray particles on each technology node.

1.2 Objectives

The main objective of this work is to simulate how particles with varying energies and angles from the original beam affect different transistor technologies. Specifically, we aim to determine whether particles from cosmic ray cascades have different impacts on planar and FinFET technologies and if these particles can affect smaller technologies.

Additionally, we seek to compare planar and FinFET technologies of different sizes by observing the impact of different particles at various energies and angles to determine if soft errors occur. The final objective is to conduct a qualitative analysis to evaluate the specific effects of each particle on each technology, providing a clear and organized comparison of particle-transistor interactions. This will offer a comprehensive understanding of the individual and specific effects of particles on electronic devices.

1.3 Contribution

Our literature review [152] contributes to the characterization of particles, facilities, and devices used in current radiation-induced experiments, bringing both quantitative and

qualitative literature analyses from the past five years. This review reports trends in radiation research, revealing which particles are currently considered most relevant, highlighting the most commonly used facilities available for testing radiation effects, and emphasizing which technological nodes and/or devices are addressed preferentially with regard to radiation-induced effects studies.

Through simulation, we gain a deeper understanding of the impact that particles with varying energy levels have on electronic devices. This research can streamline the process of understanding and mitigating soft errors. Despite the abundance of these particles in the atmosphere, there seems to be a lack of studies on analyzing the effect of various particles from the cosmic cascade. Thus, a thorough investigation into these effects could help develop strategies for mitigating errors in electronic systems. Another contribution is the development of the Geant4 code, which includes a detailed construction of the selected technologies based on literature references.

A complete set of the data results are made available on a GitHub website [151].

1.4 Document Organization

This document is organized as follows:

- Cosmic Rays in Different Technologies (Chapter 2): Describes the impact of cosmic rays on various technologies. It includes a discussion on fundamental concepts, their effects in the atmosphere, and their influence of particles such as neutrons, alpha particles, pions, and muons. This chapter also covers planar and FinFET technologies, and the use of Geant4 for simulations.
- Literature Review (Chapter 3): Provides a comprehensive analysis of current research. It summarizes discoveries and patterns, including the annual number of published articles, targeted journals, radiation facilities, and their locations, types of particles, and impacts from circuit technology. It also discusses emerging trends in the field.
- Methodology (Chapter 4): Describes the methods and procedures used in the research, including Geant4 parameters, technology parameters, simulation results, data manipulation, and current calculation.
- Results (Chapter 5): Presents the research findings, offering a thorough analysis and interpretation of the data obtained from simulations and calculations.
- Conclusion (Chapter 6): Summarizes the main findings, discusses their implications, and proposes future research directions.

2. BACKGROUND KNOWLEDGE

This Chapter presents the fundamental concepts of this research. We detail cosmic rays, including their source, atmospheric interactions, secondary particles, and energy distribution at different atmospheric levels. We also discuss the selected devices for study and their significance in the market. We also explain the Geant4 simulation toolkit and review related research that has utilized this tool.

2.1 Cosmic Rays in atmosphere

Cosmic rays are high-energy particles originating from various astrophysical sources, such as supernovae, black holes, and active galactic nuclei, they consist of high-energy particles, mostly protons, alpha particles, and heavy ions atomic nuclei [73] and are constantly entering Earth's atmosphere. Before reaching Earth's atmosphere, they travel through space with energies ranging from 10^9 eV to above 10^{20} eV [73].

When cosmic rays enter Earth's atmosphere, they collide with its atoms and molecules, resulting in a cascade of secondary particles. These secondary particles include muons, electrons, photons, neutrons, pions (both charged and neutral), and neutrinos, leading to the formation of an extensive air shower [182]. The composition, energy, and quantity of secondary particles generated by cosmic ray interactions depend on various factors, including the primary cosmic ray's energy and composition, as well as the altitude at which the interactions occur.

As we can see in Figure 2.1 we can describe each level of the atmosphere:

- **Deep Space:** in deep space there are up to $300,000 \text{ particles/cm}^2/\text{h}$, mainly protons (90%) with some alpha particles (9%) and heavy ions(1%).
- **Geosynchronous Orbit:** up to $500,000 \text{ particles/cm}^2/\text{h}$, mainly electrons and protons. But as we can see in [67] there are also pions and neutrons generated by the primary particle interaction with the atmosphere.
- **Low Earth Orbit:** Up to $100,000 \text{ particles/cm}^2/\text{h}$, mainly protons and electrons. As in Geosynchronous Orbit there are also pions, neutrons and muons.
- **Airplane Altitudes:** $6,000 - 9,000 \text{ neutrons/cm}^2/\text{h}$ and muons.
- **Ground Level:** $10 - 15 \text{ neutrons/cm}^2/\text{h}$, $60 \text{ muons/cm}^2/\text{h}$ and neutrinos.

In this dissertation, the author focuses on protons, neutrons, alpha particles, pions, and muons.

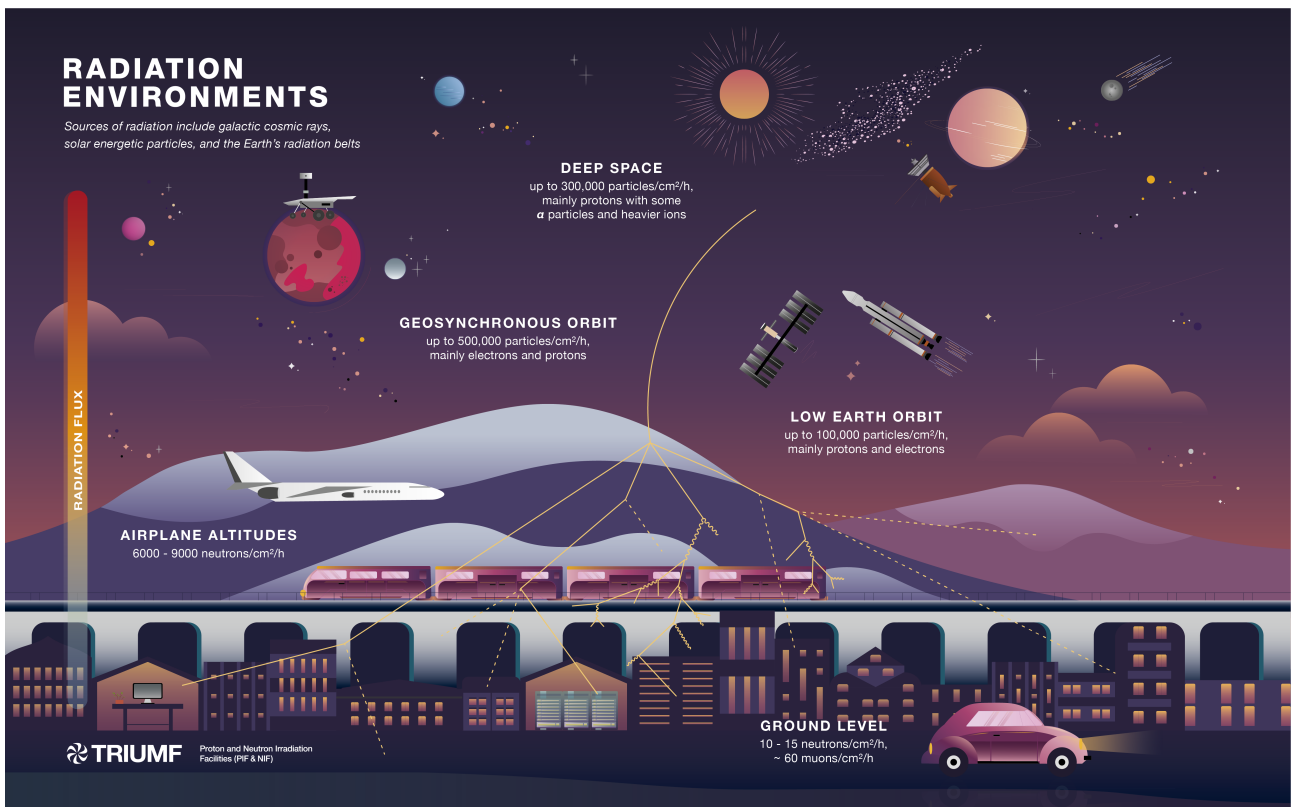


Figure 2.1 – Air shower generated from cosmic rays [192].

2.1.1 Protons

Protons (p) are the predominant particles among cosmic rays entering the atmosphere, with initial energies ranging from 100 MeV to 100 TeV [67]. A proton is a baryon (<https://en.wikipedia.org/wiki/Baryon>) with an electric charge of +1, spin $\frac{1}{2}$, and has a mass of approximately one u (atomic mass unit).

2.1.2 Neutrons

Neutrons (n) are particles generated during the initial collisions of cosmic rays in the atmosphere. Like protons, they are baryons with spin $\frac{1}{2}$, but they have no electric charge and their mass is slightly greater than the proton. However, since this difference is minimal, they are typically described as having a mass of approximately one u . Neutrons initial energy depend if they are cosmic neutrons, atmospheric neutrons or ground level neutrons, but they can get to 10 GeV [198].

2.1.3 Alpha Particle

An alpha particle (α) is composed of 4 particles: 2 protons and 2 neutrons, forming what can be called a helium nucleus. Although it is not a fundamental particle, being a stable nucleus, it is considered a composite boson (<https://en.wikipedia.org/wiki/Boson>). Its electric charge is +2, and its spin is 0. Its mass is, as expected, approximately 4 u . This particle makes up about 9% of cosmic rays and the initial energy are commonly ranging between 40GeV and 250 TeV [2].

2.1.4 Pions

Pions (π), like neutrons, are among the particles most frequently produced in the early layers of the atmosphere and can reach an initial energy of up to 10 GeV [114]. Pions can be positively charged (π^+), neutral (π^0), or negatively charged (π^-) and are mesons with spin 0. Their mass varies depending on their charge but is somewhat greater than the mass of a muon.

2.1.5 Muons

A muon (μ) is a lepton with an electric charge of $-e$, spin $\frac{1}{2}$, and a mass approximately 207 times greater than that of an electron. It is often described as “very similar to the electron, but heavier.” Due to its high mass, the muon’s stopping power is relatively low, resulting in only a slight energy loss as it travels through the atmosphere. Combined with the relativistic effects of its high velocities, muons can reach the Earth’s surface. In addition to the muon, there is also the antimuon, which is identical to the muon but with a positive electric charge. Both are common in the atmosphere.

2.2 Planar and FinFET Transistors

Transistors are semiconductor devices that can amplify electrical signals as they are transferred from input to output terminals [211]. Transistors can be viewed as electrically controlled switches with a control terminal and two other terminals that are connected or disconnected depending on the voltage or current applied to the gate [211]. This work evaluates the effects of the particles in two different devices, presented in Figure 2.2:

- **Planar transistors**, specifically MOSFETs (Metal-Oxide-Semiconductor Field-Effect Transistors), are traditional semiconductor devices used in various electronic circuits. These transistors have a flat, planar structure where the current flows horizontally from the source to the drain through a channel controlled by the gate.
- **FinFETs** (Fin Field-Effect Transistors) are a type of multi-gate transistor designed to overcome the limitations of planar transistors. They feature a 3D structure with a thin silicon fin extending from the substrate, providing better control over the channel and reducing short-channel effects.

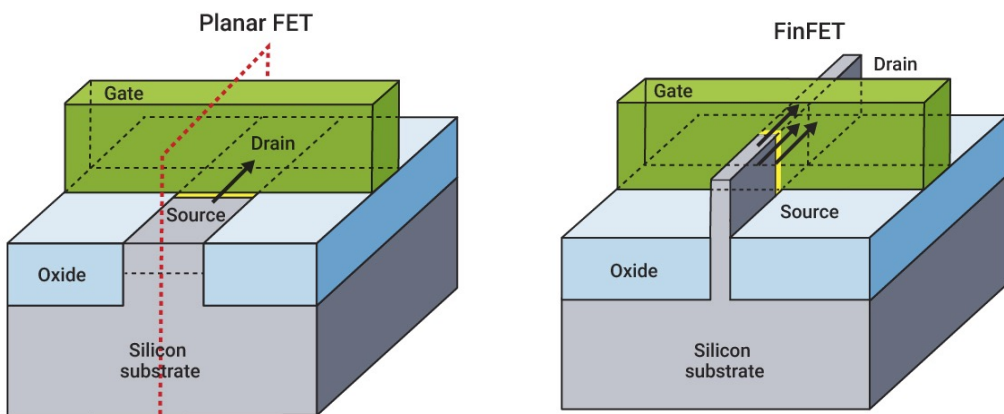


Figure 2.2 – Planar and FinFET transistors (Source: <https://www.synopsys.com/glossary/what-is-a-finfet.html>).

In planar technology, the channel is formed on a flat surface of the semiconductor substrate. The gate, which controls the current flow through the channel, is placed directly on top of this flat surface. However, in smaller process nodes, planar technology faces challenges related to leakage current and power consumption due to limitations in gate control [211]. To overcome the planar transistors' limitations, a new type of transistor was created, FinFETs, first commercialized in 2010. FinFETs offer better performance, lower power consumption, and improved scalability than planar transistors, especially as transistor sizes shrink. Thus, it permits transistors to keep reducing sizes, as Moore's Law proposes [211].

In these dissertation we focus on 2 planar technologies and 3 FinFET technologies:

- **65nm Technology (Planar):** This refers to the semiconductor manufacturing process technology node where the transistor gate length is approximately 65 nanometers. During this time, planar technology was primarily used. Commercial integrated circuit manufacturing using 65nm process began in 2005. The 65nm technology supports for a wide range of applications, such as mobile devices, computers, automotive electronics, IoT, and smart wearables [194].

- **32nm Technology (Planar):** This node is an advancement over the 65nm node. Commercial integrated circuit manufacturing using 32nm process began in 2010 [215].
- **22nm Technology (FinFET):** At this node, the technology is already FinFET. It offered significant improvements over the previous planar technology in terms of performance and power efficiency. The memory first production was in 2008 [214].
- **14nm Technology (FinFET):** This node is another FinFET technology. It offers better performance and energy efficiency than previous nodes, enabling the development of more powerful and energy-efficient electronic devices. It was introduced in 2015 [174].
- **7nm Technology (FinFET):** Introduced in 2019, it has even better performance than 14nm node, having 50% less power consumption, 0 to 50% increase in switching performance and 4 times higher density [177].

2.3 GEANT4

Geant4 [3, 7, 8, 53] is an open-source toolkit designed to simulate the trajectory of particles or radiation as they pass through various materials. Its application areas include high-energy physics, technology transfer, space and radiation studies, and medical physics (e.g., X-rays, proton therapy). Geant4 is utilized by many research institutions, including the European Organization for Nuclear Research (CERN).

Geant4 (Geometry and Tracking 4) was developed to provide a reliable simulation environment for studying particle interactions in various experimental setups. It builds upon its predecessors, GEANT and GEANT3. The primary goal of Geant4 is to simulate the interaction of particles with matter, enabling researchers to design and optimize detectors and experiments.

Geant4 can replicate an experimental setup or a detector, simulate radiation sources, and capture specific physical quantities resulting from the interaction of source particles and secondaries with the material. This toolkit covers a large spectrum of particle transport simulation, allowing users to model geometry, navigate tracks, apply physics interactions, generate secondary particles, record relevant information, visualize setups, and interact with the application through a flexible interface. Geant4 also encompasses a comprehensive set of physics processes, spanning electromagnetic, strong, and weak interactions across a broad energy range. It is also important to note that Geant4 is an open-source platform associated with a global collaboration of scientists and software engineers dedicated to its development, maintenance, and support, with ongoing research and code enhancement. Its open-source nature, readable source code, and example applications make it adaptable for various domains, enabling the creation of custom applications or the utilization of existing configurations.

Example of applications of Geant4 in MOS device studies:

- **Radiation Environment Simulation:** Geant4 can simulate the radiation environment that MOS devices are exposed to. This includes cosmic rays, solar particle events, and secondary particles generated in the Earth's atmosphere or in shielding materials. By simulating these environments, researchers can predict the types and energies of particles interacting with the MOS devices.
- **Particle Interaction Modeling:** Geant4 provides detailed models of particle interactions with matter, including the ionization and displacement damage that occur within the semiconductor material of MOS devices. These interactions are critical for understanding how radiation affects device performance. Geant4 can simulate the tracks of individual particles as they pass through the device, providing insights into the spatial distribution of energy deposition.
- **Damage and Degradation Analysis:** Using Geant4, researchers can model the cumulative effects of radiation exposure on MOS devices. This includes the generation of defects in the silicon lattice and the buildup of charge in the oxide layer. These simulations help identify the mechanisms of radiation-induced degradation and quantify the extent of damage over time.
- **Shielding and Mitigation Strategies:** Geant4 can be used to design and evaluate shielding strategies to protect MOS devices from radiation. By simulating different shielding materials and configurations, researchers can optimize the shielding to reduce the radiation dose the devices receive. This is particularly important for space applications, where weight and volume constraints are critical.
- **Testing and Validation:** Simulations with Geant4 can complement experimental testing of MOS devices. By comparing simulation results with experimental data, researchers can validate their models and improve their understanding of radiation effects. This iterative process helps in refining both the simulation tools and the design of radiation-hardened devices.

2.3.1 Related Work Using Geant4 in FET Devices

Takashi *et al.* [100] show that the negative muon induces considerable multiple-cell upsets (MCUs) in 65nm and 28nm bulk planar SRAMs. In contrast, positive muons do not result in such upsets [120, 121]. This research notes that the susceptibility to MCUs increases as SRAM cells shrink and that due to transistor miniaturization, the MCU mechanism becomes more complex, including the induction of parasitic bipolar effects (PBEs)

due to well-potential perturbation [75, 149]. In conclusion, it is necessary to investigate the muon-induced MCUs in more advanced devices.

Deng *et al.* [62] propose a method based on a proton acceleration test using Geant4 simulation to predict single event upsets (SEUs) caused by positive muons in 65nm bulk SRAM. The researchers compared the experimental data of muon-induced SEUs and the simulation result of proton-induced ones. They concluded that the fluxes of incident particles reaching the semiconductor devices are different between protons and positive muons due to the energy straggling in the device. The researchers emphasized the following assertion: Neutrons indirectly induce soft errors through nuclear interactions with atomic nuclei in the device, while muons can deposit energy directly through the ionization process in the device, causing SEUs.

Hubert *et al.* [91] demonstrated that protons and muons must be considered for ground environments. They also reported that noteworthy differences were observed for bulk, FDSOI, and FinFET technologies since the downscaling increases SEU susceptibility to radiation. Thus, the muon SERs are expected to increase as the critical charge decreases with miniaturization of semiconductors.

Additionally, Hao *et al.* [86] studied the difference between gamma ray radiation in planar and FinFET devices. The study concluded that a FinFET exhibits lower sensitivity to transient radiation than a planar MOSFET.

3. LITERATURE REVIEW

To obtain a better understanding of the advancements and current state of research on radiation-induced errors, the Author conducted a survey on the subject [152]. The aim is to know the state-of-the-art regarding the progress of studies on soft errors. This survey analyzed a collection of 295 articles published between 2018 and 2022, aiming to characterize the current state of research on radiation-induced errors. The focus is on experimental research considering radiation effects on electronic devices, excluding works that solely involve simulation and radiation modeling. Additionally, it narrows the scope of analysis to effects of particle radiation from space, disregarding radiation sources related to devices or materials, such as those from specific chip packaging or solder bumps.

This Chapter starts by presenting the methodology used in the survey, followed by the evaluation of the selected papers according to different criteria. The Chapter finish with the observed trends in the field.

3.1 Survey Methodology

To execute the survey we used the “Scopus advanced search” functionality¹ on the Scopus website to identify articles meeting our specified criteria. The search string crafted for this work is shown in Algorithm 3.1.

The search string starts with terms associated with radiation and single events, encompassing SEE, SEU, and SET, which are the keywords of this survey. Then, some particles used in acceleration facilities were included. Note that the intention is to compile articles relevant to the fields of computer science and engineering. Moreover, these articles must be written in English and hold the status of either “article” or “in press”.

The search string was run on March 6, 2023, identifying more than 300 articles potentially relevant. To restrict the analysis to a five-year period, articles from 2023 were intentionally excluded since it did not constitute, at the time, a full year. This resulted in a dataset of 295 articles. Following the Scopus search, the articles were downloaded and a spreadsheet was compiled with the basic results for each article. Next, articles were revised, to determine which ones met or did not meet this survey’s specific requirements, formulated as follows:

- Articles containing particle acceleration and collision facilities involving electronic devices, which aim to investigate phenomena such as single-event effects, single-event upsets (i.e., bit flips) and single-event transients.

¹<https://www.scopus.com/search/form.uri?display=advanced>

Algorithm 3.1 Scopus search string.

```
(TITLE-ABS-KEY("radiation"))
AND (TITLE-ABS-KEY("bitflip")
OR TITLE-ABS-KEY("bit flip")
OR TITLE-ABS-KEY("Single Event")
OR TITLE-ABS-KEY("Single-Event"))

AND (TITLE-ABS-KEY("proton")
OR TITLE-ABS-KEY("neutron")
OR TITLE-ABS-KEY("heavy ion")
OR TITLE-ABS-KEY("laser")
OR TITLE-ABS-KEY("x-ray")
OR TITLE-ABS-KEY("muon")
OR TITLE-ABS-KEY("electron")
OR TITLE-ABS-KEY("alpha"))

AND NOT TITLE-ABS-KEY("simulation")

AND (SUBJAREA(COMP) OR SUBJAREA(ENGI))

AND (LANGUAGE(English))

AND (DOCTYPE(ar) OR DOCTYPE(ip))

AND PUBYEAR > 2017
```

– Articles falling into the following categories were excluded from our analysis:

- ✓ Simulation-only articles;
- ✓ Articles relying on radiation modeling only (we focused on works that employ particles accelerated in facilities);
- ✓ Articles that, despite featuring physical experiments, omitted crucial details about the facility, particles, or specific electronic devices under test.

The outcome was a set of 174 articles that satisfied the established criteria, and these articles constitute the focus of this survey [1, 4–6, 9–17, 19, 21–24, 26–52, 54, 55, 57, 58, 60, 61, 65, 66, 68–70, 72, 74, 78–82, 84, 85, 87–90, 92, 94–96, 98–110, 112, 113, 115, 117–119, 122–130, 132–141, 143–146, 148, 150, 153–161, 163–173, 178–181, 183–189, 196, 197, 199, 201–210, 212, 219–229, 231].

This study contains the number of published articles and preferred communication channels within the research community of radiation-induced soft errors. It also identifies the most active countries and commonly used particles for assessing the impact of radiation on electronic circuits. Additionally, it provides a qualitative analysis of the studies conducted over the last five years, offering insights into how certain particles are used to analyze their impact on electronic devices and the technological advances in this area.

3.2 Publications by Year

Given the global impact of the COVID-19 pandemic within this five-year period, the annual distribution of research studies may be relevant. Figure 3.1 illustrates the number of articles published per year based on our search criteria. The results indicate a consistent number of articles published throughout this period, aligning with an average of 35 articles per year. Note that some of the articles published in 2020 were grounded in experiments and simulations conducted in 2018 and 2019, with subsequent data analysis carried out in 2020. This suggests that the pandemic had no significant impact on the overall quantity of articles published during this five-year period.

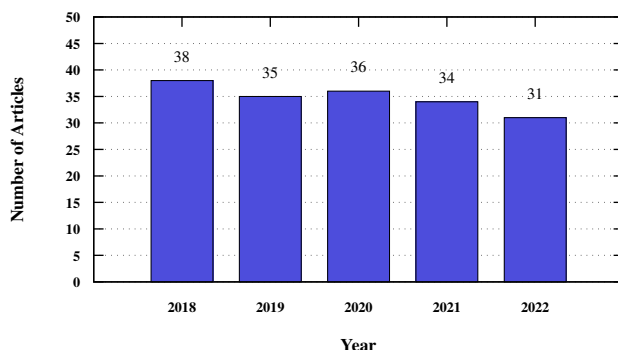


Figure 3.1 – Number of publications per year.

3.3 Journals Targeted by Articles

Concerning the preferred communication channels within the radiation research community, Figure 3.2 depicts the number of publications per journal. The findings highlight two main journals, IEEE Transactions on Nuclear Science (TNS) and Microelectronics Reliability (MR). Notably, TNS exhibits a significant publication volume compared to any other journal. One possible explanation is that TNS publishes special issues based upon manuscripts presented at the RADiation and its Effects on Components and Systems (RADECS) Conference. This conference, held annually in Europe, serves as a scientific and industrial forum focusing on the effects of radiation on electronics and photonic materials, devices, circuits, sensors, and systems. A notable criterion for acceptance at this conference is a strong emphasis on presenting works with experiments describing result from real radiation campaigns. On the other hand, Microelectronics Reliability is a journal with a broader scope, encompassing topics related to the reliability of microelectronic devices. This includes the measurement, evaluation and mitigation of failures induced by radiation. Consequently, it serves as a communication channel catering to both the radiation community and the systems reliability community.

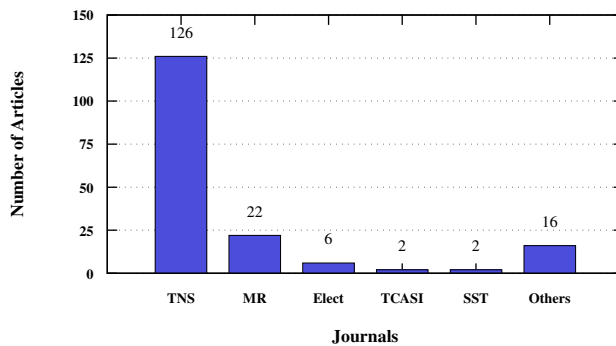


Figure 3.2 – Publication per journals – **TNS**: IEEE Transactions on Nuclear Science, **MR**: Microelectronics Reliability, **Elect**: Electronics (Switzerland), **TCASI**: IEEE Transactions on Circuits and Systems I, **SST**: Semiconductor Science and Technology.

3.4 Radiation Facilities and Country Locations

Figure 3.3 displays a heat map illustrating the distribution of publications by country. This map elucidates the nations that have exhibited the highest number of publications in radiation-induced research over the past 5 years. Unsurprisingly, United States of America and China emerge as the primary contributors, reflecting their substantial investments in research and development in this field [56].

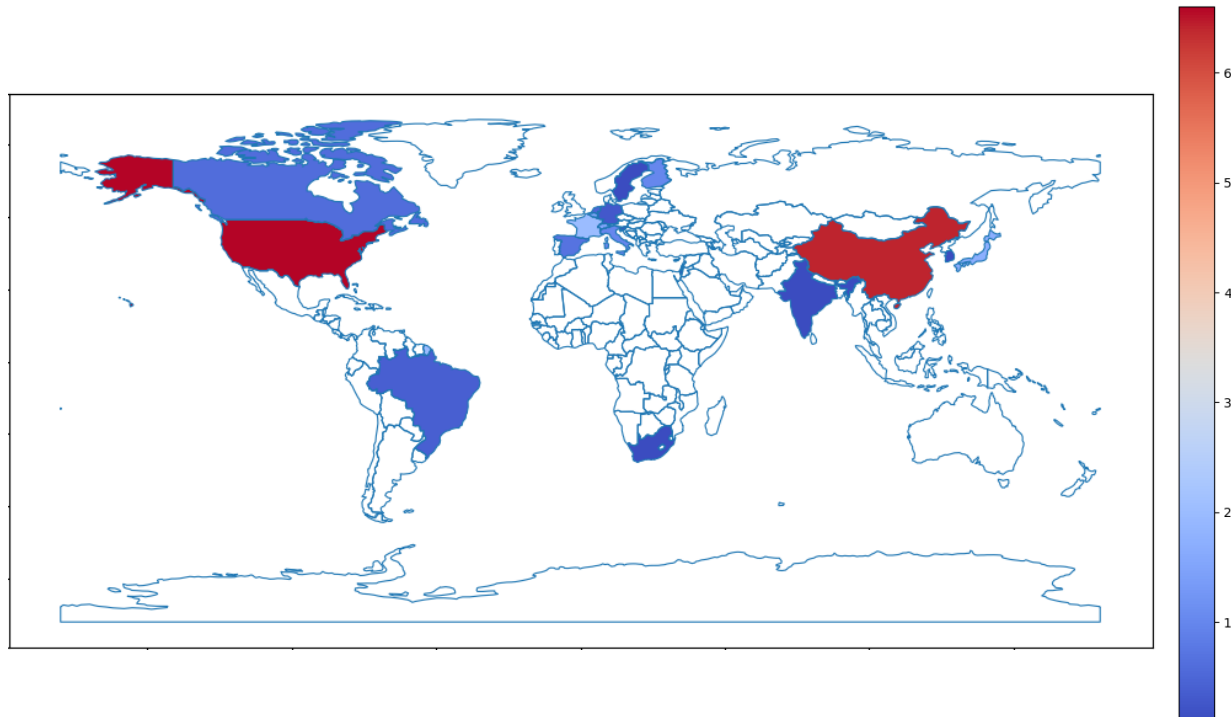


Figure 3.3 – Heat map indicating the number of publications by countries.

In Europe, a notable number of experiments were also conducted, with Belgium and France standing out as significant contributors. Japan helped push the Asian continent forward in this field with 17 publications. In contrast, Brazil stands as the sole representative

from South America, with four publications, while South Africa is the only African representative with just one publication. The global distribution of these research endeavors underscores the international collaboration and diverse geographical representation in the field of radiation-induced research, as depicted in Figure 3.3.

In terms of facilities, Table 3.1 shows the paper-to-facility distribution, arranged by the number of publications each of these has generated, restricted to facilities mentioned by four or more articles. Leading the list are two Chinese facilities the HI-13 in Beijing and the HIRFL in Lanzhou with several papers mentioned the use of both facilities. Follows the HIF-UCL, the heavy ion facility at the Université Catholique de Louvain in Belgium and some major labs in USA (the Los Alamos Neutron Science Center facility - LANSCE and the Lawrence Berkeley National Laboratory - LBNL). A variety of other countries contribute with the rest of mentioned facilities in Europe, Asia and Americas.

Table 3.1 – Relationship between facilities and publications originating from these in the years 2018-2022.

Number of Papers	Facility Name	Country	Articles
20	HI-13	China	[173], [132], [226], [74], [223], [30], [209], [32], [181], [220], [28], [130], [31], [161], [224], [43], [69], [183], [125], [128]
20	HIRFL	China	[226], [74], [30], [127], [209], [32], [45], [29], [227], [28], [130], [31], [144], [124], [46], [42], [225], [90], [125], [128]
14	HIF-UCL	Belgium	[27] [199], [106], [105], [5], [157], [139], [10], [228], [148], [14], [118], [52], [143]
13	LANSCE	USA	[159], [150], [35], [153], [172], [95], [23], [34], [103], [4], [126], [104]
12	LBNL	USA	[145], [163], [92], [84], [102], [134], [41], [88], [44], [110], [37], [164]
10	CERN	Switzer-land	[158], [187], [70], [105], [65], [188], [39], [201], [202], [184]
10	USNRL	USA	[163], [169], [48], [92], [109], [47], [180], [189], [140], [164]
9	RADEF	Finland	[132], [136], [158], [9], [188], [24], [167], [206], [184]
8	NSSC	China	[173], [32], [45], [227], [22], [203], [89], [125]
8	GENEPI2	France	[51], [154], [68], [113], [197], [50], [155], [115]
8	ISDE-SE-VU	USA	[26], [165], [119], [208], [229], [166], [33], [17]
7	TAMU	USA	[85], [36], [222], [41], [170], [66], [37], [160]
6	Peking Univ.	China	[221], [210], [127], [220], [129], [42]
6	Öhicplr	U.K.	[87], [156], [146], [13], [219], [17]
5	ILL	France	[51], [212], [171], [155], [115]
5	INFN	Italy	[49], [80], [12], [1], [14]
5	TIARA	Japan	[186], [112], [141], [185], [168]
5	CNA	Spain	[153], [51], [172], [38], [206]
5	PSI	Switzer-land	[55], [171], [15], [11], [196]
5	APS-ANL	USA	[145], [108], [107], [24], [164]
4	LAFN-USP	Brazil	[21], [82], [6], [81]
4	TRIUMF	Canada	[40], [16], [58], [170]
4	KVI - CART	Nether-lands	[199], [105], [57], [206]

It is interesting to note that, although the United States leads in the number of experiments (Figure 3.3), the extensive range of facilities contributes to a dispersion in the

count of articles published per facility. Some notable facilities in the United States comprise the Los Alamos Neutron Science Center (LANSCE), the Lawrence Berkeley National Laboratory (LBNL), and the U.S. Naval Research Laboratory (USNRL).

In Europe, all experiments conducted at CERN were attributed to Switzerland. Additionally, in France, many experiments took place at the GEnérateur à NEutrons Pulsés Intenses (GENEPI2) neutron source. The ISIS Neutron and Muon Source (ChiPIr) in the UK, along with facilities in Spain, Italy, and the Netherlands, further contribute to the robust development of the European radiation research community.

Table 3.2 – An account of particles and the frequency with which survey papers mention their use.

Number of Papers	Percent-age of total	Particle	Articles
87	50.00%	heavy ion	[21], [173], [132], [226], [74], [223], [136], [30], [145], [163], [27], [82], [49], [127], [137], [209], [32], [45], [60], [29], [181], [227], [138], [199], [158], [92], [220], [84], [28], [130], [9], [106], [207], [85], [186], [70], [105], [65], [31], [22], [161], [144], [36], [102], [5], [134], [224], [12], [112], [222], [41], [157], [170], [43], [124], [88], [141], [139], [46], [10], [24], [228], [1], [110], [69], [201], [66], [42], [225], [14], [167], [118], [185], [90], [183], [6], [81], [202], [125], [37], [206], [52], [128], [164], [168], [143], [160]
43	24.71%	neutron	[159], [87], [150], [79], [35], [153], [51], [98], [204], [40], [156], [154], [68], [99], [172], [146], [16], [113], [95], [54], [23], [34], [58], [101], [13], [197], [103], [39], [212], [50], [4], [117], [171], [155], [115], [126], [205], [104], [219], [17], [123], [100], [61]
34	19.54%	laser	[173], [132], [165], [163], [169], [154], [32], [45], [29], [227], [158], [48], [92], [119], [85], [186], [22], [96], [203], [109], [47], [208], [180], [157], [231], [139], [189], [140], [89], [57], [125], [184], [166], [164]
33	18.97%	proton	[221], [74], [179], [26], [153], [51], [210], [178], [172], [80], [138], [199], [158], [220], [9], [129], [105], [41], [170], [38], [78], [110], [148], [171], [15], [57], [11], [196], [19], [206], [135], [33], [168]
8	4.60%	xray	[145], [49], [108], [9], [107], [24], [229], [164]
8	4.60%	alpha	[87], [40], [106], [44], [229], [66], [17], [100]
7	4.02%	gamma	[127], [199], [187], [9], [42], [81], [160]
5	2.87%	electron	[187], [94], [72], [188], [184]
3	1.72%	muon	[133], [122], [100]
1	0.57%	pion	[55]

3.5 Particles

A key aspect involves understanding the specific particles employed in facilities to induce soft errors due to radiation in electronic devices. This knowledge unveils the intended application environments for these devices, such as space or sea-level, and provides insights into the challenges that researchers presently identify in the development of electronic device technology, which these particles can help clarify.

Table 3.2 provides a summary of particles and the frequency with which they are mentioned in the surveyed papers. Note that the total number of papers (211) exceeds the 174 articles selected based on the criteria outlined in Section 3.1. This discrepancy arises,

of course, because certain articles present radiation experiments involving more than one particle. For instance, Clemente *et al.* [51] conducted experiments with both neutrons and protons, while Bosser *et al.* [24] used heavy ions and x-rays. The outcomes reveal a significant number of experiments conducted with heavy ions, followed by neutrons, lasers, and protons. Collectively, the remaining particles are mentioned in only 16.67% of the articles.

Half of the articles employ heavy ions to assess their influence on electronic devices. However, the category of heavy ions is extensive, encompassing various chemical elements. Figure 3.4 provides a heat map featuring the elements corresponding to ions employed in heavy ion experiments within the articles reviewed in this survey.

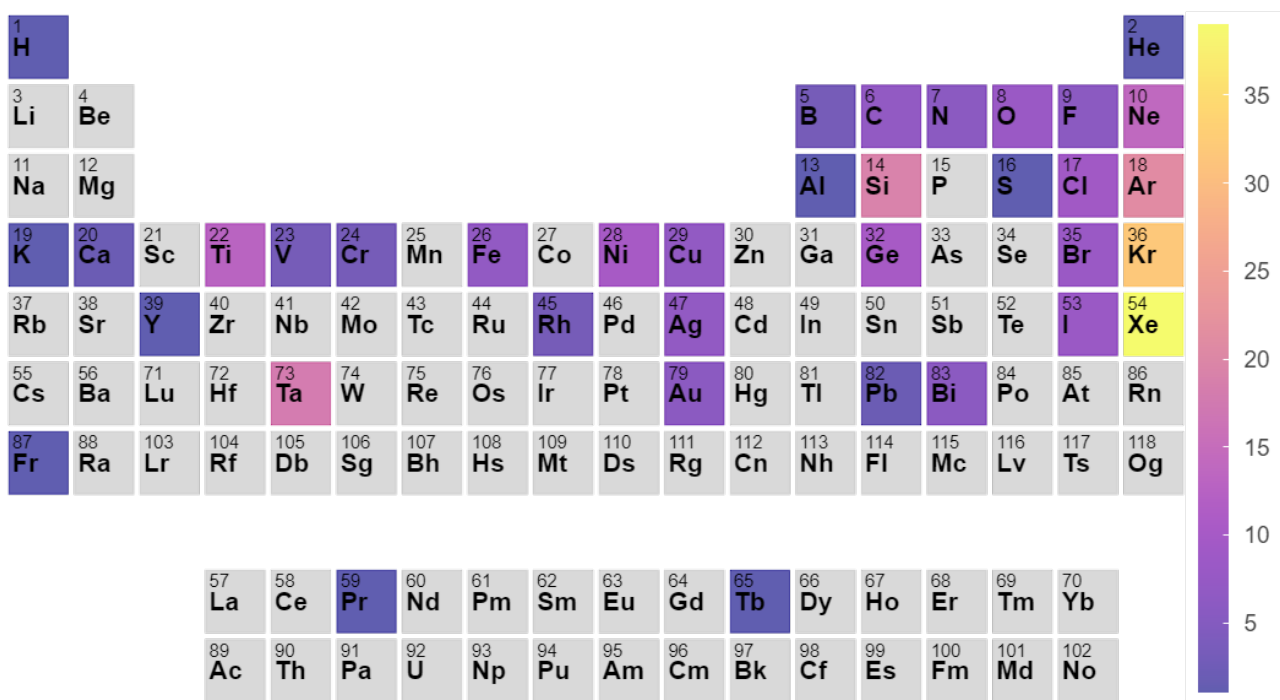


Figure 3.4 – Heat map of heavy ion experiments (obtained using the Periodic Trend Plotter Tool [162]).

The diversity of ions in Figure 3.4 is attributed to the common use of ion cocktails in various experiments. Ion cocktails are mixtures of ions of near-identical mass-to-charge (m/q) ratios. The injector mass-analyzing magnet cannot separate the ions, so it ejects them together from the ion source [116]. When simulating the space radiation environment, it is crucial to consider beam modification and dosimetry, since the beam intensity must be low, and new processing techniques require more energetic beams, posing a challenge for accelerator and ion source physicists. The spectroscopic properties of the beam must be defined in each test run, and calibration and monitoring of parameters like homogeneity, flux, and fluence are necessary during irradiation. Time-saving solutions are also important in building irradiation facilities for space projects, since this decreases costs, and quick ion

changes can be achieved with cocktail beams [200], making them the best option for space radiation simulations.

3.6 Particles and Countries

Research on bit flips has been consistently undertaken over the last five years. As demonstrated in Section 3.5, the particles predominantly employed in the reviewed studies encompass heavy ions, neutrons, and protons. Heavy ions and protons are considered high-energy particles capable of penetrating materials and inducing ionization. This characteristic makes them pivotal in comprehending the effects of space radiation. Furthermore, heavy ions are extensively employed due to their high linear energy transfer and their potential to induce single-event upsets in electronic devices.

Through a careful analysis of each particle, it becomes evident that heavy ions stand out as the preferred choice due to their capability to induce significant damage, enabling a prompt observation of their effects. This is particularly advantageous in radiation experiments, considering their costliness. This feature facilitates the planning of experiments, such as case studies, where there is a higher likelihood of obtaining results that reveal defects. In the United States, numerous articles have been published on the utilization of heavy ions, with Texas A&M University (TAMU) and the Lawrence Berkeley National Laboratory (LBNL) serving as primary facilities for heavy ion research.

Neutrons, as uncharged particles, do not have a direct impact on electronic devices, except for thermal neutrons. These low-energy neutrons, with energy below 25 MeV, can undergo exothermic reactions with specific isotopes, particularly boron-10 in semiconductor devices [154]. Nevertheless, high-energy neutrons can interact with the atomic nuclei of materials, resulting in the emission of secondary ionizing particles, either a charged alpha particle (+2) or a proton (+1) [54]. These ionizing particles have the potential to alter internal logic states in electronic devices, leading to SEUs. Studies indicate that energetic neutrons are responsible for 95% of soft errors [40]. However, gaining access to neutron facilities can be challenging. In this context, France stands out in neutron incidence research, in part, due to the availability of suitable facilities (GENEPI2 and ILL).

Similar to neutrons, protons also have a particular significance given their substantial impact within the atmosphere [96, 154]. Therefore, works involving protons exhibit a wide range, spanning applications in deep learning processors [135] and error correction codes [51] to the assessment of highly complex circuits, such as mixed-signal ASICs [85]. It is noteworthy that a substantial amount of research on protons is conducted in Europe, given that facilities are distributed across multiple countries, including Switzerland (Paul Scherrer Institute, PSI), the Netherlands (Kernfysisch Versneller Instituut, KVI-CART), and Spain (Centro Nacional de Aceleradores, CNA).

Lasers, in turn, consist of focused photon beams and are preferred for their experimental convenience. The United States has conducted a greater number of laser experiments than any other country, indicating their emphasis on cost reduction. As highlighted in Hales *et al.* [84], there is an increasing interest in using lasers to simulate excitation-induced SEEs caused by heavy ions, particularly in cases where access to heavy-ion test facilities is limited. This accounts for the widespread adoption of laser-based experiments globally.

Some works, including Ryder *et al.* [164] and Ildefonso *et al.* [92], have identified x-rays as a viable alternative for reproducing single event effects induced by heavy ions. However, due to variations in dosimetry between heavy-ion and laser sources, the outcomes of pulsed-laser-induced SEEs are predominantly qualitative. Consequently, researchers endeavor to establish a quantitative relationship between measurements induced by heavy ions and lasers, aiming to correlate experiments conducted with lasers to those with heavy ions.

As devices decrease in size and incorporate a larger number of transistors, the occurrence of SEUs per unit area increases [95]. In such a scenario, particles such as alpha become increasingly significant. As elucidated by Chandrashekhar *et al.* [40], the reduction in charge induced by alpha particles is similar to that caused by neutrons. However, in this scenario, charges result from the Coulombic interaction between the alpha particle and silicon atoms as the former traverses the floating gate. These particles exhibit robust ionizing capabilities, generating a multitude of electron-hole pairs within the crystalline lattice of silicon.

Regarding other particles that are less commonly employed in radiation experiments for electronic circuits, electrons demand high energy, and photons have the potential to harm the sample, making them less suitable for specific applications. These factors contribute to their limited usage. On the other hand, muon and pion accelerators are more accessible than facilities for protons and neutrons. However, they hold lesser significance due to their reduced interaction with electronics devices. Nonetheless, Kato *et al.* [100] have shown that muons, particularly negative ones, can induce SEUs and multiple-cell upsets (MCU). As semiconductor components scale down, the probability of muon affecting devices increases due to the reduction in critical charge required for low-linear energy transfer (LET) events. In this regard, Japan is notably concerned about SEUs caused by muons, as evidenced by the majority of related articles originating from the country [100, 122, 133].

3.7 Impacts from Circuit Technology

The effects of radiation on electronic circuits are intricately linked to technological advancements, indicating that specific technological nodes are more or less utilized in particular applications. For instance, this survey illustrated that older technology nodes,

specifically 130nm and above, are widely employed in developing space applications. Fan *et al.* [69] present the work that utilizes the oldest technology in this survey (500nm or 0.5 μ m CMOS technology). They introduce a radiation-tolerant circuit design for a four-channel 12-bit digital-to-analog (DAC) converter. Chen *et al.* [45] also present development work targeted at space applications, specifically a radiation-hardened phase-locked loop (PLL) fabricated in a 130nm technology node. Another device extensively utilized in space applications is the CMOS image sensor, employed as star trackers and image generators for astronomical observations [195]. To address this device, Cai *et al.* [32] evaluated the soft error susceptibility of digital peripheral circuits within commercial CIS fabricated in 180nm (0.18 μ m) CMOS process.

In the intermediate range of technological nodes, radiation research is applied to FPGAs. For instance, Keren *et al.* [106] introduced a novel approach to analyze the effects of single-event transients in SRAM-based FPGA devices. The experiments were conducted using a 45nm SRAM-based FPGA, and the results provide a cross-sectional analysis for both SET and SEU effects at low linear energy transfers. The experiments took place at the UCL Cyclotron (Belgium) accelerator, involving heavy ions and alpha source irradiation. Wang *et al.* [210], on the other hand, conducted proton experiments, while Fabero *et al.* [68] assessed neutron particles using 28nm FPGAs. Both studies focused on characterizing the sensitivity of FPGAs to single-event effects. Moreover, Cai *et al.* [29] also assess the radiation sensitivity of an FPGA. The significant distinction lies in the technological shift, transitioning from CMOS to FinFET through the evaluation of a 16nm FinFET SRAM-based FPGA.

Over the past five years, transformations have occurred not only in technological nodes but also in applications exposed to radiation. Currently, assessments are underway to understand the impact of radiation in machine learning applications using devices with newer technological nodes. Maillard *et al.* [135] introduced a platform and design methodology aimed at facilitating radiation-tolerant deep learning acceleration on FPGAs. They devised a solution tailored for executing image classification applications on a 20nm SRAM-based FPGA. The study included experiments involving a proton beam test with the ResNet-18 convolutional neural network (CNN) for image classification on the radiation-tolerant platform. Additionally, a technique called fault-aware training (FAT) was employed to effectively mitigate single-event effects in the CNN datapath. The findings indicate that employing FAT resulted in a 50% reduction in the overall cross-section of the radiation-tolerant system compared to the design without mitigation during training. In turn, Wang *et al.* [135] assessed the effects of SEUs on CNNs through the utilization of a 28nm SRAM-based FPGA. Similarly, Benevenuti *et al.* [21] evaluated a CNN on a 28nm SRAM-based FPGA. They delved into the main aspects of vulnerability and accuracy degradation of an image classification engine implemented on SRAM-based FPGAs subjected to faults induced by heavy-ion accelerated irradiation.

Lastly, there is radiation research focusing on newer technologies, including FinFETs with nodes ranging from 16nm down to 7nm. Yaqing *et al.* [225] and Takeuchi *et al.* [185] conducted a characterization of single-event effects on 16nm bulk FinFETS, evaluating both single-bit upsets and multiple-cell upsets resulting from heavy ion irradiation. Their findings suggest that the parasitic bipolar effect remains a significant concern for 16nm FinFET SRAMs, similar to planar SRAMs in previous technologies. Nevertheless, the charge-sharing effect is efficiently mitigated due to the narrow connection between the fin and the bulk region in FinFETs. Furthermore, it was observed that works involving recent technologies are carried out using simpler circuits. For instance, Huang *et al.* [90] performed a heavy ion experiment involving a 14/16nm bulk FinFET inverter chains. Similarly, Ball *et al.* [17] investigated the reliability of inverters, NAND gates, and D flip-flop chains when subjected to radiation from neutron and alpha particles.

3.8 Trends

The research into particle acceleration to investigate bit flips and single-event effects in electronic devices is marked by diverse trends, encompassing different radiation sources and international research collaborations. Heavy ions have emerged as a primary choice for simulating space radiation and assessing the resilience of electronic components. Notably, countries such as the United States, China, Belgium, and Switzerland, along with facilities like LBNL, HIRFL, HIF-UCL, and CERN, have been at the forefront of heavy ion experiments.

Heavy ions and protons pose significant challenges in microelectronics research. Their prevalence in space, coupled with their ability to penetrate materials and induce ionization, has a profound impact on electronic devices. Looking ahead, it is expected an increasing dependence on these high-energy particles, particularly as space exploration and satellite technologies advance. Due to their capacity to swiftly induce substantial damage, heavy ions are likely to see heightened usage for prompt effect observation.

The use of laser experiments in radiation research is anticipated to expand, with USA taking a leading role and pursuing cost reduction. Researchers are increasingly working towards establishing a quantitative relationship between heavy-ion and laser-induced measurements to enable correlation with space radiation and heavy-ion experiments. The global interest in laser experiments has the potential to surge, particularly as they provide a means for assessing single-event effects induced by heavy ions.

Continued exploration of muons and pions is anticipated. Despite their lower interaction with electronic circuits, there is a growing concern regarding their potential to induce SEUs and MCUs. This concern is particularly noteworthy as semiconductor components scale down, increasing the susceptibility to muon-induced effects.

Looking ahead, it seems that the focus is shifting towards the research of lower-power and smaller-sized devices. This shift is driven by their increased susceptibility to soft errors caused by accelerated particles. In the last five years, there has been a rise in studies concentrating on SEEs in more advanced technologies, such as FinFET technology, while research on SRAMs has remained consistent, as they continue to be among the most affected components in electronic devices.

4. METHODOLOGY

This chapter summarizes the methodology employed in this work, including the Geant4 simulations, calculations, and comparisons essential for a comprehensive analysis of the results. We describe and explain the chosen Geant4 parameters, including the software version and physics libraries, as well as the selected technological parameters, such as physical compositions and dimensions. Furthermore, we detail the simulation parameters, including the particles, their energies, and incidence angles. Finally, we present the fundamentals of the calculations used to analyze the simulation results.

4.1 Geant4: Basic information

The Geant4 toolkit was used to perform the simulations. This toolkit enables the creation of device geometries, the specification of the physical composition of each component, and the simulation of particle interactions at various angles and energies. For this study, Geant4 version 11.2.1 (2024) was employed as the simulation framework, using the FTFP_BERT physics list [77].

Given the substantial volume of data generated, the simulations were resource-intensive and exceeded the capacity of a standard machine. To accelerate the simulation process, multicore workstations were employed. Geant4's multi-threading capability was utilized, running eight parallel threads, with five different simulations executed simultaneously, each corresponding to a specific technology. Python and bash scripts were developed not only for data analysis and selection but also for computational loops to optimize the Geant4 code implementation.

4.2 Technology parameters

For this study, we selected five technologies: two planar (65nm and 32nm) and three FinFETs (22nm, 14nm, and 7nm). The construction process involved incrementally building each component of the structure. We researched and detailed the technologies' compositions and dimensions, which are summarized in Tables 4.1, 4.2, 4.3, 4.4, and 4.5, with coordinates set as shown in Figure 4.1. The geometrical representations of these technologies are illustrated in Figure 4.3, and the detailed segmentation is illustrated in Figure 4.4.

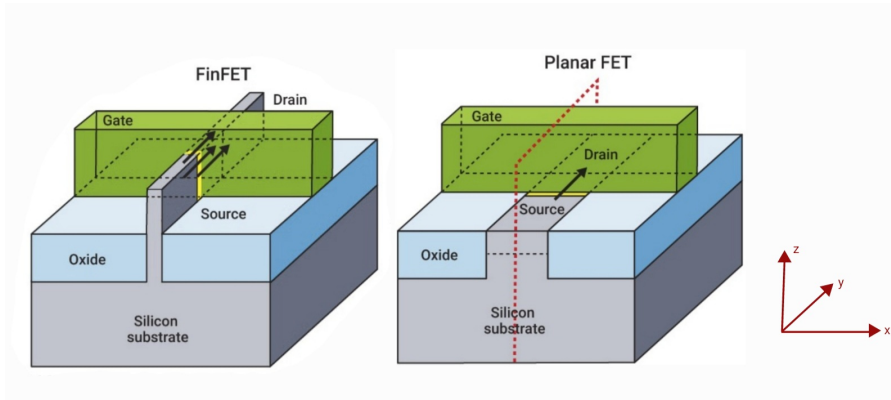


Figure 4.1 – Coordinates used to characterize planar and FinFET transistors (Source: <https://www.synopsys.com/glossary/what-is-a-finfet.html> - modified).

The planar technologies feature the channel and effective channel lengths as described in [175, 176], which are crucial components of the device for reducing drive current and enhancing switching performance. To aid in the understanding of the geometry, we present an illustration of the 65nm channel from [176] in Figure 4.2.

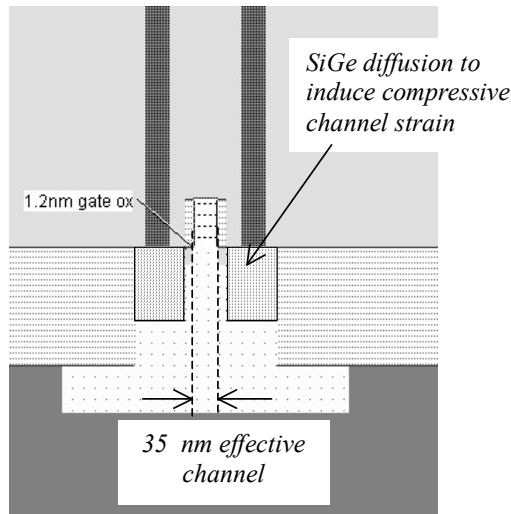


Figure 4.2 – Planar channel and effective channel (Source: [176]).

Figure 4.3(a) shows the planar architecture design. The figure shows the device structure, with the gray region representing pure silicon. The blue regions indicate the source and drain electrodes, the green region represents the gate, and the light blue area beneath the gate denotes the oxide layer. This is a 65nm representation produced with Geant4, and it is one of the geometries used in this work for simulation.

Figure 4.3(b) shows the FinFET design structure where the gray area represents pure silicon, the light blue area indicates the oxide layer, the blue regions denote the source and drain electrodes, the green area represents the gate, and the yellow region beneath the gate is the insulating oxide. This is 22nm representation produced with Geant4 and it is one of the geometries used in this work for simulation.

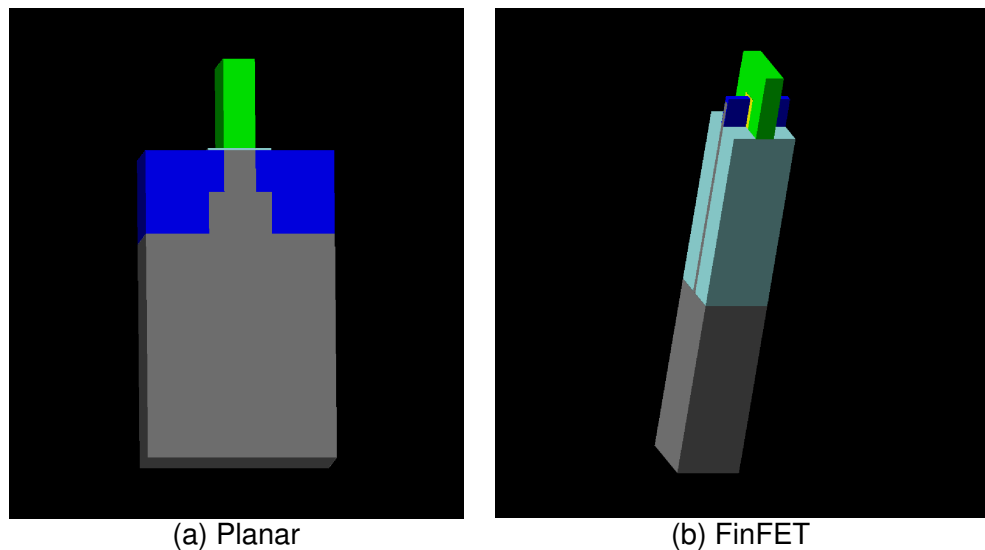


Figure 4.3 – Planar and FinFET architecture design.

Figure 4.4 present the geometric parameters used in Tables 4.1, 4.2, 4.3, 4.4, and 4.5. Such geometric parameters were used to build the devices.

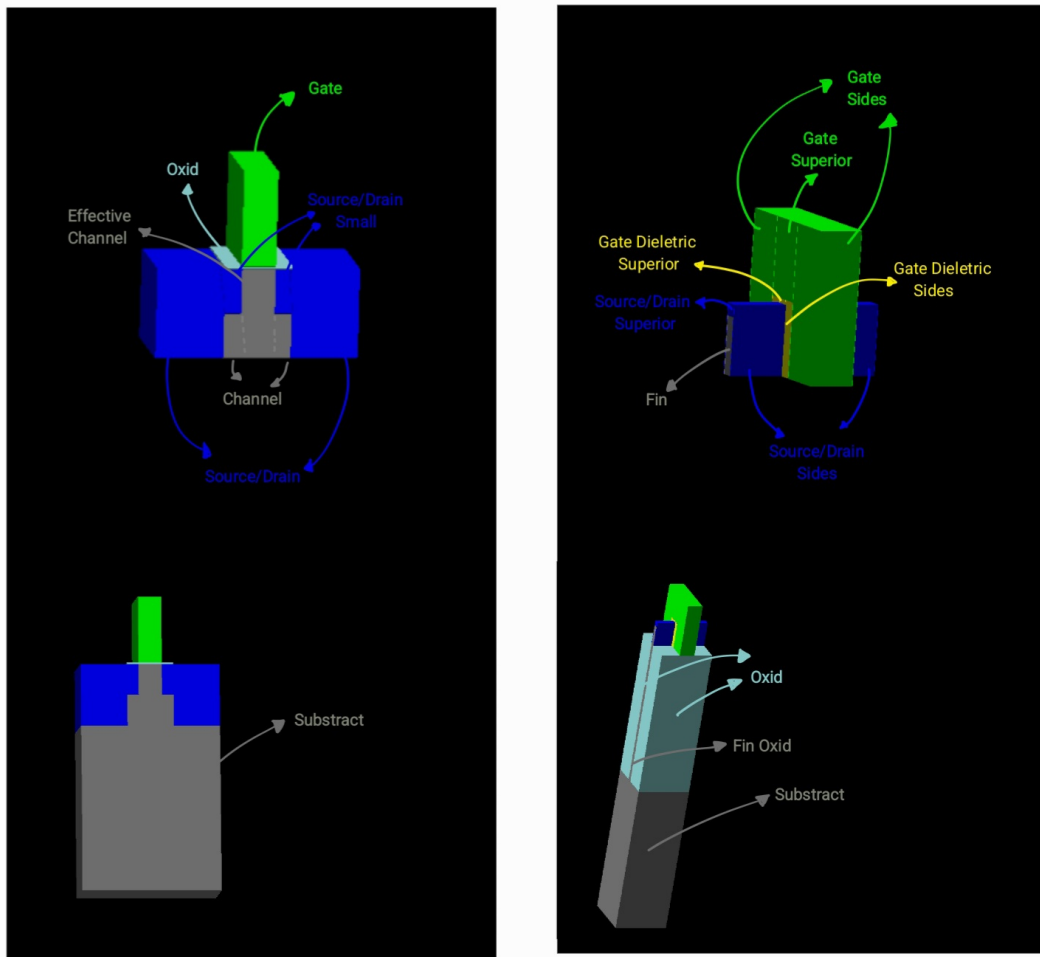


Figure 4.4 – FET architectures design detailed segmentation.

Table 4.1 – 65nm Technology Details.

65nm					
Material	Component	Reference	Position	Value (nm)	Reference
Substract	Si	[176]	x	210	[216]
			y	110	[216]
			z	250	
Source/Drain	SiGe	[176]	x	70	(xSubstract - xOxid)/2
			y	110	ySubstract
			z	93.33	[142]
Source/Drain Small	SiGe	[176]	x	17.5	(xOxid - xFin)/2
			y	110	ySubstract
			z	46.67	zSource/Drain/2
Effective Channel	Si	[176]	x	35	[176]
			y	110	ySubstract
			z	93.33	zSource/Drain
Channel	Si	[176]	x	17.5	(xOxid - xFin)/2
			y	110	ySubstract
			z	46.67	zSource/Drain/2
Oxid	SiON	[176]	x	70	[176]
			y	110	ySubstract
			z	2.5	[176]
Gate	Si	[176]	x	35	xFin
			y	110	ySubstract
			z	100	

Table 4.2 – 32nm Technology Details.

32nm					
Material	Component	Reference	Position	Value (nm)	Reference
Substract	Si	[175]	x	112.5	[215]
			y	56.25	[215]
			z	250	
Source/Drain	SiGe	[175]	x	38.25	(xSubstract - xOxid)/2
			y	56.25	ySubstract
			z	48	[142]
Source/Drain Small	SiGe	[175]	x	2	zSource/Drain/2
			y	56.25	ySubstract
			z	24	zSource/Drain/2
Effective Channel	Si	[175]	x	32	[175]
			y	56.25	ySubstract
			z	48	zSource/Drain
Channel	Si	[175]	x	2	(xOxid - xFin)/2
			y	56.25	ySubstract
			z	24	zSource/Drain/2
Oxid	HfO ₂	[175]	x	36	[175]
			y	56.25	ySubstract
			z	2.5	[175]
Gate	SiN	[175]	x	32	xFin
			y	56.25	ySubstract
			z	57.15	

Table 4.3 – 22nm Technology Details.

22nm					
Material	Component	Reference	Position	Value (nm)	Reference
Substract	Si	[64]	x	90	ySubstract
			y	90	[214]
			z	250	zoxid
Oxid	SiO2	[64]	x	41	(ySubstract - xFin)/2
			y	90	ySubstract
			z	250	[64]
Fin Oxid	Si	[193]	x	8	xFin
			y	90	ySubstracttract
			z	250	zOxid
Fin	Si	[193]	x	8	[214]
			y	90	ySubstracttract
			z	34	[214]
Source/Drain Sides	As (2.5 g/cm ³ 5%) + SiO2 (95%)	[193]	x	0.74	[193]: (xFin × 4)/43
			y	32	(ySubstract - yGate)/2
			z	41.12	(zFin + zSource/Drain Superior)
Source/Drain Superior	As (2.2 g/cm ³ 1%) + SiO2 (99%)	[193]	x	8	xFin
			y	32	(ySubstract - yGate)/2
			z	7.12	[193]: (zFin × 9)/43
Gate Dielectric Sides	HfO2	[64]	x	10	[64]
			y	26	yGate Superior
			z	44	(zFin + zGate Dielectric Superior)
Gate Dielectric Superior	HfO2	[64]	x	8	xFin
			y	26	yGate Superior
			z	10	zGate Dielectric Sides
Gate Sides	TiN	[174]	x	31	(xsub - (xFin + 2*zGate Dielectric Sides))/2
			y	90	ySubstract
			z	90	ySubstract
Gate Superior	TiN	[174]	x	28	(xFin + 2*zGate Dielectric Sides)
			y	26	[214]
			z	46	ySubstract - (zFin + zGate Dielectric Superior)

Table 4.4 – 14nm Technology Details.

14nm					
Material	Component	Reference	Position	Value (nm)	Reference
Substract	Si	[64]	x	70	ySubstract
			y	70	[213]
			z	250	zOxid
Oxid	SiO2	[64]	x	31	(ySubstract - yFinOxid)/2
			y	70	ySubstract
			z	250	[64]
Fin Oxid	Si	[193]	x	8	xFin
			y	70	ySubstract
			z	250	zOxid
Fin	Si	[193]	x	8	[213]
			y	70	ySubstract
			z	42	[213]
Source/Drain Sides	As (2.5 g/cm ³ 5%) + SiO2 (95%)	[193]	x	0.74	[193]: (xFin × 4)/43
			y	25	(ySubstract - yGate)/2
			z	50.79	(zFin + zSource/Drain Superior)
Source/Drain Superior	As (2.2 g/cm ³ 1%) + SiO2 (99%)	[193]	x	8	xFin
			y	25	(ySubstract - yGate)/2
			z	8.79	[193]: (zFin × 9)/43
Gate Dielectric Sides	HfO2	[64]	x	3	[177]
			y	20	yGate Superior
			z	45	(zFin + zGate Dielectric Superior)
Gate Dielectric Superior	HfO2	[64]	x	8	xFin
			y	20	yGate Superior
			z	3	xhfo2lat
Gate Sides	TiN	[174]	x	28	(xsub - (xFin + 2*zGate Dielectric Sides))/2
			y	20	yGate Superior
			z	90	ySubstract
Gate Superior	TiN	[174]	x	14	(xFin + 2*zGate Dielectric Sides)
			y	20	[213]
			z	25	ySubstract - (zFin + zGate Dielectric Superior)

Table 4.5 – 7nm Technology Details.

7nm					
Material	Component	Reference	Position	Value (nm)	Reference
Substract	Si	[64]	x	57	ySubstract
			y	57	[217]
			z	250	zOxid
Oxid	SiO2	[64]	x	25.5	(ySubstract - yFinOxid)/2
			y	57	ySubstract
			z	250	[64]
Fin Oxid	Si	[193]	x	6	xFin
			y	57	ySubstract
			z	250	zOxid
Fin	Si	[193]	x	6	[217]
			y	57	ySubstract
			z	52	[217]
Source/Drain Sides	As (2.5 g/cm ³ 5%) + SiO2 (95%)	[193]	x	0.56	[193]: (xFin × 4)/43
			y	24	(ySubstract - yGate)/2
			z	62.88	zFin + zSource/Drain Superior
Source/Drain Superior	As (2.2 g/cm ³ 1%) + SiO2 (99%)	[193]	x	6	xFin
			y	24	(ySubstract - yGate)/2
			z	10.88	[193]: (zFin × 9)/43
Gate Dielectric Sides	HfO2	[64]	x	1.4	[177]
			y	9	yGate Superior
			z	53.4	(zFin + zGate Dielectric Superior)
Gate Dielectric Superior	HfO2	[64]	x	6	xFin
			y	9	yGate Superior
			z	1.4	xGate Dielectric Sides
Gate Sides	TiN	[174]	x	24.1	(xSubstract - (xFin + 2*zGate Dielectric Sides))/2
			y	9	yGate Superior
			z	57	ySubstract
Gate Superior	TiN	[174]	x	8.8	xFin + 2*zGate Dielectric Sides
			y	9	[213]
			z	3.6	ySubstract - (zFin + zGate Dielectric Superior)

4.3 Simulation parameters

Once the geometries are constructed, simulations are conducted using Geant4. In this phase, the incident particles, their angles of incidence, energies, and the number of initial particles per run are specified. Protons, neutrons, muons, alpha particles, and pions are selected based on discussions made in Chapter 2. From the same discussion, the initial particle energy range is selected from 0.5 MeV to 100 TeV. To cover this range, the following energies are chosen: 0.5 MeV, 1 MeV, 2 MeV, 5 MeV, 10 MeV, 100 MeV, 500 MeV, 1 GeV, 500 GeV, 1 TeV, 10 TeV, and 100 TeV. The initial particle angles of incidence are also strategically selected and are depicted in Figure 4.5, which illustrates four distinct angular measurement groups:

- **Planar a:** angles range from perpendicular to the gate to lateral orientations that pass through the source and drain regions.
- **Planar b:** the angles that vary from above and perpendicular to the gate to a 90° angle that directly traverses the pure silicon substrate.
- **FinFET a:** angles vary from perpendicular to the gate to those that pass through the entire fin structure.
- **FinFET b:** angles ranging from above the gate to lateral orientations relative to the gate.

It is important to note that for both Planar a and Planar b, and respectively for FinFET a and FinFET b, the 0° and 180° incidence angles are equivalent.

In each simulation, 10,000 incidents of identical particles with the same initial energy and angle of incidence were performed to ensure statistically representative data. The simulation results reflect what occurs within the sensitive area. In this work, the sensitive area is defined as the pure silicon region below the gate. For FinFETs, this includes the region below the gate and between the source and drain, while for MOSFETs, it covers the entire area between the source and drain. Although the simulation output provides various data, our focus was specifically on the distinct electrons and the energy deposited by all detected particles.

Table 4.6 summarizes the experimental parameters and conditions used in the study. It details the types of particles involved, the semiconductor technologies, the initial energy levels of the particles, the range of incident angles considered, and the number of particles simulated. This information is crucial for understanding the experimental setup and the conditions under which the simulations were conducted.

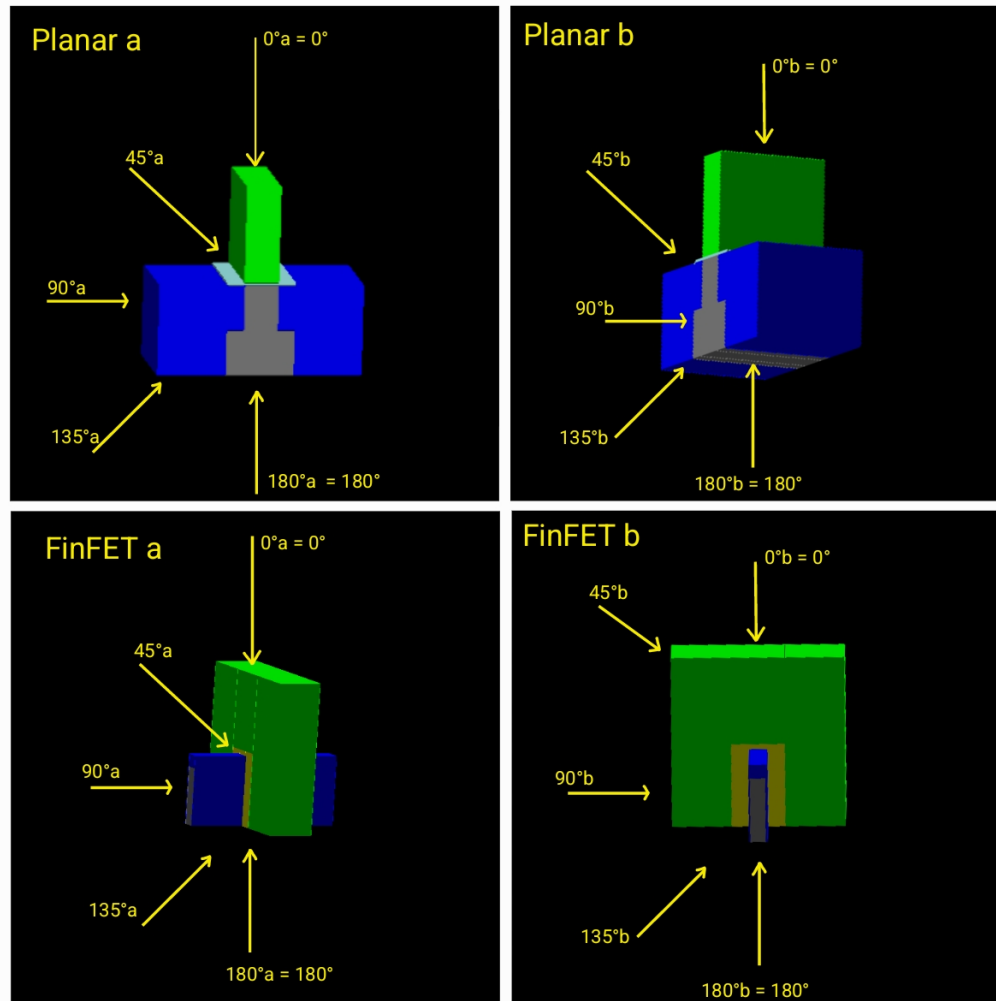


Figure 4.5 – Geant4-based simulation for 65nm and 22nm technology nodes, removing the substrate area, bringing the chosen four distinct angular measurement groups.

Table 4.6 – Summary of experimental parameters and conditions.

Parameter	Description
Particles	Protons, neutrons, positive muons, negative muons, alpha particles, positive pions, negative pions, neutral pions
Technology	Two planar (65 nm and 32 nm) and three FinFETs (22 nm, 14 nm, and 7 nm)
Initial Particle Energy	0.5 MeV, 1 MeV, 2 MeV, 5 MeV, 10 MeV, 100 MeV, 500 MeV, 1 GeV, 500 GeV, 1 TeV, 10 TeV, 100 TeV
Incident Angles in Technology	0°, 45°a, 90°a, 135°a, 180°a, 45°b, 90°b, 135°b (Figure 4.5)
Number of Particles per Simulation	10,000 incidents of identical particles

4.4 Simulation results data manipulation

To calculate the total number of electrons contributing to the current, two factors from the simulation must be considered: the number of detected electrons in the sensitive area and the electrons generated by the energy deposited by particles going through the sensitive area. This calculation is necessary because Geant4 standard libraries accounts only for electrons generated by ionization with energies above 10 eV [63], while low-energy electrons also contribute to the current. Electrons are added to the current if the deposited energy exceeds the threshold for pair creation. The number of generated electrons is computed by dividing the initial energy by the energy required to create pairs, which is 3.6 eV [25] for silicon. The total number of electrons is then divided by 10,000 to determine the number of electrons per incident particle. With this information, the drain current and voltage generated can be calculated, as presented in the next session.

4.5 Current Calculus

In MOS transistors, both planar and FinFETs, current and voltage are fundamental parameters that significantly affect device performance, efficiency, and reliability. In this section, we present the formulas to convert the number of electrons resulting from the Geant4 simulations into current values.

According to Nussenzveig [147] (p. 99), the current can be described as follows:

$$I = \frac{\Delta q}{\Delta t} \quad (4.1)$$

where: Δq is the charge variation and Δt is the time variation.

Since we have the information about the number of electrons, we have:

$$\Delta q = N q_0 \quad (4.2)$$

where: N is the number of electrons and q_0 is the elementary charge of the electron [147] (p. 11) given by:

$$q_0 = 1.6 \cdot 10^{-19} C \quad (4.3)$$

The unit of charge is Coulombs [147] (p. 8), defined as the electric charge transported in 1 second by a current of 1 ampere ($C = sA$).

It is known that velocity is the derivative of displacement (which we will call l) with respect to time (t):

$$v = \frac{\Delta I}{\Delta t}$$

thus,

$$\Delta t = \frac{\Delta I}{v} \quad (4.4)$$

The drift velocity [218] is the velocity a particle reaches due to an electric field and can be expressed as:

$$v = \mu E \quad (4.5)$$

where: μ is the electron mobility in $\frac{m^2}{Vs}$ and E is the electric field in $\frac{V}{m}$.

The electric field [83] (p. 79) can be defined as the negative gradient of the electric potential (voltage):

$$\vec{E} = -\vec{\nabla} V \Rightarrow E = -\frac{\Delta V}{\Delta I} \quad (4.6)$$

Substituting the magnitude of 4.6 into 4.5:

$$v = \mu \frac{\Delta V}{\Delta I} \quad (4.7)$$

Substituting 4.7 into 4.4:

$$\Delta t = \frac{\Delta I}{\mu \left(\frac{\Delta V}{\Delta I} \right)} \therefore \Delta t = \frac{\Delta I^2}{\mu \Delta V} \quad (4.8)$$

Substituting 4.8 into 4.1:

$$I = \frac{\Delta q}{\left(\frac{\Delta I^2}{\mu \Delta V} \right)} \quad (4.9)$$

Finally, substituting 4.2 into 4.9:

$I = \frac{N q_0 \mu \Delta V}{\Delta I^2}$

(4.10)

From [59] (65nm technology):

$$\Delta V_{65nm} \simeq 1 V \quad (4.11)$$

$$\mu = 1.4 \frac{cm^2}{Vs} \therefore \mu = 1.4 \cdot 10^{-4} \frac{m^2}{Vs}$$

Since ΔI is on the order of nanometers, then:

$$\Delta I = x \cdot 10^{-9} \therefore \Delta I^2 = x^2 \cdot 10^{-18} \quad (4.12)$$

Substituting 4.3, 4.11, and 4.12, we get:

$$I = \frac{N \cdot 1.6 \cdot 10^{-19} \cdot 1.4 \cdot 10^{-4} \cdot 1}{x^2 \cdot 10^{-18}} \quad As \cdot \frac{m^2}{Vs} \cdot V \cdot \frac{1}{m^2} \quad (4.13)$$

$$I = 2.24 \cdot 10^{-5} \frac{N}{x^2} A \quad (4.14)$$

In MOS devices, I_{dsat} (also called I_{ON}), or saturation current, is the drain current when the MOS operates in the saturation region (also called the active region). In this region, the MOS is turned on, and the current is independent of the drain-source voltage (V_{DS}) and primarily controlled by the gate-source voltage (V_{GS}). Jena [97] (p. 437) defines I_{dsat} as:

$$I_{dsat} = \frac{I}{W} \quad (4.15)$$

where: W is the width of the technology. For planar MOS, W is the y value of the silicon area below the gate and in case of the FinFETs it is the z value of the fin.

We can now use the current equations and technology definitions to simulate and compare the number of electrons generated in each simulation with the resulting current. That allows us to assess and compare the results against Spectre simulations and tabulated values to determine if the device is susceptible to inducing bitflips.

5. RESULTS

This chapter presents the results obtained from simulations performed with Geant4. It is organized as follows:

- Section 5.1 presents the average number of electrons each particle produces, demonstrating that protons are the most prevalent.
- Section 5.2 evaluates the average number of electrons produced at different energy levels, showing that 0.5 MeV results in the highest number of electrons.
- Section 5.3 discusses the SPICE simulation of a memory cell, aimed at quantifying the current required to induce a bit flip.
- Section 5.4 examines the current induced by incident particles at various angles, using 0.5 MeV energy, in comparison with the current defined in the SPICE simulation. The results indicate that the current induced by the particles effectively causes bit flips.
- Section 5.5 presents normalized results related to the number of electrons and current for different technologies and incidence angles.
- Section 5.6 summarizes the main findings of this chapter.

5.1 Particle versus Average Number of Electrons

In this section, we present the average number of electrons produced by each particle, as shown in Figure 5.1. In this figure, the y-axis represents the average number of electrons produced, while the x-axis corresponds to the particle type. From the figure, we observe that:

- **Alpha** particles lead to a significant production of electrons. However, since alpha particles only constitute 9% of cosmic rays and are early stopped in the atmosphere, their impact should be considered only in outer and near-outer space.
- **Protons**, which appear second in the figure, account for 90% of cosmic rays and are also generated during cosmic cascades. This aligns with Table 3.2, which shows many experiments involving protons, emphasizing the necessity of these studies.
- **Positive pions** are abundantly generated at higher atmospheric levels during cascades and rank third in electron generation.

- **Positive muon** come in fourth. Despite their lower ranking, muons are predominant at ground level. Although they generate fewer electrons, if the current or voltage generated by muons under certain conditions is sufficient to cause a SEE, these errors may have a more significant impact at ground level than those caused by protons, which typically do not reach this atmospheric layer in large quantities.
- **Neutrons** and **neutral pions** were not detected in our simulation. A more detailed study, which is beyond the scope of this dissertation due to time constraints, would be needed to investigate these particles. This could serve as a starting point for future research.

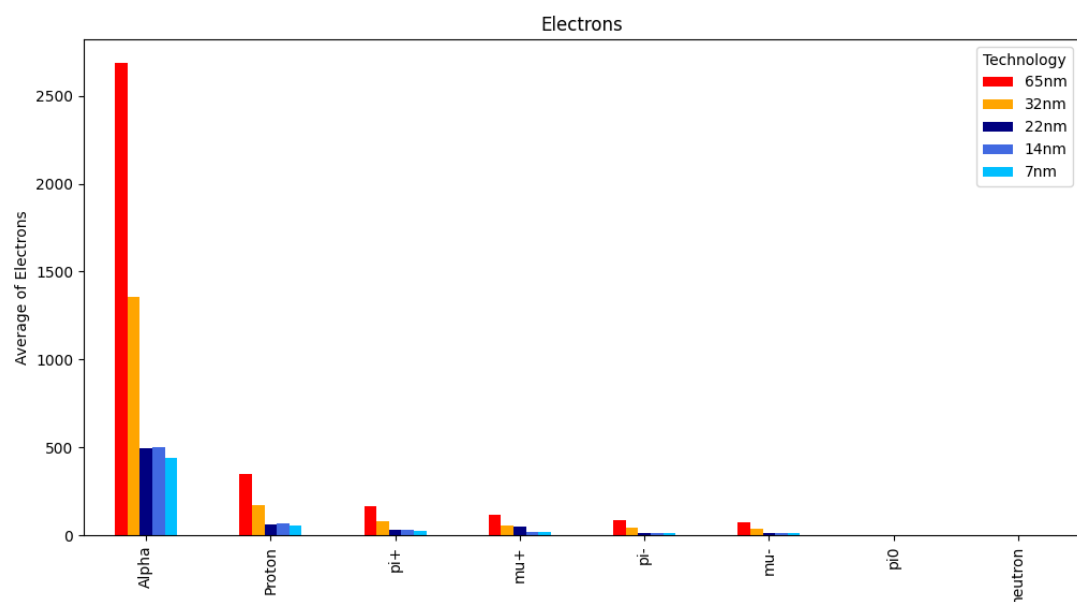


Figure 5.1 – Particle (x-axis) versus Average Number of Electrons (y-axis). This graph shows the average number of electrons measured for each particle. The average is calculated over the angle of incidence and energies.

Figure 5.1 also shows that planar technologies, particularly the 65nm technology, produce more electrons due to their larger sensitive area. However, this does not necessarily indicate a higher number of single event effects, as the current required to induce a bit flip varies between different technologies.

5.2 Energy versus Average Number of Electrons

Figure 5.2 presents the average number of electrons (y-axis) produced at different energy levels (x-axis). The figure shows that the number of generated electrons decreases as energy increases. At higher energies, particles tend to traverse the material more quickly,

resulting in fewer collisions and, consequently, a lower production of secondary electrons. This phenomenon explains why the number of produced electrons decreases as the particle's energy increases.

Another key concept in understanding the relationship between electrons and energy levels is *stopping power*. In particle and radiation physics, it describes the rate at which a charged particle loses energy as it travels through a material. It is defined as the energy loss per unit distance traveled by the particle within the medium, typically expressed in units of energy per unit length (e.g., MeV/cm).

In our experiments, since higher-energy particles interact less with the medium, it is reasonable to focus on the results for the initial energy of 0.5 MeV. At this energy level, the stopping power is greater, interactions are more frequent, and more electrons are produced.

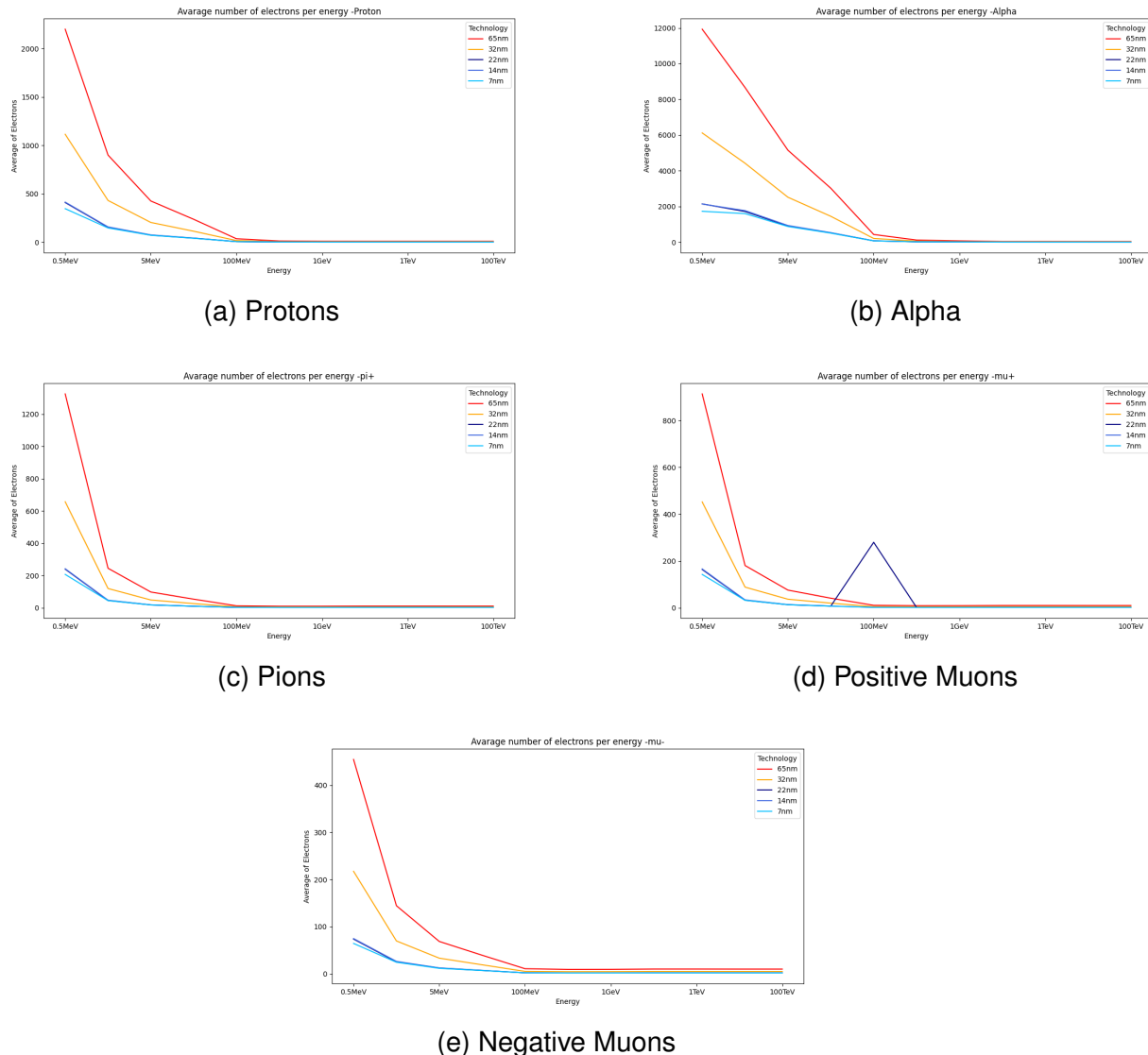


Figure 5.2 – Energy versus Average Number of Electrons per Particle.

5.3 Cell Memory Simulation

This section presents the electrical stimulation of cell memory across 65nm (planar), 28nm (planar), and 7nm (FinFET) technology nodes to determine the current needed to produce a bitflip. Figure 5.3 shows the structure of the circuit being simulated. In this figure, we observe four sections [211]:

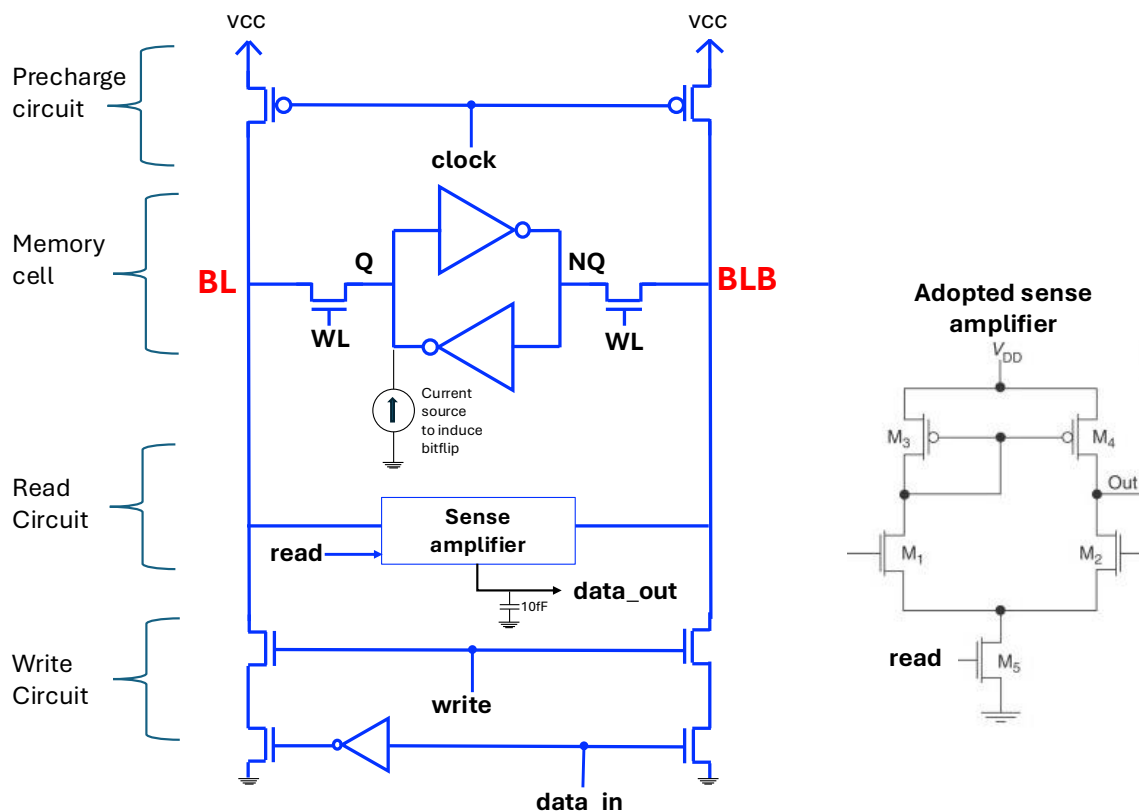


Figure 5.3 – Circuitry for the memory cell, with the read and write circuits.

- **Precharge circuit**, responsible for precharging the data lines (BL and BLB) when $clock=0$.
 - **Memory cell**. The core component of the circuit, the memory cell, stores a single bit of data (either 0 or 1). The memory cell is connected to the word line (WL) and the bit lines (BL and BLB). The WL is activated during both reading and writing operations. The logic value in Q corresponds to the stored data. A current source is connected to Q to simulate the current generated by particle interactions (similarly, a similar current source is also simulated on NQ). The WL is obtained by *oring* *read* and *write* signals.
 - **Read circuit**. This is implemented using a sense amplifier. The sense amplifier detects the small voltage difference between the bit lines (BL and BLB) and amplifies it to a recognizable logic level (0 or 1) during a read operation. It ensures that the data read from the memory cell, $data_out$, is accurate.

- **Write circuit**, activated by the *write* signal, this circuit discharges either *BL* or *BLB*, allowing the *data_in* value to be stored in the memory cell.

Figure 5.4 illustrates the operation of the memory cell without current injection to simulate particles. Write or read operations occur when *clock*=‘1’, following the precharging of the *BL* and *BLB* signals. In this simulation, 4 write operations are performed with the values 1-0-1-0. The logic value is stored in the pair of inverters. After each write operation, a read operation (*read* signal) is performed, and the correctly read value is observed at the output signal. The simulation also presents the *BL* and *BLB* signals.

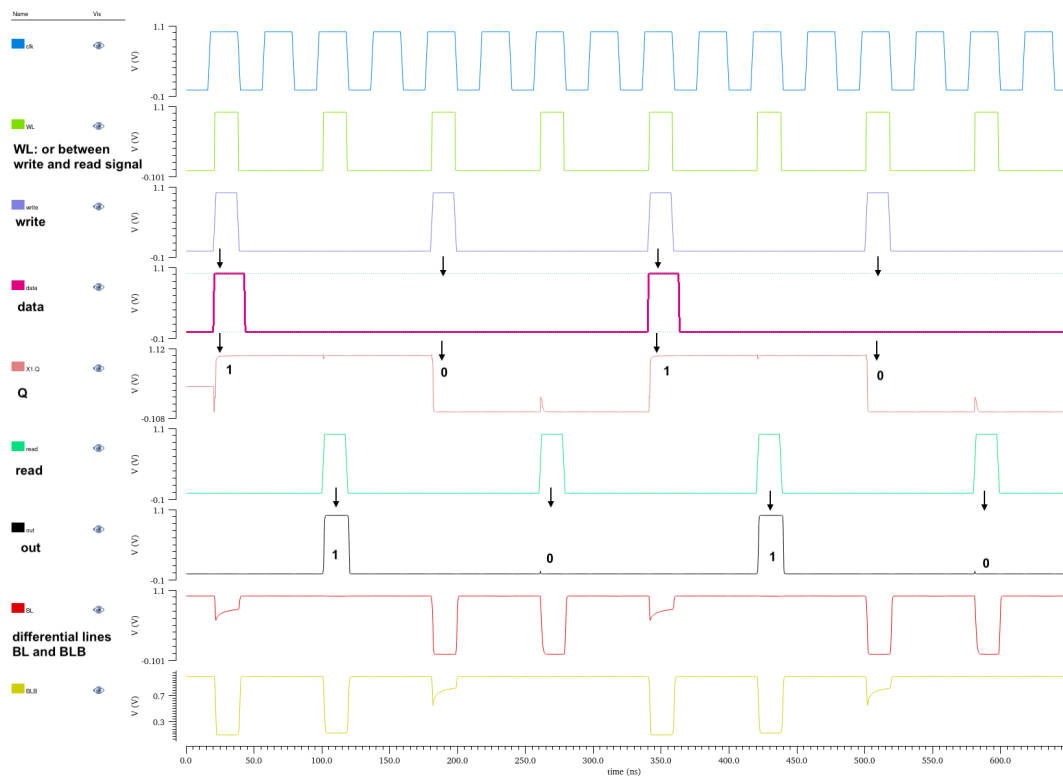


Figure 5.4 – Simulation of a memory cell in 65nm technology, with 4 write and 4 read operations. The differential lines, *BL* and *BLB*, are pre-charged when the *clk* signal is equal to ‘0’.

Figure 5.5 presents the same simulation scenario with 4 write and 4 read operations; however, current sources are activated at *Q* and *NQ* after the first and second write operations, respectively. These current sources increase the current on their connected nodes from 0 to 100 mA. It is observed that as the current increases, the voltage on the affected node decreases, eventually causing the stored value to change state and resulting in a bitflip. The simulation induces bitflips for both logical levels. As a result, the read operation returns 0-1-1-0 instead of 1-0-1-0, as seen in the first simulation.

Figure 5.6 provides a close-up view of the moments when bitflips occur in the simulation for 65nm, 28nm, and 7nm technologies. Table 5.1 presents the current required to induce a bitflip, as measured using commands from the Spectre simulator. A lower current value was expected for the 28nm technology. This is probably due to differences in transistor

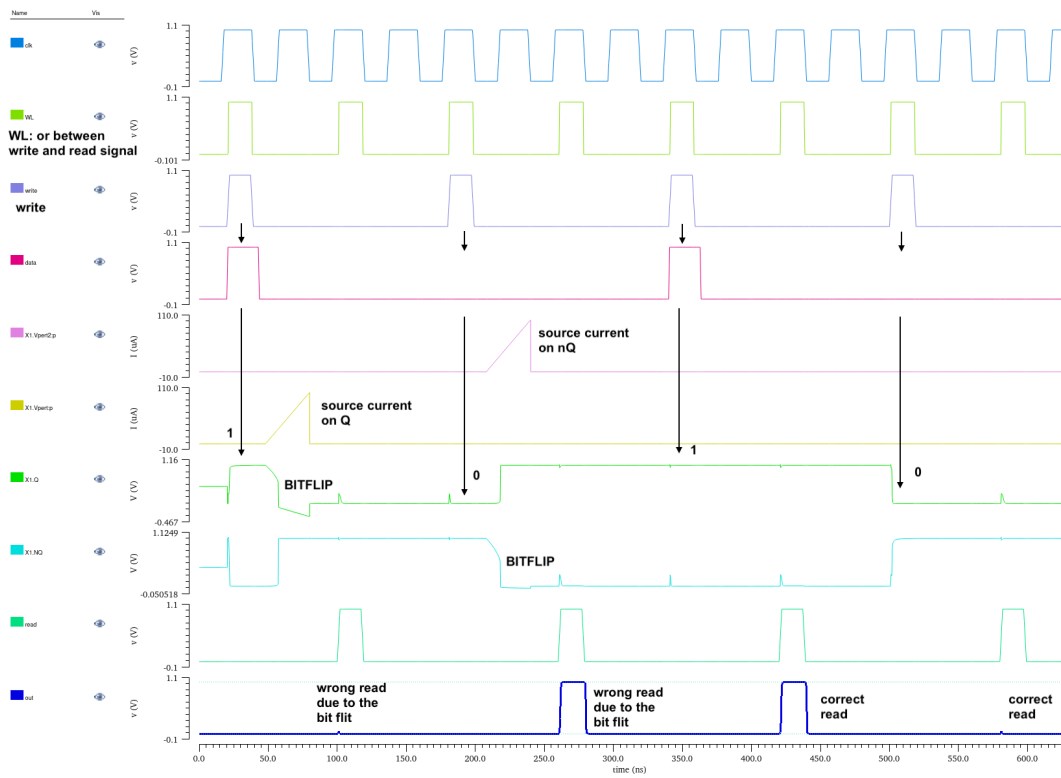


Figure 5.5 – Simulation of a memory cell in 65nm technology, with 4 write and 4 read operations. Note the two source currents on 'Q' and 'nQ' signals inducing bitflips.

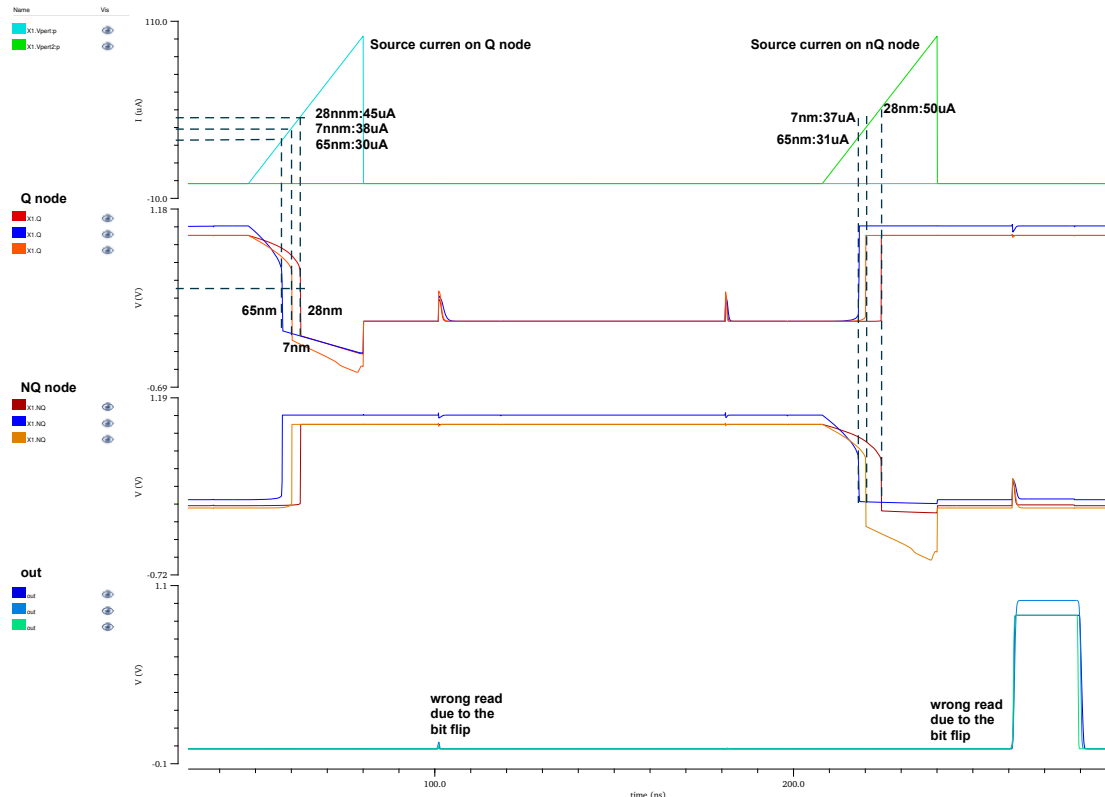


Figure 5.6 – Simulation of bitflips on 65nm, 28nm, and 7nm. The simulation highlights the current inducing the bitflips for each technology.

sizing and type. The key finding is the quantification of the current that particles must induce in real technologies for bitflips to occur.

Table 5.1 – Current, in μA , to induce a bitflip for different technology nodes. We consider the smallest current to induce a bitflip.

Technology node	65nm	28nm	7nm
bitflip 1 → 0	30	45	38
bitflip 0 → 1	31	50	37

5.4 Angle of Incidence versus Current

From the incidence angles shown in Figure 4.5, we created graphs with the incidence angle on the x-axis and the current generated by the resulting electrons on the y-axis for an energy of 0.5 MeV, as specified for the proton sample in Table 5.2. These graphs were produced for different technologies. The maximum current (I) on the y-axis is determined by the number of electrons generated for each particle, as calculated using Equation 4.14, where x represents the effective length (L_{eff}) in meters.

Table 5.2 – Number of electrons (N) across different technologies and angles. I: current (μA). Complete table with other particles in GitHub [151].

Angle	65nm – $L_{\text{eff}}=35\text{nm}$		32nm – $L_{\text{eff}}=32\text{nm}$		22nm – $L_{\text{eff}}=26\text{nm}$		14nm – $L_{\text{eff}}=20\text{nm}$		7nm – $L_{\text{eff}}=9\text{nm}$	
	N	I	N	I	N	I	N	I	N	I
0	1573	28.8	801	17.5	567	18.8	692	38.8	850	235.0
45a	2511	45.9	1229	26.9	599	19.9	463	25.9	207	57.2
45b	2205	40.3	1117	24.4	190	6.3	189	10.6	141	39.0
90a	4382	80.1	2294	50.2	427	14.2	324	18.1	147	40.6
90b	1836	33.6	922	20.2	135	4.5	133	7.5	100	27.7
135a	2526	46.2	1241	27.1	600	19.9	464	26.0	205	56.8
135b	2218	40.6	1127	24.7	189	6.3	188	10.5	142	39.2
180	1583	28.9	804	17.6	411	13.6	499	27.9	412	113.9

In Figure 5.7, the golden line represents the minimum current required to cause a bitflip in the technology. This current value, obtained from electrical simulation with Spectre (presented in Section 5.3), indicates the threshold for bitflips. Since a model for the 32nm technology was not available, we used the 28nm model as a good approximation. The violet line shows the calculated current by replacing I_{ON} from the literature with I_{dsat} in Equation 4.15. These results are detailed in Table 5.3 and are only used for the FinFET comparison, as we do not have simulation data for 22nm and 14nm technologies.

From Figure 5.7 we observe:

- **65nm:** Protons generate currents above the bitflip threshold regardless of the incidence angle. Positive pions and muons can also induce bitflips when incident at an angle of 90°a, particularly as they pass through the source/drain area.

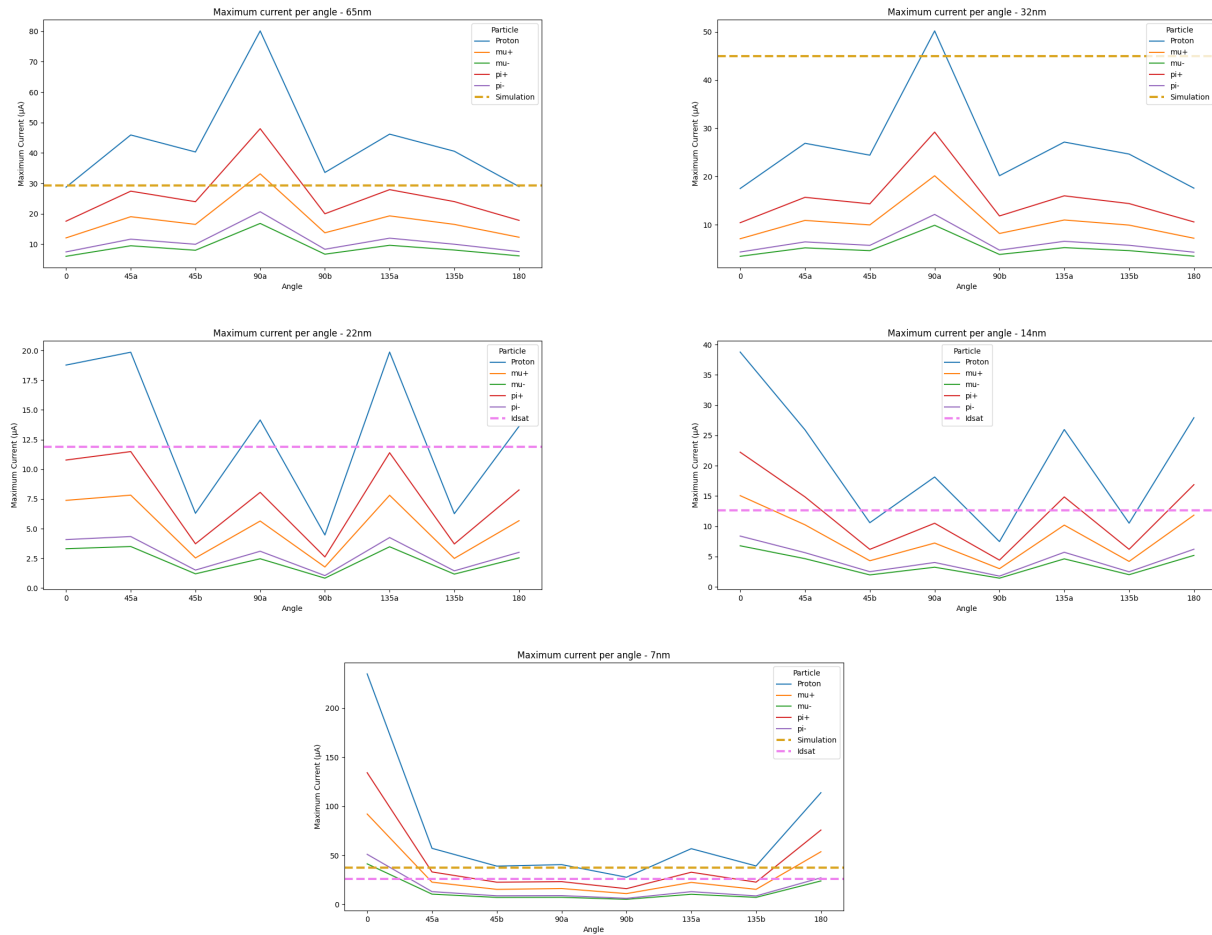


Figure 5.7 – Current per incidence angle for different particles. Gold line: minimum current needed to cause a bitflip obtained from electrical simulation. Violet line: minimum current calculated by replacing I_{ON} with I_{dsat} in Equation 4.15.

Table 5.3 – Simulation and Saturation Current Values for Different Technologies. The I_{ON} saturation values are from references [174–177, 214].

Technology	Simulation (μA)	I_{on} ($mA/\mu m$)	I_{on} Current (μA)
65nm	30	-	-
32nm	45	-	-
22nm	-	0.35	12
14nm	-	0.3	13
7nm	38	0.5	26

- **32nm:** This technology shows strong resilience to bitflips, with only protons causing issues at $90^\circ a$ through the source/drain area.
- **22nm:** Protons can cause bitflips at various angles, while positive pions approach the bitflip threshold at $45^\circ a$ and $135^\circ a$.
- **14nm:** Both protons and positive pions can induce bitflips, with positive muons also capable of causing bitflips at 0° .

- **7nm:** All particles can induce bitflips at 0° ; however, due to the specific angle and small affected region, fewer events may occur despite the increased sensitivity. At other angles, protons are the primary contributors to bitflips.

5.5 Qualitative Comparison between Technology, Angle of Incidence, and Incident Particles

Figures 5.8 and 5.9 present a selected set of normalized data showing the simulation results. The angles and particles are those deemed most expressive based on the previous figures. The data is presented as a qualitative comparison, with results normalized on a scale from 0 and 5.

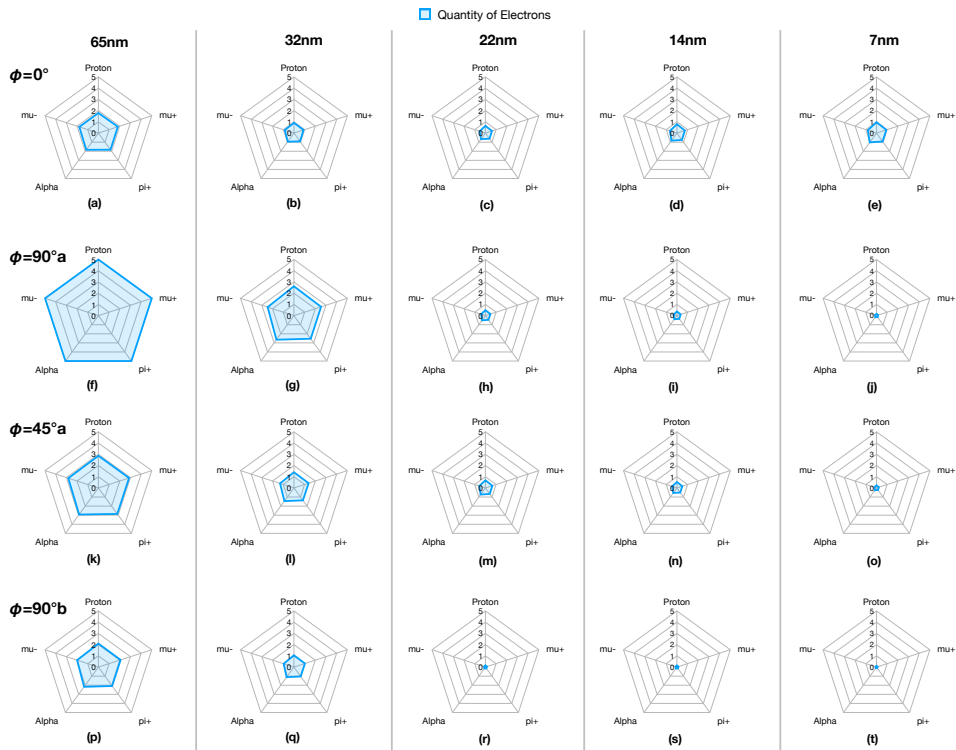


Figure 5.8 – Radar chart showing the number of electrons, comparing different technologies and angles normalized by particles.

In Figure 5.8, we observe that the 65nm technology shows a higher occurrence of electrons for all particles. However, as previously mentioned, this does not necessarily lead to more bitflips, as this effect also depends on the component dimensions. Another interesting observation is that at an incidence angle of $\phi = 0^\circ$, the number of electrons decreases with smaller technology sizes but increases again starting from 14nm. This is due to the dimensions of FinFET technology, where the fin height increases with smaller technology nodes. Details of the fin heights are provided in Tables 4.1, 4.2, 4.3, 4.4, showing

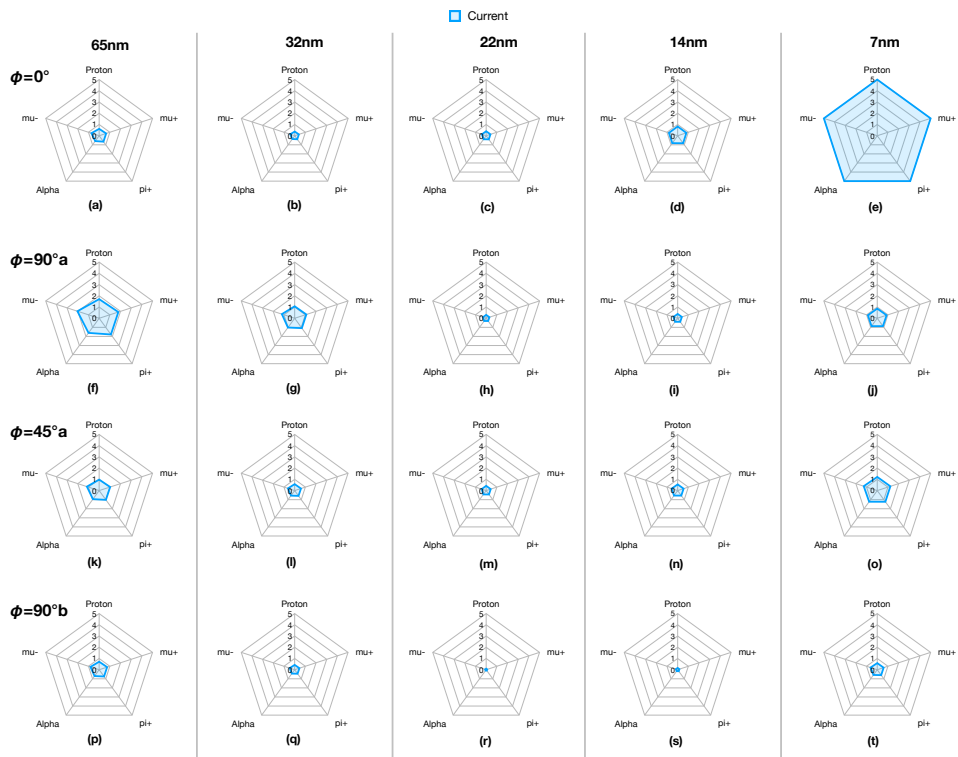


Figure 5.9 – Radar chart showing the current, comparing different technologies and angles normalized by particles.

heights of 93.33nm for 65nm, 48nm for 32nm, 34nm for 22nm, 42nm for 14nm, and 52nm for 7nm.

Figure 5.9 presents a qualitative radar chart comparing current, technology, particle, and angle of incidence. Although the 7nm technology generates fewer electrons due to its smaller size, it produces a higher current than earlier FET technologies. This increased current is attributed to the smaller channel size, as indicated by Equation 4.10, where the current is inversely proportional to the square of the channel size. Additionally, in planar technologies, particles striking at a 90-degree angle and passing through the source and drain produce a higher current.

Both images suggest that, in this qualitative analysis, there is no apparent difference between particles. However, this conclusion may arise from misinterpreting the data, as the graphs are normalized by the number of electrons generated for each particle. A proper analysis of the radar chart should recognize that the behavior appears similar across particles. Nonetheless, as the current figure demonstrates, there are significant differences in current when viewed in absolute terms.

5.6 Final Remarks

In this chapter, we presented simulation results to investigate the potential impacts of cosmic ray interactions with FET devices. As highlighted throughout, lower energies generate more electrons, suggesting that devices might remain unaffected by particles with energies above 5 MeV. We also observed that alpha particles and protons have a higher probability of causing bitflips across all the technologies analyzed. In contrast, positive muons and pions primarily affect FinFET technologies, aligning with findings from the literature, particularly the study by Takashi [100], which inspired this research.

The 32nm technology seems to be the most resilient to cosmic-ray-induced bitflips, being primarily affected by protons at specific incidence angles. In contrast, the 7nm technology demonstrated a concerning vulnerability when particles strike directly above the fin and pass through the gate. This configuration appears susceptible to all charged particles at this particular angle. However, since the affected area is extremely small (around $2.8 \mu m^3$), such events are likely to be rare in this region.

6. CONCLUSION

This dissertation investigated the impact of different cosmic ray particles on various transistor technologies. Simulations conducted with Geant4 were used to examine electron generation and the potential for Single Event Effects in FET technologies.

The simulations revealed some key insights:

- **Particle versus Average Number of Electrons:** Although alpha particles make up only 9% of cosmic rays, they generate a significant number of electrons. Protons, constituting 90% of cosmic rays, also produce a substantial number of electrons and are prominent in experimental studies. Positive pions and muons, while less prolific in generating electrons, are significant due to their presence at lower atmospheric levels and ground levels.
- **Angle of Incidence versus Current:** The current induced by electrons varies with the angle of incidence. Planar technologies are at higher risk for Single Event Upsets when particles pass through the source and drain at an angle of 90° , as shown in Figure 4.5. In contrast, FinFET technologies are more vulnerable when particles strike from above the fin and pass through the gate at 0° , as depicted in Figure 4.5. The simulations highlight the importance of considering angular dependence when evaluating SEE risks and demonstrate that positive pions and muons can induce bitflips in FinFET technologies.
- **Qualitative Comparison between Technologies:** The 65nm planar technology presents a higher occurrence of electrons, attributed to its larger sensitive area. However, despite generating fewer electrons, FinFET technologies are more susceptible to bitflips due to their architecture design and size.

These observations accentuate the complex nature of particle interactions with different technologies. The electron generation by alpha particles near outer space suggests that there is a need for robust protective measures in space electronics. Protons' substantial contribution to SEEs indicates a need for strategies to mitigate their impact, particularly in low Earth orbit applications where they are prevalent.

It is also need to consider the angle of incidence in SEE evaluations, as certain angles can significantly increase the risk of SEEs. The qualitative comparison between planar and FinFET technologies indicates that device geometry and structure play key roles in determining susceptibility to SEEs.

Finally, it is important to note that our work provides a basic approach. This proposal can be extended into a more complex research. We suggest that a natural continuation could include:

- **Extended Particle Studies:** Further research should encompass a wider range of particles, including neutrons and neutral pions, using more detailed physical models and libraries to understand their impacts comprehensively.
- **Advanced Technology Nodes:** Future studies should investigate newer technology nodes beyond 7nm to assess how further miniaturization affects SEE susceptibility and to explore mitigation strategies.

6.1 Publications During the MSc Program

1. A Complementary Survey of Radiation-Induced Soft Error Research: Facilities, Particles, Devices and Trends

PEREIRA, Elisa G.; GARIBOTTI, Rafael; OST, L.; CALAZANS, Ney; MORAES, Fernando Gehm.

Journal of Integrated Circuits and Systems (JICS), vol. 19, n. 2, pp. 1-18, August 2024.

<https://jics.org.br/ojs/index.php/JICS/article/view/846/499>

2. Assessment of Radiation-Induced Soft Error on Unmanned Surface Vehicles

FLECK, Marcos A.; PEREIRA, Elisa G.; GAVA, Jonas F.; SILVA, Henrique B.; MORAES, Fernando Gehm; CALAZANS, Ney L. V.; MENEGUZZI, Felipe; BASTOS, Rodrigo P.; REIS, Ricardo A. L.; OST, Luciano; GARIBOTTI, Rafael.

IEEE Transactions On Nuclear Science, March 2024

<https://ieeexplore.ieee.org/document/10474396>

REFERENCES

- [1] Abbate, C.; Busatto, G.; Mattiazzo, S.; Sanseverino, A.; Silvestrin, L.; Tedesco, D.; Velardi, F. "Progressive drain damage in SiC power MOSFETs exposed to ionizing radiation", *Microelectronics Reliability*, vol. 88-90, 2018, pp. 941–945.
- [2] Adriani, O.; Akaike, e. a. "Direct Measurement of the Cosmic-Ray Helium Spectrum from 40 GeV to 250 TeV with the Calorimetric Electron Telescope on the International Space Station", *Phys. Rev. Lett.*, vol. 130, 2023, pp. 171002.
- [3] Agostinelli, S.; Allison, J.; Amako, K. a.; Apostolakis, J.; Araujo, H.; Arce, P.; Asai, M.; Axen, D.; Banerjee, S.; Barrand, G.; et al.. "GEANT4—a simulation toolkit", *Nuclear instruments and methods in physics research section A: Accelerators, Spectrometers, Detectors and Associated Equipment*, vol. 506–3, 2003, pp. 250–303.
- [4] Akturk, A.; Wilkins, R.; Gunthoti, K.; Wender, S. A.; Goldsman, N. "Energy Dependence of Atmospheric Neutron-Induced Failures in Silicon Carbide Power Devices", *IEEE Transactions on Nuclear Science*, vol. 69–4, 2022, pp. 900–907.
- [5] Al Youssef, A.; Artola, L.; Ducret, S.; Hubert, G.; Buiron, R.; Poivey, C.; Perrier, F.; Parola, S. "Single-Event Transients in Readout Circuitries at Low Temperature Down to 50 K", *IEEE Transactions on Nuclear Science*, vol. 65–1, 2018, pp. 119–125.
- [6] Alberton, S. G.; Aguiar, V.; Medina, N.; Added, N.; Macchione, E.; Menegasso, R.; Cesário, G.; Santos, H.; Scarduelli, V.; Alcántara-Núñez, J.; Guazzelli, M.; Santos, R.; Flechas, D. "Charge deposition analysis of heavy-ion-induced single-event burnout in low-voltage power VDMOSFET", *Microelectronics Reliability*, vol. 137, 2022, pp. 114784.
- [7] Allison, J.; et al.. "Geant4 developments and applications", *IEEE Transactions on Nuclear Science*, vol. 53, 2006, pp. 270–278.
- [8] Allison, J.; et al.. "Recent developments in Geant4", *Nuclear Instruments and Methods in Physics Research Section A: Accelerators, Spectrometers, Detectors and Associated Equipment*, vol. 835, 2016, pp. 186–225.
- [9] Andreou, C. M.; González-Castaño, D. M.; Gerardin, S.; Bagatin, M.; Gómez Rodriguez, F.; Paccagnella, A.; Prokofiev, A. V.; Javanainen, A.; Virtanen, A.; Liberali, V.; Calligaro, C.; Nahmad, D.; Georgiou, J. "Low-Power, Subthreshold Reference Circuits for the Space Environment: Evaluated with γ -rays, X-rays, Protons and Heavy Ions", *Electronics*, vol. 8–5, 2019, pp. 1–24.

- [10] Artola, L.; Hubert, G.; Ducret, S.; Mekki, J.; Al Youssef, A.; Ricard, N. "Impact of D-Flip-Flop Architectures and Designs on Single-Event Upset Induced by Heavy Ions", *IEEE Transactions on Nuclear Science*, vol. 65–8, 2018, pp. 1776–1782.
- [11] Azimi, S.; De Sio, C.; Portaluri, A.; Rizzieri, D.; Sterpone, L. "A comparative radiation analysis of reconfigurable memory technologies: FinFET versus bulk CMOS", *Microelectronics Reliability*, vol. 138, 2022, pp. 114733.
- [12] Bagatin, M.; Gerardin, S.; Paccagnella, A.; Beltrami, S.; Camerlenghi, E.; Bertuccio, M.; Costantino, A.; Zadeh, A.; Ferlet-Cavrois, V.; Santin, G.; Daly, E. "Effects of Heavy-Ion Irradiation on Vertical 3-D NAND Flash Memories", *IEEE Transactions on Nuclear Science*, vol. 65–1, 2018, pp. 318–325.
- [13] Bagatin, M.; Gerardin, S.; Paccagnella, A.; Beltrami, S.; Cazzaniga, C.; Frost, C. D. "Atmospheric Neutron Soft Errors in 3-D NAND Flash Memories", *IEEE Transactions on Nuclear Science*, vol. 66–7, 2019, pp. 1361–1367.
- [14] Bagatin, M.; Gerardin, S.; Paccagnella, A.; Costantino, A.; Ferlet-Cavrois, V.; Pesce, A.; Beltrami, S. "Single Event Effects in 3-D NAND Flash Memory Cells With Replacement Gate Technology", *IEEE Transactions on Nuclear Science*, vol. 70–4, 2023, pp. 308–313.
- [15] Bagatin, M.; Gerardin, S.; Paccagnella, A.; Costantino, A.; Ferlet-Cavrois, V.; Santin, G.; Muschitiello, M.; Pesce, A.; Beltrami, S. "Secondary Particles Generated by Protons in 3-D nand Flash Memories", *IEEE Transactions on Nuclear Science*, vol. 69–7, 2022, pp. 1461–1466.
- [16] Bak, G.; Baeg, S. "Failure Analysis of Galaxy S7 Edge Smartphone Using Neutron Radiation", *IEEE Transactions on Nuclear Science*, vol. 67–11, 2020, pp. 2370–2381.
- [17] Ball, D. R.; Sheets, C. B.; Xu, L.; Cao, J.; Wen, S.-J.; Fung, R.; Cazzaniga, C.; Kauppila, J. S.; Massengill, L. W.; Bhuva, B. L. "Single-Event Latchup in a 7-nm Bulk FinFET Technology", *IEEE Transactions on Nuclear Science*, vol. 68–5, 2021, pp. 830–834.
- [18] Bandeira, V.; Sampford, J.; Garibotti, R.; Trindade, M. G.; Bastos, R. P.; Reis, R.; Ost, L. "Impact of radiation-induced soft error on embedded cryptography algorithms", *Microelectronics Reliability*, vol. 126, 2021, pp. 114349.
- [19] Bazzano, G.; Ampollini, A.; Cardelli, F.; Fortini, F.; Nenzi, P.; Palmerini, G.; Picardi, L.; Piersanti, L.; Ronsivalle, C.; Surrenti, V.; Trinca, E.; Vadrucci, M.; Sabatini, M. "Radiation testing of a commercial 6-axis MEMS inertial navigation unit at ENEA Frascati proton linear accelerator", *Advances in Space Research*, vol. 67–4, 2021, pp. 1379–1391.

- [20] Benevenuti, F.; Gonçalves, M. M.; Pereira, E. C. F.; Vaz, R. G.; Gonçalez, O. L.; Bastos, R. P.; Letiche, M.; Kastensmidt, F. L.; Azambuja, J. R. "Investigating the reliability impacts of neutron-induced soft errors in aerial image classification CNNs implemented in a softcore SRAM-based FPGA GPU", *Microelectronics Reliability*, vol. 138, 2022, pp. 114738.
- [21] Benevenuti, F.; Kastensmidt, F.; Oliveira, A.; Adde, N.; Aguiar, V.; Medina, N.; Guazzelli, M. "Robust Convolutional Neural Networks in SRAM-based FPGAs: a Case Study in Image Classification", *Journal of Integrated Circuits and Systems*, vol. 16–2, 2021.
- [22] Bi, J.; Li, B.; Xi, K.; Luo, L.; Ji, L.; Wang, H.; Liu, M. "Total ionization dose and single event effects of a commercial stand-alone 4 Mb resistive random access memory (ReRAM)", *Microelectronics Reliability*, vol. 100-101, 2019, pp. 1–5.
- [23] Bohman, M.; James, B.; Wirthlin, M. J.; Quinn, H.; Goeders, J. "Microcontroller Compiler-Assisted Software Fault Tolerance", *IEEE Transactions on Nuclear Science*, vol. 66–1, 2019, pp. 223–232.
- [24] Bosser, A. L.; Gupta, V.; Javanainen, A.; Tsiliogiannis, G.; LaLumondiere, S. D.; Brewe, D.; Ferlet-Cavrois, V.; Puchner, H.; Kettunen, H.; Gil, T.; Wrobel, F.; Saigné, F.; Virtanen, A.; Dilillo, L. "Single-Event Effects in the Peripheral Circuitry of a Commercial Ferroelectric Random Access Memory", *IEEE Transactions on Nuclear Science*, vol. 65–8, 2018, pp. 1708–1714.
- [25] Bossini, E.; Minafra, N. "Diamond Detectors for Timing Measurements in High Energy Physics", *Frontiers in Physics*, vol. 8, 2020, pp. 1–14.
- [26] Brewer, R. M.; Moran, S. L.; Cox, J.; Sierawski, B. D.; McCurdy, M. W.; Zhang, E. X.; Iyer, S. S.; Schrimpf, R. D.; Alles, M. L.; Reed, R. A. "The Impact of Proton-Induced Single Events on Image Classification in a Neuromorphic Computing Architecture", *IEEE Transactions on Nuclear Science*, vol. 67–1, 2020, pp. 108–115.
- [27] Budrowiet, J.; Jaksch, M.; Alía, R. G.; Coronetti, A.; Kölpin, A. "Heavy Ion Induced Single Event Effects Characterization on an RF-Agile Transceiver for Flexible Multi-Band Radio Systems in NewSpace Avionics", *Aerospace*, vol. 7–2, 2020.
- [28] Cai, C.; Fan, X.; Liu, J.; Li, D.; Liu, T.; Ke, L.; Zhao, P.; He, Z. "Heavy-Ion Induced Single Event Upsets in Advanced 65 nm Radiation Hardened FPGAs", *Electronics*, vol. 8–3, 2019, pp. 1–13.
- [29] Cai, C.; Gao, S.; Zhao, P.; Yu, J.; Zhao, K.; Xu, L.; Li, D.; He, Z.; Yang, G.; Liu, T.; Liu, J. "SEE Sensitivity Evaluation for Commercial 16 nm SRAM-FPGA", *Electronics*, vol. 8–12, 2019, pp. 1–12.

- [30] Cai, C.; Liu, T.; Zhao, P.; Fan, X.; Huang, H.; Li, D.; Ke, L.; He, Z.; Xu, L.; Chen, G.; Liu, J. "Multiple Layout-Hardening Comparison of SEU-Mitigated Filp-Flops in 22-nm UTBB FD-SOI Technology", *IEEE Transactions on Nuclear Science*, vol. 67–1, 2020, pp. 374–381.
- [31] Cai, C.; Zhao, P.; Xu, L.; Liu, T.; Li, D.; Ke, L.; He, Z.; Liu, J. "SEU tolerance improvement in 22 nm UTBB FDSOI SRAM based on a simple 8T hardened cell", *Microelectronics Reliability*, vol. 100-101, 2019, pp. 1–6.
- [32] Cai, Y.; Wen, L.; Li, Y.; Guo, Q.; Zhou, D.; Feng, J.; Zhang, X.; Liu, B.; Fu, J. "Single-Event Effects in Pinned Photodiode CMOS Image Sensors: SET and SEL", *IEEE Transactions on Nuclear Science*, vol. 67–8, 2020, pp. 1861–1868.
- [33] Cannon, J. M.; Loveless, T. D.; Estrada, R.; Boggs, R.; Lawrence, S. P.; Santos, G.; McCurdy, M. W.; Sternberg, A. L.; Reising, D. R.; Finzell, T.; Cannon, A. "Electrical Measurement of Cell-to-Cell Variation of Critical Charge in SRAM and Sensitivity to Single-Event Upsets by Low-Energy Protons", *IEEE Transactions on Nuclear Science*, vol. 68–5, 2021, pp. 815–822.
- [34] Cannon, M. J.; Keller, A. M.; Rowberry, H. C.; Thurlow, C. A.; Pérez-Celis, A.; Wirthlin, M. J. "Strategies for Removing Common Mode Failures From TMR Designs Deployed on SRAM FPGAs", *IEEE Transactions on Nuclear Science*, vol. 66–1, 2019, pp. 207–215.
- [35] Cannon, M. J.; Keller, A. M.; Thurlow, C. A.; Pérez-Celis, A.; Wirthlin, M. J. "Improving the Reliability of TMR With Nontriplicated I/O on SRAM FPGAs", *IEEE Transactions on Nuclear Science*, vol. 67–1, 2020, pp. 312–320.
- [36] Casey, M. C.; Lauenstein, J.-M.; Weachock, R. J.; Wilcox, E. P.; Hua, L. M.; Campola, M. J.; Topper, A. D.; Ladbury, R. L.; LaBel, K. A. "Failure Analysis of Heavy Ion-Irradiated Schottky Diodes", *IEEE Transactions on Nuclear Science*, vol. 65–1, 2018, pp. 269–279.
- [37] Casey, M. C.; Stansberry, S. D.; Seidleck, C. M.; Maharrey, J. A.; Gamboa, D.; Pellish, J. A.; Label, K. A. "Single-Event Response of 22-nm Fully Depleted Silicon-on-Insulator Static Random Access Memory", *IEEE Transactions on Nuclear Science*, vol. 68–4, 2021, pp. 402–409.
- [38] Cazzaniga, C.; Alía, R. G.; Coronetti, A.; Bilko, K.; Morilla, Y.; Martin-Holgado, P.; Kastriotou, M.; Frost, C. D. "Measurements of Low-Energy Protons Using a Silicon Detector for Application to SEE Testing", *IEEE Transactions on Nuclear Science*, vol. 69–3, 2022, pp. 485–490.

- [39] Cecchetto, M.; García Alía, R.; Gerardin, S.; Brugger, M.; Infantino, A.; Danzeca, S. “Impact of Thermal and Intermediate Energy Neutrons on SRAM SEE Rates in the LHC Accelerator”, *IEEE Transactions on Nuclear Science*, vol. 65–8, 2018, pp. 1800–1806.
- [40] Chandrashekhar, S.; Puchner, H.; Mitani, J.; Shinozaki, S.; Sardi, M.; Hoffman, D. “Radiation induced soft errors in 16 nm floating gate SLC NAND flash memory”, *Microelectronics Reliability*, vol. 108, 2020, pp. 113631.
- [41] Chen, D.; Wilcox, E.; Ladbury, R. L.; Seidleck, C.; Kim, H.; Phan, A.; LaBel, K. A. “Heavy Ion and Proton-Induced Single Event Upset Characteristics of a 3-D NAND Flash Memory”, *IEEE Transactions on Nuclear Science*, vol. 65–1, 2018, pp. 19–26.
- [42] Chen, J.; Chi, Y.; Liang, B.; Yuan, H.; Wen, Y.; Xing, H.; Yao, X. “ASET and TID Characterization of a Radiation Hardened Bandgap Voltage Reference in a 28-nm Bulk CMOS Technology”, *IEEE Transactions on Nuclear Science*, vol. 69–5, 2022, pp. 1141–1147.
- [43] Chen, J.; Yu, J.; Yu, P.; Liang, B.; Chi, Y. “Characterization of the Effect of Pulse Quenching on Single-Event Transients in 65-nm Twin-Well and Triple-Well CMOS Technologies”, *IEEE Transactions on Device and Materials Reliability*, vol. 18–1, 2018, pp. 12–17.
- [44] Chen, R. M.; Mahatme, N. N.; Diggins, Z. J.; Wang, L.; Zhang, E. X.; Chen, Y. P.; Liu, Y. N.; Narasimham, B.; Witulski, A. F.; Bhuvan, B. L.; Fleetwood, D. M. “Analysis of Temporal Masking Effects on Master- and Slave-Type Flip-Flop SEUs and Related Applications”, *IEEE Transactions on Nuclear Science*, vol. 65–8, 2018, pp. 1823–1829.
- [45] Chen, Z.; Ding, D.; Dong, Y.; Shan, Y.; Zeng, Y.; Gao, J. “Design of a High-Performance Low-Cost Radiation-Hardened Phase-Locked Loop for Space Application”, *IEEE Transactions on Aerospace and Electronic Systems*, vol. 56–5, 2020, pp. 3588–3598.
- [46] Chi, Y.; Cai, C.; He, Z.; Wu, Z.; Fang, Y.; Chen, J.; Liang, B. “SEU Tolerance Efficiency of Multiple Layout-Hardened 28 nm DICE D Flip-Flops”, *Electronics*, vol. 11–7, 2022, pp. 1–11.
- [47] Cho, M.-K.; Song, I.; Pavlidis, S.; Fleetwood, Z. E.; Buchner, S. P.; McMorrow, D.; Paki, P.; Cressler, J. D. “An Electrostatic Discharge Protection Circuit Technique for the Mitigation of Single-Event Transients in SiGe BiCMOS Technology”, *IEEE Transactions on Nuclear Science*, vol. 65–1, 2018, pp. 426–431.

- [48] Cho, M.-K.; Song, I.; Zachary, F. E.; Khachatrian, A.; Warner, J. H.; Buchner, S. P.; McMorrow, D.; Paki, P.; Cressler, J. D. "Best Practices for Using Electrostatic Discharge Protection Techniques for Single-Event Transient Mitigation", *IEEE Transactions on Nuclear Science*, vol. 66–1, 2019, pp. 240–247.
- [49] Ciarpi, G.; Magazzù, G.; Palla, F.; Saponara, S. "Design, Implementation, and Experimental Verification of 5 Gbps, 800 Mrad TID and SEU-Tolerant Optical Modulators Drivers", *IEEE Transactions on Circuits and Systems I: Regular Papers*, vol. 67–3, 2020, pp. 829–838.
- [50] Clemente, J. A.; Hubert, G.; Fraire, J.; Franco, F. J.; Villa, F.; Rey, S.; Baylac, M.; Puchner, H.; Mecha, H.; Velazco, R. "SEU Characterization of Three Successive Generations of COTS SRAMs at Ultralow Bias Voltage to 14.2-MeV Neutrons", *IEEE Transactions on Nuclear Science*, vol. 65–8, 2018, pp. 1858–1865.
- [51] Clemente, J. A.; Rezaei, M.; Franco, F. J. "Reliability of Error Correction Codes Against Multiple Events by Accumulation", *IEEE Transactions on Nuclear Science*, vol. 69–2, 2022, pp. 169–180.
- [52] Coi, O.; Pendina, G. D.; Sousa, R.; Adrianjohany, N.; Dangla, D.; Ecoffet, R.; Torres, L. "Heavy-Ion Irradiation Effects on Advanced Perpendicular Anisotropy Spin-Transfer Torque Magnetic Tunnel Junction", *IEEE Transactions on Nuclear Science*, vol. 68–5, 2021, pp. 588–596.
- [53] Collaboration, G. "Geant4 Toolkit". Source: <https://geant4.web.cern.ch/>, January 2024.
- [54] Conway, P. M.; Gadlage, M. J.; Ingalls, J. D.; Williams, A. M.; Bruce, D. I.; Bossev, D. P. "Impact of the Elemental Makeup of an IC in Generating Single-Event Upsets From Low-Energy (<10 MeV) Neutrons: A 3-D nand Flash Case Study", *IEEE Transactions on Nuclear Science*, vol. 66–1, 2019, pp. 466–473.
- [55] Coronetti, A.; Alía, R. G.; Cecchetto, M.; Hajdas, W.; Söderström, D.; Javanainen, A.; Saigné, F. "The Pion Single-Event Effect Resonance and its Impact in an Accelerator Environment", *IEEE Transactions on Nuclear Science*, vol. 67–7, 2020, pp. 1606–1613.
- [56] Crane, B. "China's Drive for Leadership in Global Research and Development". Source: <https://www.csis.org/analysis/chinas-drive-leadership-global-research-and-development>, 2023-11-25.
- [57] Da Costa Lopes, I.; Pouget, V.; Wrobel, F.; Touboul, A.; Saigne, F.; Roed, K. "Bridging RHA Methodology From Component to System Level Applied to System-on-Modules", *IEEE Transactions on Nuclear Science*, vol. 69–7, 2022, pp. 1747–1756.

- [58] Darvishi, M.; Audet, Y.; Blaquier, Y.; Thibeault, C.; Pichette, S. "On the Susceptibility of SRAM-Based FPGA Routing Network to Delay Changes Induced by Ionizing Radiation", *IEEE Transactions on Nuclear Science*, vol. 66–3, 2019, pp. 643–654.
- [59] Database, M. M. P. "Silicon: Electrical Properties". Source: http://www.matprop.ru/Si_electric, 2024-07-06.
- [60] de Bibikoff, A.; Lamberbourg, P. "Method for System-Level Testing of COTS Electronic Board Under High-Energy Heavy Ions", *IEEE Transactions on Nuclear Science*, vol. 67–10, 2020, pp. 2179–2187.
- [61] Dekkers, S.; Nakazawa, Y.; Fujii, Y.; Yoshida, H.; Wong, T. S.; Ueno, K.; Nash, J. "Radiation Tolerance of Online Trigger System for COMET Phase-I", *IEEE Transactions on Nuclear Science*, vol. 68–8, 2021, pp. 2020–2027.
- [62] Deng, Y.; Watanabe, Y. "A Method of Predicting Muon-Induced SEUs Using Proton Tests and Monte Carlo Simulation", *IEEE Transactions on Nuclear Science*, vol. 70–8, 2023, pp. 1775–1782.
- [63] Derós, M. A. d. O. "Estudo das Propriedades de Diamantes Policristalinos para Uso em Detectores de Partículas de Alta Energia", Master's Thesis, Universidade Federal do Rio Grande do Sul. Instituto de Física. Programa de Pós-Graduação em Física, 2024, 99p.p.
- [64] Doornbos, G.; James, R.; Lander, P. "Fin field effect transistor (FinFET)". Patent US 2015/0200302 A1, Source: <https://patents.google.com/patent/US20150200302A1/en>, 2024-07-29.
- [65] Du, B.; Sterpone, L.; Azimi, S.; Merodio Codinachs, D.; Ferlet-Cavrois, V.; Boatella Polo, C.; Alía, R. G.; Kastriotou, M.; Fernandez-Martínez, P. "Ultrahigh Energy Heavy Ion Test Beam on Xilinx Kintex-7 SRAM-Based FPGA", *IEEE Transactions on Nuclear Science*, vol. 66–7, 2019, pp. 1813–1819.
- [66] Elash, C. J.; Li, Z.; Jin, C.; Chen, L.; Xing, J.; Yang, Z.; Shi, S. "Efficacy of Transistor Interleaving in DICE Flip-Flops at a 22 nm FD SOI Technology Node", *Applied Sciences*, vol. 12–9, 2022, pp. 1–10.
- [67] et al, F. B. "Cosmic rays with portable Geiger counters: from sea level to airplane cruise altitudes". Source: <https://iopscience.iop.org/article/10.1088/0143-0807/30/4/003/pdf>, 2024-05-01.
- [68] Fabero, J. C.; Mecha, H.; Franco, F. J.; Clemente, J. A.; Korkian, G.; Rey, S.; Cheymol, B.; Baylac, M.; Hubert, G.; Velazco, R. "Single Event Upsets Under 14-MeV Neutrons in a 28-nm SRAM-Based FPGA in Static Mode", *IEEE Transactions on Nuclear Science*, vol. 67–7, 2020, pp. 1461–1469.

- [69] Fan, H.; Li, D.; Zhang, K.; Cen, Y.; Feng, Q.; Qiao, F.; Heidari, H. "A 4-Channel 12-Bit High-Voltage Radiation-Hardened Digital-to-Analog Converter for Low Orbit Satellite Applications", *IEEE Transactions on Circuits and Systems I: Regular Papers*, vol. 65–11, 2018, pp. 3698–3706.
- [70] Fernández-Martínez; Pablo; Alía; García, R.; Cecchetto; Matteo; Kastriotou; Maria; Kerboub; Nourdine; Tali; Maris; Wyrwoll; Vanessa; Brugger; Markus; Cangialosi; Chiara; Cerutti; Francesco; Danzeca; Salvatore; Delrieux; Marc; Froeschl; Robert; Gatignon; Lau; Gilardoni; Simone; Lendaro; Jerome; Mateu; Isidre; Ravotti; Federico; Wilkens; Henric; Gaillard; Remi. "SEE Tests With Ultra Energetic Xe Ion Beam in the CHARM Facility at CERN", *IEEE Transactions on Nuclear Science*, vol. 66–7, 2019, pp. 1523–1531.
- [71] Findelsen, C.; Herr, E.; Schenkel, M.; Schlegel, R.; Zeller, H. "Extrapolation of cosmic ray induced failures from test to field conditions for IGBT modules", *Microelectronics Reliability*, vol. 38–6, 1998, pp. 1335–1339.
- [72] Gadlage, M. J.; Roach, A. H.; Duncan, A. R.; Williams, A. M.; Bossev, D. P.; Kay, M. J. "Multiple-Cell Upsets Induced by Single High-Energy Electrons", *IEEE Transactions on Nuclear Science*, vol. 65–1, 2018, pp. 211–216.
- [73] Gaisser, T. K.; Engel, R.; Resconi, E. "Cosmic Rays and Particle Physics". Cambridge University Press, 2016, 444p.p.
- [74] Gao, J.; Zhang, Q.; Xi, K.; Li, B.; Li, B.; Wang, C.; Lu, P.; Wang, K.; Zhang, G.; Zhao, F.; Li, J.; Hao, L.; Wang, L.; Luo, J.; Han, Z.; Liu, J.; Guo, G. "Impacts of carbon ions on SEU in SOI SRAM", *Microelectronics Reliability*, vol. 126, 2021, pp. 114341.
- [75] Gasiot, G.; Giot, D.; Roche, P. "Multiple Cell Upsets as the Key Contribution to the Total SER of 65 nm CMOS SRAMs and Its Dependence on Well Engineering", *IEEE Transactions on Nuclear Science*, vol. 54–6, 2007, pp. 2468–2473.
- [76] Gava, J.; Moura, N.; Lucena, J.; Rocha, V. d.; Garibotti, R.; Calazans, N.; Cuenca-Asensi, S.; Bastos, R. P.; Reis, R.; Ost, L. "Assessment of Radiation-Induced Soft Errors on Lightweight Cryptography Algorithms Running on a Resource-Constrained Device", *IEEE Transactions on Nuclear Science*, vol. 70–8, 2023, pp. 1805–1813.
- [77] Geant4. "Reference Physics Lists". Source: https://geant4-userdoc.web.cern.ch/UsersGuides/PhysicsListGuide/html/reference_PL/FTFP_BERT.html, July 4, 2023.
- [78] Giordano, R.; Barbieri, D.; Perrella, S.; Catalano, R.; Milluzzo, G. "Configuration Self-Repair in Xilinx FPGAs", *IEEE Transactions on Nuclear Science*, vol. 65–10, 2018, pp. 2691–2698.

- [79] Giordano, R.; Lai, Y.; Korpar, S.; Pestotnik, R.; Lozar, A.; Šantelj, L.; Shoji, M.; Nishida, S. “Frame-Level Intermodular Configuration Scrubbing of On-Detector FPGAs for the ARICH at Belle II”, *IEEE Transactions on Nuclear Science*, vol. 68–12, 2021, pp. 2810–2817.
- [80] Giordano, R.; Perrella, S.; Barbieri, D.; Izzo, V. “A Radiation-Tolerant, Multigigabit Serial Link Based on FPGAs”, *IEEE Transactions on Nuclear Science*, vol. 67–8, 2020, pp. 1852–1860.
- [81] Gonzalez, C. J.; Machado, D. N.; Vaz, R. G.; Bôas, A. C. V.; Gonçalez, O. L.; Puchner, H.; Added, N.; Macchione, E. L. A.; Aguiar, V. A. P.; Kastensmidt, F. L.; Medina, N. H.; Guazzelli, M. A.; Balen, T. R. “Testing a Fault Tolerant Mixed-Signal Design Under TID and Heavy Ions”, *Journal of Integrated Circuits and Systems*, vol. 16–3, 2021.
- [82] González, C. J.; Added, N.; Macchione, E. L. A.; Aguiar, V. A. P.; Kastensmidt, F. G. L.; Puchner, H. K.; Guazzelli, M. A.; Medina, N. H.; Balen, T. R. “Reducing Soft Error Rate of SoCs Analog-to-Digital Interfaces With Design Diversity Redundancy”, *IEEE Transactions on Nuclear Science*, vol. 67–3, 2020, pp. 518–524.
- [83] Griffiths, D. J. “Introduction to Electrodynamics”. Cambridge University Press, 2017, 618p.p.
- [84] Hales, J. M.; Ildefonso, A.; Buchner, S. P.; Khachatrian, A.; Allen, G.; McMorrow, D. “Quantitative Prediction of Ion-Induced Single-Event Transients in an Operational Amplifier Using a Quasi-Bessel Beam Pulsed-Laser Approach”, *IEEE Transactions on Nuclear Science*, vol. 70–4, 2023, pp. 354–362.
- [85] Hales, J. M.; Khachatrian, A.; Ildefonso, A.; Buchner, S.; Adams, D.; Wheeler, D.; Messenger, S.; Mishler, C.; Budzinski, N.; Jordan, S.; Van Art, R.; McMorrow, D. “Pulsed-Laser Testing to Quantitatively Evaluate Latchup Sensitivity in Mixed-Signal ASICs”, *IEEE Transactions on Nuclear Science*, vol. 69–3, 2022, pp. 429–435.
- [86] Hao, J.-B.; Liu, Y.; Wang, Z. “Research of transient radiation effects on FinFET SRAMs compared with planar SRAMs”. In: International Conference on Solid-State and Integrated Circuit Technology (ICSICT), 2016, pp. 1005–1007.
- [87] Haran, A.; Yitzhak, N. M.; Mazal-Tov, E.; Keren, E.; David, D.; Refaeli, N.; Preziosi, E.; Senesi, R.; Cazzaniga, C.; Frost, C. D.; Hadas, T.; Zangi, U.; Andreani, C. “Ultralow Power System-on-Chip SRAM Characterization by Alpha and Neutron Irradiation”, *IEEE Transactions on Nuclear Science*, vol. 68–11, 2021, pp. 2598–2608.
- [88] Harrington, R. C.; Maharrey, J. A.; Kauppila, J. S.; Nsengiyumva, P.; Ball, D. R.; Haeffner, T. D.; Zhang, E. X.; Bhuva, B. L.; Massengill, L. W. “Effect of Transistor

Variants on Single-Event Transients at the 14-/16-nm Bulk FinFET Technology Generation”, *IEEE Transactions on Nuclear Science*, vol. 65–8, 2018, pp. 1807–1813.

- [89] Hengzhou, Y.; Hao, S.; Bin, L.; Jianjun, C.; Yaqing, C.; Weixia, X.; Yang, G. “A SET-Tolerant High-Frequency Multibiased Multiphase Voltage-Controlled Oscillator for Phase Interpolator-Based Clock and Data Recovery”, *IEEE Transactions on Nuclear Science*, vol. 69–7, 2022, pp. 1725–1732.
- [90] Huang, P.; Yue, D.; Chi, Y.; Sun, Q.; Liang, B. “Characterization of charge sharing induced by high LET heavy ions using inverter chains in a commercial bulk FinFET process”, *Semiconductor Science and Technology*, vol. 37–8, 2022, pp. 1–7.
- [91] Hubert, G.; Artola, L.; Regis, D. “Impact of scaling on the soft error sensitivity of bulk, FDSOI and FinFET technologies due to atmospheric radiation”, *Integration*, vol. 50, 2015, pp. 39–47.
- [92] Ildefonso, A.; Fleetwood, Z. E.; Tzintzarov, G. N.; Hales, J. M.; Nergui, D.; Frounchi, M.; Khachatrian, A.; Buchner, S. P.; Mcmorrow, D.; Warner, J. H.; Harms, J.; Erickson, A.; Voss, K.; Ferlet-Cavrois, V.; Cressler, J. D. “Optimizing Optical Parameters to Facilitate Correlation of Laser- and Heavy-Ion-Induced Single-Event Transients in SiGe HBTs”, *IEEE Transactions on Nuclear Science*, vol. 66–1, 2019, pp. 359–367.
- [93] Indriolo, N.; Fields, B. D.; McCall, B. J. “The Implications of a High Cosmic-ray Ionization Rate in Diffuse Interstelar Clouds”, *The Astrophysical Journal*, vol. 694–1, 2009, pp. 257.
- [94] Irom, F.; Edmonds, L. D.; Allen, G. R.; Kim, W.; Vartanian, S. “Electron Irradiation of Samsung 8-Gb NAND Flash Memory”, *IEEE Transactions on Nuclear Science*, vol. 65–1, 2018, pp. 27–33.
- [95] Iwashita, H.; Funatsu, G.; Sato, H.; Kamiyama, T.; Furusaka, M.; Wender, S. A.; Pitcher, E.; Kiyanagi, Y. “Energy-Resolved Soft-Error Rate Measurements for 1–800 MeV Neutrons by the Time-of-Flight Technique at LANSCE”, *IEEE Transactions on Nuclear Science*, vol. 67–11, 2020, pp. 2363–2369.
- [96] Jagtap, S.; Anmadwar, S.; Rudrapati, S.; Gupta, S. “A Single-Event Transient-Tolerant High-Frequency CMOS Quadrature Phase Oscillator”, *IEEE Transactions on Nuclear Science*, vol. 66–9, 2019, pp. 2072–2079.
- [97] Jena, D. “Quantum Physics of Semiconductor Materials and Devices”. Oxford University Press, 2022, 896p.p.
- [98] Kanno, Y.; Toba, T.; Shimamura, K.; Kanekawa, N. “Design Method for Online Totally Self-Checking Comparators Implementable on FPGAs”, *IEEE Transactions on Very Large Scale Integration (VLSI) Systems*, vol. 28–3, 2020, pp. 726–735.

- [99] Kato, T.; Hashimoto, M.; Matsuyama, H. "Angular Sensitivity of Neutron-Induced Single-Event Upsets in 12-nm FinFET SRAMs With Comparison to 20-nm Planar SRAMs", *IEEE Transactions on Nuclear Science*, vol. 67–7, 2020, pp. 1485–1493.
- [100] Kato, T.; Tampo, M.; Takeshita, S.; Tanaka, H.; Matsuyama, H.; Hashimoto, M.; Miyake, Y. "Muon-Induced Single-Event Upsets in 20-nm SRAMs: Comparative Characterization With Neutrons and Alpha Particles", *IEEE Transactions on Nuclear Science*, vol. 68–7, 2021, pp. 1436–1444.
- [101] Kato, T.; Yamazaki, T.; Saito, N.; Matsuyama, H. "Neutron-Induced Multiple-Cell Upsets in 20-nm Bulk SRAM: Angular Sensitivity and Impact of Multiwell Potential Perturbation", *IEEE Transactions on Nuclear Science*, vol. 66–7, 2019, pp. 1381–1389.
- [102] Kauppila, J. S.; Maharrey, J. A.; Harrington, R. C.; Haeffner, T. D.; Nsengiyumva, P.; Ball, D. R.; Sternberg, A. L.; Zhang, E. X.; Bhuvan, B. L.; Massengill, L. W. "Exploiting Parallelism and Heterogeneity in a Radiation Effects Test Vehicle for Efficient Single-Event Characterization of Nanoscale Circuits", *IEEE Transactions on Nuclear Science*, vol. 65–1, 2018, pp. 486–494.
- [103] Keller, A. M.; Whiting, T. A.; Sawyer, K. B.; Wirthlin, M. J. "Dynamic SEU Sensitivity of Designs on Two 28-nm SRAM-Based FPGA Architectures", *IEEE Transactions on Nuclear Science*, vol. 65–1, 2018, pp. 280–287.
- [104] Keller, A. M.; Wirthlin, M. J. "Partial TMR for Improving the Soft Error Reliability of SRAM-Based FPGA Designs", *IEEE Transactions on Nuclear Science*, vol. 68–5, 2021, pp. 1023–1031.
- [105] Kerboub, N.; Alia, R. G.; Mekki, J.; Bezerra, F.; Monteuijs, A.; Fernández-Martínez, P.; Danzeca, S.; Brugger, M.; Standarovski, D.; Rauch, J. "Comparison Between In-flight SEL Measurement and Ground Estimation Using Different Facilities", *IEEE Transactions on Nuclear Science*, vol. 66–7, 2019, pp. 1541–1547.
- [106] Keren, E.; Greenberg, S.; Yitzhak, N. M.; David, D.; Refaeli, N.; Haran, A. "Characterization and Mitigation of Single-Event Transients in Xilinx 45-nm SRAM-Based FPGA", *IEEE Transactions on Nuclear Science*, vol. 66–6, 2019, pp. 946–954.
- [107] Khachatrian, A.; Buchner, S.; Koehler, A.; Affouda, C.; McMorrow, D.; LaLumondiere, S. D.; Dillingham, E. C.; Bonsall, J. P.; Scofield, A. C.; Brewe, D. L. "The Effect of the Gate-Connected Field Plate on Single-Event Transients in AlGaN/GaN Schottky-Gate HEMTs", *IEEE Transactions on Nuclear Science*, vol. 66–7, 2019, pp. 1682–1687.
- [108] Khachatrian, A.; Roche, N. J.-H.; Buchner, S. P.; Koehler, A. D.; Anderson, T. J.; McMorrow, D.; Lalumondiere, S. D.; Bonsall, J. P.; Dillingham, E. C.; Brewe, D. L.

“Investigation of Single-Event Transients in AlGaN/GaN MIS-Gate HEMTs Using a Focused X-Ray Beam”, *IEEE Transactions on Nuclear Science*, vol. 66–1, 2019, pp. 368–375.

- [109] Khachatrian, A.; Roche, N. J.-H.; Ruppalt, L. B.; Champlain, J. G.; Buchner, S.; Koehler, A. D.; Anderson, T. J.; Hobart, K. D.; Warner, J. H.; Mcmorrow, D. “Correlation of the Spatial Variation of Single-Event Transient Sensitivity With Thermoreflectance Thermography in $Al_x Ga_{1-x}$ N/GaN HEMTs”, *IEEE Transactions on Nuclear Science*, vol. 65–1, 2018, pp. 369–375.
- [110] Kireeff Covo, M.; Albright, R.; Ninemire, B.; Johnson, M.; Hodgkinson, A.; Loew, T.; Benitez, J.; Todd, D.; Xie, D.; Perry, T.; Phair, L.; Bernstein, L.; Bevins, J.; Brown, J.; Goldblum, B.; Harasty, M.; Harrig, K.; Laplace, T.; Matthews, E.; Bushmaker, A.; Walker, D.; Oklejas, V.; Hopkins, A.; Bleuel, D.; Chen, J.; Cronin, S. “The 88-Inch Cyclotron: A one-stop facility for electronics radiation and detector testing”, *Measurement*, vol. 127, 2018, pp. 580–587.
- [111] Kobayashi, D. “Scaling Trends of Digital Single-Event Effects: A Survey of SEU and SET Parameters and Comparison With Transistor Performance”, *IEEE Transactions on Nuclear Science*, vol. 68–2, 2021, pp. 124–148.
- [112] Kobayashi, D.; Hirose, K.; Ito, T.; Kakehashi, Y.; Kawasaki, O.; Makino, T.; Ohshima, T.; Matsuura, D.; Narita, T.; Kato, M.; Ishii, S.; Masukawa, K. “Heavy-Ion Soft Errors in Back-Biased Thin-BOX SOI SRAMs: Hundredfold Sensitivity Due to Line-Type Multicell Upsets”, *IEEE Transactions on Nuclear Science*, vol. 65–1, 2018, pp. 523–532.
- [113] Korkian, G.; Fabero, J. C.; Hubert, G.; Rezaei, M.; Mecha, H.; Franco, F. J.; Puchner, H.; Clemente, J. A. “Experimental and Analytical Study of the Responses of Nanoscale Devices to Neutrons Impinging at Various Incident Angles”, *IEEE Transactions on Nuclear Science*, vol. 67–11, 2020, pp. 2345–2352.
- [114] Kortland, K. “Air Showers”. 2024-07-29, Source: https://docs.hisparc.nl/routenet/en/Air_Showers.pdf, 2023-10-30.
- [115] Kraemer Sarzi Sartori, T.; Fourati, H.; Letiche, M.; Bastos, R. P. “Assessment of Radiation Effects on Attitude Estimation Processing for Autonomous Things”, *IEEE Transactions on Nuclear Science*, vol. 69–7, 2022, pp. 1610–1617.
- [116] Leitner, D.; McMahan, M. A.; Argento, D.; Gimpel, T.; Guy, A.; Morel, J.; Siero, C.; Thatcher, R.; Lyneis, C. M. “Heavy Ion Cocktail Beams at the 88 Inch Cyclotron”, Technical Report, Lawrence Berkeley National Laboratory, 2002, 4p.p.

- [117] Li, M.; Fan, Y.; Jia, X.; Cui, H.; Liang, Z.; Zhao, M.; Yang, T.; Wu, K.; Li, S.; Yu, C.; Liu, B.; Wang, W.; Yang, X.; Tan, Y.; Shi, X.; da Costa, J. G.; Heng, Y.; Xu, G.; Zhai, Q.; Yan, G.; Ding, M.; Luo, J.; Yin, H.; Li, J.; Howard, A.; Kramberger, G. "Effects of Shallow Carbon and Deep N++ Layer on the Radiation Hardness of IHEP-IME LGAD Sensors", *IEEE Transactions on Nuclear Science*, vol. 69–5, 2022, pp. 1098–1103.
- [118] Li, Z.; Berti, L.; Wouters, J.; Wang, J.; Leroux, P. "Characterization of the Total Charge and Time Duration for Single-Event Transient Voltage Pulses in a 65-nm CMOS Technology", *IEEE Transactions on Nuclear Science*, vol. 69–7, 2022, pp. 1593–1601.
- [119] Liang, C.; Ma, R.; Li, K.; Su, Y.; Gong, H.; Ryder, K. L.; Wang, P.; Sternberg, A. L.; Zhang, E. X.; Alles, M. L.; Reed, R. A.; Koester, S. J.; Fleetwood, D. M.; Schrimpf, R. D. "Laser-Induced Single-Event Transients in Black Phosphorus MOSFETs", *IEEE Transactions on Nuclear Science*, vol. 66–1, 2019, pp. 384–388.
- [120] Liao, W.; Hashimoto, M.; Manabe, S.; Watanabe, Y.; Abe, S.-I.; Nakano, K.; Sato, H.; Kin, T.; Hamada, K.; Tampo, M.; Miyake, Y. "Measurement and Mechanism Investigation of Negative and Positive Muon-Induced Upsets in 65-nm Bulk SRAMs", *IEEE Transactions on Nuclear Science*, vol. 65–8, 2018, pp. 1734–1741.
- [121] Liao, W.; Hashimoto, M.; Manabe, S.; Watanabe, Y.; Abe, S.-I.; Nakano, K.; Takeshita, H.; Tampo, M.; Takeshita, S.; Miyake, Y. "Negative and Positive Muon-Induced SEU Cross Sections in 28-nm and 65-nm Planar Bulk CMOS SRAMs". In: Reliability Physics Symposium (IRPS), 2019, pp. 1–5.
- [122] Liao, W.; Hashimoto, M.; Manabe, S.; Watanabe, Y.; Abe, S.-i.; Tampo, M.; Takeshita, S.; Miyake, Y. "Impact of the Angle of Incidence on Negative Muon-Induced SEU Cross Sections of 65-nm Bulk and FDSOI SRAMs", *IEEE Transactions on Nuclear Science*, vol. 67–7, 2020, pp. 1566–1572.
- [123] Liao, W.; Ito, K.; Abe, S.-i.; Mitsuyama, Y.; Hashimoto, M. "Characterizing Energetic Dependence of Low-Energy Neutron-Induced SEU and MCU and Its Influence on Estimation of Terrestrial SER in 65-nm Bulk SRAM", *IEEE Transactions on Nuclear Science*, vol. 68–6, 2021, pp. 1228–1234.
- [124] Liu, T.; Liu, J.; Xi, K.; Zhang, Z.; He, D.; Ye, B.; Yin, Y.; Ji, Q.; Wang, B.; Luo, J.; Sun, Y.; Zhai, P. "Heavy Ion Radiation Effects on a 130-nm COTS NVSRAM Under Different Measurement Conditions", *IEEE Transactions on Nuclear Science*, vol. 65–5, 2018, pp. 1119–1126.
- [125] Long Cai, Y.; Guo, Q.; Wen, L.; Zhou, D.; Feng, J.; Kai Liu, B.; Fu, J.; Li, Y. D. "Single Event Effects in 0.18 μm Pinned Photodiode CMOS Image Sensors: SEU and SEFI", *Microelectronics Reliability*, vol. 117, 2021, pp. 114038.

- [126] Longofono, S.; Kline, D.; Melhem, R.; Jones, A. K. "Predicting and mitigating single-event upsets in DRAM using HOTH", *Microelectronics Reliability*, vol. 117, 2021, pp. 114024.
- [127] Lu, B.; Li, B.; Huo, J.; Chen, Y.; Zhao, W.; Gao, J.; Wang, C.; Liu, H.; Luo, J.; Zhou, Y. "Design and Characterizations of the Radiation-Hardened XCR4C ASIC for X-Ray CCDs for Space Astronomical Applications", *IEEE Transactions on Nuclear Science*, vol. 67–6, 2020, pp. 1175–1184.
- [128] Luo, Y.; Zhang, F.; Chen, W.; Ding, L.; Wang, T. "The Influence of Ion Track Characteristics on Single-Event Upsets and Multiple-Cell Upsets in Nanometer SRAM", *IEEE Transactions on Nuclear Science*, vol. 68–5, 2021, pp. 1111–1119.
- [129] Luo, Y.; Zhang, F.; Pan, X.; Guo, H.; Wang, Y. "Impact of Total Ionizing Dose on Low Energy Proton Single Event Upsets in Nanometer SRAM", *IEEE Transactions on Nuclear Science*, vol. 66–7, 2019, pp. 1848–1853.
- [130] Luo, Y.; Zhang, F.; Wei, C.; Ding, L.; Pan, X. "The orientational dependence of single event upsets and multiple-cell upsets in 65 nm dual DICE SRAM", *Microelectronics Reliability*, vol. 94, 2019, pp. 24–31.
- [131] Luza, L. M.; Ruospo, A.; Söderström, D.; Cazzaniga, C.; Kastriotou, M.; Sanchez, E.; Bosio, A.; Dilillo, L. "Emulating the Effects of Radiation-Induced Soft-Errors for the Reliability Assessment of Neural Networks", *IEEE Transactions on Emerging Topics in Computing*, vol. 10–4, 2022, pp. 1867–1882.
- [132] Lyu, H.; Zhang, H.; Mei, B.; Yu, Q.; Mo, R.; Sun, Y.; Gao, W. "Research on single event effect test of a RRAM memory and space flight demonstration", *Microelectronics Reliability*, vol. 126, 2021, pp. 114347.
- [133] Mahara, T.; Manabe, S.; Watanabe, Y.; Liao, W.; Hashimoto, M.; Saito, T. Y.; Niikura, M.; Ninomiya, K.; Tomono, D.; Sato, A. "Irradiation Test of 65-nm Bulk SRAMs With DC Muon Beam at RCNP-MuSIC Facility", *IEEE Transactions on Nuclear Science*, vol. 67–7, 2020, pp. 1555–1559.
- [134] Maharrey, J. A.; Kauppila, J. S.; Harrington, R. C.; Nsengiyumva, P.; Ball, D. R.; Haeffner, T. D.; Zhang, E. X.; Bhuva, B. L.; Holman, W. T.; Massengill, L. W. "Impact of Single-Event Transient Duration and Electrical Delay at Reduced Supply Voltages on SET Mitigation Techniques", *IEEE Transactions on Nuclear Science*, vol. 65–1, 2018, pp. 362–368.
- [135] Maillard, P.; Chen, Y. P.; Vidmar, J.; Fraser, N.; Gambardella, G.; Sawant, M.; Voogel, M. L. "Radiation-Tolerant Deep Learning Processor Unit (DPU)-Based Platform Using

Xilinx 20-nm Kintex UltraScale FPGA”, *IEEE Transactions on Nuclear Science*, vol. 70–4, 2023, pp. 714–721.

- [136] Martinella, C.; Natzke, P.; Alia, R.; Kadi, Y.; Niskanen, K.; Rossi, M.; Jaatinen, J.; Kettunen, H.; Tsibizov, A.; Grossner, U.; Javanainen, A. “Heavy-ion induced single event effects and latent damages in SiC power MOSFETs”, *Microelectronics Reliability*, vol. 128, 2022, pp. 114423.
- [137] Martinella, C.; Ziemann, T.; Stark, R.; Tsibizov, A.; Voss, K. O.; Alia, R. G.; Kadi, Y.; Grossner, U.; Javanainen, A. “Heavy-Ion Microbeam Studies of Single-Event Leakage Current Mechanism in SiC VD-MOSFETs”, *IEEE Transactions on Nuclear Science*, vol. 67–7, 2020, pp. 1381–1389.
- [138] Martinez, M. J.; King, M. P.; Baca, A. G.; Allerman, A. A.; Armstrong, A. A.; Klein, B. A.; Douglas, E. A.; Kaplar, R. J.; Swanson, S. E. “Radiation Response of AlGaN-Channel HEMTs”, *IEEE Transactions on Nuclear Science*, vol. 66–1, 2019, pp. 344–351.
- [139] Mauguet, M.; Lagarde, D.; Widmer, F.; Chatry, N.; Marie, X.; Lorfrevre, E.; Bezerra, F.; Marec, R.; Calvel, P. “Single Events Induced By Heavy Ions and Laser Pulses in Silicon Schottky Diodes”, *IEEE Transactions on Nuclear Science*, vol. 65–8, 2018, pp. 1768–1775.
- [140] Mishu, P. K. C.; Cho, M.-K.; Khachatrian, A.; Buchner, S. P.; McMorrow, D.; Paki, P.; Cressler, J. D.; Song, I. “Voltage-Controlled Oscillator Utilizing Inverse-Mode SiGe-HBT Biasing Circuit for the Mitigation of Single-Event Effects”, *IEEE Transactions on Nuclear Science*, vol. 69–6, 2022, pp. 1242–1248.
- [141] Mizuta, E.; Kuboyama, S.; Nakada, Y.; Takeyama, A.; Ohshima, T.; Iwata, Y.; Suzuki, K. “Single-Event Damage Observed in GaN-on-Si HEMTs for Power Control Applications”, *IEEE Transactions on Nuclear Science*, vol. 65–8, 2018, pp. 1956–1963.
- [142] Moon, U.-K. “Avant! Star-Hspice Manual”. Source: <https://web.engr.oregonstate.edu/~moon/ece323/hspice98/>, 2024-07-29.
- [143] Morand, S.; Binois, C.; de Fleurieu, H. C.; Carvalho, A.; Samaras, A.; Clatworthy, T.; Kruckmeyer, K.; Marin, M.; Mangeret, R.; Salvaterra, G.; Staerk, D. “Simultaneous Single-Event Transient (SET) Observation on LM139A Wired-and Comparator Circuit”, *IEEE Transactions on Nuclear Science*, vol. 68–6, 2021, pp. 1279–1285.
- [144] nan Yin, Y.; Liu, J.; qi Liu, T.; Ye, B.; gang Ji, Q.; mei Sun, Y.; jie Zhou, X. “Heavy-ion induced radiation effects in 50 nm NAND floating gate flash memories”, *Microelectronics Reliability*, vol. 102, 2019, pp. 1–6.

- [145] Nergui, D.; Ildefonso, A.; Tzintzarov, G. N.; Lourenco, N. E.; Omprakash, A. P.; Goley, P. S.; Fleetwood, Z. E.; LaLumondiere, S. D.; Bonsall, J. P.; Monahan, D. M.; Kettering, H.; Brewe, D. L.; Cressler, J. D. "Single-Event Transients in SiGe HBTs Induced by Pulsed X-Ray Microbeam", *IEEE Transactions on Nuclear Science*, vol. 67–1, 2020, pp. 91–98.
- [146] Niskanen, K.; Touboul, A. D.; Germanicus, R. C.; Michez, A.; Javanainen, A.; Wrobel, F.; Boch, J.; Pouget, V.; Saigné, F. "Impact of Electrical Stress and Neutron Irradiation on Reliability of Silicon Carbide Power MOSFET", *IEEE Transactions on Nuclear Science*, vol. 67–7, 2020, pp. 1365–1373.
- [147] Nussenzveig, H. M. "Curso de Física Básica: Eletromagnetismo". Editora Edgard Blücher, 2002, 2 ed., 394p.p.
- [148] Ogiers, W.; Ruythooren, K.; Van Wichelen, K.; et al.. "FAINTSTAR: an intelligent single-chip sensor head for star trackers—prototype results", *CEAS Space Journal*, vol. 10–4, 2018, pp. 605—619.
- [149] Osada, K.; Yamaguchi, K.; Saitoh, Y.; Kawahara, T. "SRAM immunity to cosmic-ray-induced multierrors based on analysis of an induced parasitic bipolar effect", *IEEE Journal of Solid-State Circuits*, vol. 39–5, 2004, pp. 827–833.
- [150] Pande, N.; Kumar, S.; Everson, L. R.; Park, G.; Ahmed, I.; Kim, C. H. "Neutron-Induced Pulsewidth Distribution of Logic Gates Characterized Using a Pulse Shrinking Chain-Based Test Structure", *IEEE Transactions on Nuclear Science*, vol. 68–12, 2021, pp. 2736–2747.
- [151] Pereira, E. "CosmicRays_FET_Simulation". Source: https://github.com/elisagarciap-egp/CosmicRays_FET_Simulation, 2024.
- [152] Pereira, E.; Garibotti, R.; Ost, L. C.; Calazans, N.; Moraes, F. G. "A Complementary Survey of Radiation-Induced Soft Error Research: Facilities, Particles, Devices and Trends", *Journal of Integrated Circuits and Systems*, vol. 19–2, 2024, pp. 1–20.
- [153] Peña-Fernandez, M.; Lindoso, A.; Entrena, L.; Garcia-Valderas, M. "The Use of Microprocessor Trace Infrastructures for Radiation-Induced Fault Diagnosis", *IEEE Transactions on Nuclear Science*, vol. 67–1, 2020, pp. 126–134.
- [154] Possamai Bastos, R.; Dutertre, J.-M.; Garay Trindade, M.; Viera, R. A. C.; Potin, O.; Letiche, M.; Cheymol, B.; Beaucour, J. "Assessment of On-Chip Current Sensor for Detection of Thermal-Neutron-Induced Transients", *IEEE Transactions on Nuclear Science*, vol. 67–7, 2020, pp. 1404–1411.

- [155] Possamai Bastos, R.; Trindade, M. G.; Garibotti, R.; Gava, J.; Reis, R.; Ost, L. “Assessment of Tiny Machine-Learning Computing Systems Under Neutron-Induced Radiation Effects”, *IEEE Transactions on Nuclear Science*, vol. 69–7, 2022, pp. 1683–1690.
- [156] Principato, F.; Altieri, S.; Abbene, L.; Pintacuda, F. “Accelerated Tests on Si and SiC Power Transistors with Thermal, Fast and Ultra-Fast Neutrons”, *Sensors*, vol. 20–11, 2020, pp. 1–15.
- [157] Prinzie, J.; Christiansen, J.; Moreira, P.; Steyaert, M.; Leroux, P. “A 2.56-GHz SEU Radiation Hard LC -Tank VCO for High-Speed Communication Links in 65-nm CMOS Technology”, *IEEE Transactions on Nuclear Science*, vol. 65–1, 2018, pp. 407–412.
- [158] Prinzie, J.; Thys, S.; Van Bockel, B.; Wang, J.; De Smedt, V.; Leroux, P. “An SRAM-Based Radiation Monitor With Dynamic Voltage Control in 0.18- μ m CMOS Technology”, *IEEE Transactions on Nuclear Science*, vol. 66–1, 2019, pp. 282–289.
- [159] Pérez-Celis, A.; Thurlow, C.; Wirthlin, M. “Identifying Radiation-Induced Micro-SEFIs in SRAM FPGAs”, *IEEE Transactions on Nuclear Science*, vol. 68–10, 2021, pp. 2480–2487.
- [160] Quilligan, G.; Aslam, S. “TID and Heavy-Ion Performance of an RHBD Multichannel Digitizer in 180-nm CMOS”, *IEEE Transactions on Nuclear Science*, vol. 68–7, 2021, pp. 1414–1422.
- [161] Ren, Z.; An, X.; Li, G.; Zhang, X.; Huang, R. “Statistical analysis on the effects of heavy ion irradiation on 65 nm bulk silicon MOS devices”, *Semiconductor Science and Technology*, vol. 34–11, 2019, pp. 115018.
- [162] Rosen, A. S. “Periodic Trend Plotter”. Source: https://github.com/Andrew-S-Rosen/periodic_trends, 2023-10-30.
- [163] Ryder, K. L.; Ryder, L. D.; Sternberg, A. L.; Kozub, J. A.; Zhang, E. X.; Khachatrian, A.; Buchner, S. P.; McMorrow, D. P.; Hales, J. M.; Zhao, Y.; Wang, L.; Wang, C.; Weller, R. A.; Schrimpf, R. D.; Weiss, S. M.; Reed, R. A. “Comparison of Sensitive Volumes Associated With Ion- and Laser-Induced Charge Collection in an Epitaxial Silicon Diode”, *IEEE Transactions on Nuclear Science*, vol. 67–1, 2020, pp. 57–62.
- [164] Ryder, K. L.; Ryder, L. D.; Sternberg, A. L.; Kozub, J. A.; Zhang, E. X.; LaLumondiere, S. D.; Monahan, D. M.; Bonsall, J. P.; Khachatrian, A.; Buchner, S. P.; McMorrow, D.; Hales, J. M.; Zhao, Y.; Wang, L.; Wang, C.; Weller, R. A.; Schrimpf, R. D.; Weiss, S. M.; Reed, R. A. “Comparison of Single-Event Transients in an Epitaxial Silicon Diode Resulting From Heavy-Ion-, Focused X-Ray-, and Pulsed Laser-Induced

- Charge Generation”, *IEEE Transactions on Nuclear Science*, vol. 68–5, 2021, pp. 626–633.
- [165] Ryder, L. D.; Ryder, K. L.; Sternberg, A. L.; Kozub, J. A.; Gong, H.; Zhang, E. X.; Linten, D.; Mitard, J.; Weller, R. A.; Schrimpf, R. D.; Weiss, S. M.; Reed, R. A. “Polarization Dependence of Pulsed Laser-Induced SEEs in SOI FinFETs”, *IEEE Transactions on Nuclear Science*, vol. 67–1, 2020, pp. 38–43.
- [166] Ryder, L. D.; Ryder, K. L.; Sternberg, A. L.; Kozub, J. A.; Zhang, E. X.; Linten, D.; Croes, K.; Weller, R. A.; Schrimpf, R. D.; Weiss, S. M.; Reed, R. A. “Single-Event Transient Response of Vertical and Lateral Waveguide-Integrated Germanium Photodiodes”, *IEEE Transactions on Nuclear Science*, vol. 68–5, 2021, pp. 801–806.
- [167] Røed, K.; Eriksen, D.; Ceccaroli, B.; Martinella, C.; Javanainen, A.; Reshanov, S.; Massetti, S. “Isotopic Enriched and Natural SiC Junction Barrier Schottky Diodes Under Heavy Ion Irradiation”, *IEEE Transactions on Nuclear Science*, vol. 69–7, 2022, pp. 1675–1682.
- [168] Sakamoto, K.; Baba, S.; Kobayashi, D.; Okamoto, S.; Shindou, H.; Kawasaki, O.; Makino, T.; Mori, Y.; Matuura, D.; Kusano, M.; Narita, T.; Ishii, S.; Hirose, K. “Investigation of Buried-Well Potential Perturbation Effects on SEU in SOI DICE-Based Flip-Flop Under Proton Irradiation”, *IEEE Transactions on Nuclear Science*, vol. 68–6, 2021, pp. 1222–1227.
- [169] Sarker, M. A. R.; Jung, S.; Ildefonso, A.; Khachatrian, A.; Buchner, S. P.; McMorrow, D.; Paki, P.; Cressler, J. D.; Song, I. “Mitigation of Single-Event Effects in SiGe-HBT Current-Mode Logic Circuits”, *Sensors*, vol. 20–9, 2020, pp. 1–10.
- [170] Scheick, L.; Allen, G.; Edmonds, L.; Schaefer, R.; Menke, R. “Observation of Single-Event Burnout During Inductive Switching”, *IEEE Transactions on Nuclear Science*, vol. 65–2, 2018, pp. 719–723.
- [171] Scialdone, A.; Ferraro, R.; Alía, R. G.; Sterpone, L.; Danzeca, S.; Masi, A. “FPGA Qualification and Failure Rate Estimation Methodology for LHC Environments Using Benchmarks Test Circuits”, *IEEE Transactions on Nuclear Science*, vol. 69–7, 2022, pp. 1633–1641.
- [172] Serrano-Cases, A.; Reyneri, L. M.; Morilla, Y.; Cuenca-Asensi, S.; Martínez-Álvarez, A. “Empirical Mathematical Model of Microprocessor Sensitivity and Early Prediction to Proton and Neutron Radiation-Induced Soft Errors”, *IEEE Transactions on Nuclear Science*, vol. 67–7, 2020, pp. 1511–1520.
- [173] Shangguan, S.; Ma, Y.; Han, J.; Cui, Y.; Wang, Y.; Chen, R.; Liang, Y.; Zhu, X.; Li, Y. “Single event effects of SiC diode demonstrated by pulsed-laser two photon absorption”, *Microelectronics Reliability*, vol. 125, 2021, pp. 114364.

- [174] Sicard, E. "HAL open science - Introducing 14-nm FinFET technology in Microwind". Source: https://hal.science/hal-01541171/file/Application_Note_mw38_14nm_v7.pdf, 2024-07-29.
- [175] Sicard, E. "HAL open science - Introducing 32 nm technology in Microwind35". Source: <https://hal.science/hal-03324299/document>, 2024-07-29.
- [176] Sicard, E. "HAL open science - Introducing 65 nm technology in Microwind3". Source: <https://hal.science/hal-03324309v1/document>, 2024-07-29.
- [177] Sicard, E. "HAL open science - Introducing 7-nm FinFET technology in Microwind". Source: <https://hal.science/hal-01558775/document>, 2024-07-29.
- [178] Siddiqui, M. S. M.; Ruchi, S.; Van Le, L.; Yoo, T.; Chang, I.-J.; Kim, T. T.-H. "SRAM Radiation Hardening Through Self-Refresh Operation and Error Correction", *IEEE Transactions on Device and Materials Reliability*, vol. 20–2, 2020, pp. 468–474.
- [179] Smith, F. "Proton Beam Validation of a New Single Event Transient Mitigation Technique", *Journal of Electronic Testing*, vol. 36, 2020, pp. 785–792.
- [180] Song, I.; Cho, M.-K.; Fleetwood, Z. E.; Gong, Y.; Pavlidis, S.; Buchner, S. P.; McMorrow, D.; Paki, P.; Kaynak, M.; Cressler, J. D. "p-n-p-Based RF Switches for the Mitigation of Single-Event Transients in a Complementary SiGe BiCMOS Platform", *IEEE Transactions on Nuclear Science*, vol. 65–1, 2018, pp. 391–398.
- [181] Song, R.; Shao, J.; Liang, B.; Chi, Y.; Chen, J. "Characterization of P-hit and N-hit single-event transient using heavy ion microbeam", *IEICE Electronics Express*, vol. 16–8, 2019, pp. 20190141–20190141.
- [182] Stanev, T. "High Energy Cosmic Rays". Springer, 2010, 333p.p.
- [183] Sun, H.; Guo, G.; Sun, R.; Zhao, W.; Zhang, F.; Liu, J.; Zhang, Z.; Chen, Y.; Zhao, Y. "Study on Single Event Upsets in a 28 nm Technology Static Random Access Memory Device Based on Micro-Beam Irradiation", *Electronics*, vol. 11–20, 2022, pp. 1–9.
- [184] Söderström, D.; Luza, L. M.; Kettunen, H.; Javanainen, A.; Farabolini, W.; Gilardi, A.; Coronetti, A.; Poivey, C.; Dilillo, L. "Electron-Induced Upsets and Stuck Bits in SDRAMs in the Jovian Environment", *IEEE Transactions on Nuclear Science*, vol. 68–5, 2021, pp. 716–723.
- [185] Takeuchi, K.; Sakamoto, K.; Yukumatsu, K.; Watanabe, K.; Tsuchiya, Y.; Kato, T.; Matsuyama, H.; Takeyama, A.; Ohshima, T.; Kuboyama, S.; Shindo, H. "Characteristic Charge Collection Mechanism Observed in FinFET SRAM Cells", *IEEE Transactions on Nuclear Science*, vol. 69–8, 2022, pp. 1833–1839.

- [186] Takeuchi, K.; Sakamoto, T.; Tada, M.; Takeyama, A.; Ohshima, T.; Kuboyama, S.; Shindou, H. "Single-Event Effects Induced on Atom Switch-based Field-Programmable Gate Array", *IEEE Transactions on Nuclear Science*, vol. 66–7, 2019, pp. 1355–1360.
- [187] Tali, M.; Alia, R. G.; Brugger, M.; Ferlet-Cavrois, V.; Corsini, R.; Farabolini, W.; Javanainen, A.; Santin, G.; Boatella Polo, C.; Virtanen, A. "Mechanisms of Electron-Induced Single-Event Latchup", *IEEE Transactions on Nuclear Science*, vol. 66–1, 2019, pp. 437–443.
- [188] Tali, M.; García Alía, R.; Brugger, M.; Ferlet-Cavrois, V.; Corsini, R.; Farabolini, W.; Javanainen, A.; Kastriotou, M.; Kettunen, H.; Santin, G.; Boatella Polo, C.; Tsiliannis, G.; Danzeca, S.; Virtanen, A. "Mechanisms of Electron-Induced Single-Event Upsets in Medical and Experimental Linacs", *IEEE Transactions on Nuclear Science*, vol. 65–8, 2018, pp. 1715–1723.
- [189] Teng, J. W.; Ringel, B. L.; Brumbach, Z. R.; Heimerl, J. P.; Mensah, Y. A.; Tzintzarov, G. N.; Ildefonso, A.; Khachatrian, A.; McMorrow, D.; Oldiges, P.; Cressler, J. D. "The Propagation of Extended SET Tails in RF Amplifiers Using 45-nm CMOS on PDSOI", *IEEE Transactions on Nuclear Science*, vol. 70–8, 2023, pp. 1829–1837.
- [190] Trindade, M. G.; Bastos, R. P.; Garibotti, R.; Ost, L.; Letiche, M.; Beaucour, J. "Assessment of Machine Learning Algorithms for Near-Sensor Computing under Radiation Soft Errors". In: IEEE International Conference on Electronics, Circuits and Systems (ICECS), 2020, pp. 494–497.
- [191] Trindade, M. G.; Coelho, A.; Valadares, C.; Viera, R. A. C.; Rey, S.; Cheymol, B.; Baylac, M.; Velazco, R.; Bastos, R. P. "Assessment of a Hardware-Implemented Machine Learning Technique Under Neutron Irradiation", *IEEE Transactions on Nuclear Science*, vol. 66–7, 2019, pp. 1441–1448.
- [192] TRIUMF. "TRIUMF's cosmic ray air shower illustrative image". Source: <https://www.triumf.ca/pif-nif>, July 4, 2023.
- [193] Trombini, H.; Marmitt, G.; Alencar, I.; et al.. "Unraveling structural and compositional information in 3D FinFET electronic devices", *Scientific Reports*, vol. 9–1, 2019.
- [194] TSMC. "65nm Technology". 2024-05-01, Source: https://www.tsmc.com/english/dedicatedFoundry/technology/logic/l_65nm, 2020.
- [195] Turchetta, R.; Berst, J.; Casadei, B.; Claus, G.; Colledani, C.; Dulinski, W.; Hu, Y.; Husson, D.; Le Normand, J.; Riester, J.; Deptuch, G.; Goerlach, U.; Higueret, S.; Winter, M. "A monolithic active pixel sensor for charged particle tracking and imaging using standard VLSI CMOS technology", *Nuclear Instruments and Methods in*

Physics Research Section A: Accelerators, Spectrometers, Detectors and Associated Equipment, vol. 458–3, 2001, pp. 677–689.

- [196] Vacca, E.; Azimi, S.; Sterpone, L. “Failure rate analysis of radiation tolerant design techniques on SRAM-based FPGAs”, *Microelectronics Reliability*, vol. 138, 2022, pp. 114778.
- [197] Vargas, V.; Ramos, P.; Velazco, R. “Evaluation by Neutron Radiation of the NMR-MPar Fault-Tolerance Approach Applied to Applications Running on a 28-nm Many-Core Processor”, *Electronics*, vol. 7–11, 2018.
- [198] Vega, H. R. “Study of the Environmental Neutron Spectrum at Zacatecas City”. In: National Congress on Solid State Dosimetry, 2003, pp. 1–13.
- [199] Virmontois, C.; Belloir, J.-M.; Beaumel, M.; Vriet, A.; Perrot, N.; Sellier, C.; Bezine, J.; Gambart, D.; Blain, D.; Garcia-Sanchez, E.; Mouallem, W.; Bardoux, A. “Dose and Single-Event Effects on a Color CMOS Camera for Space Exploration”, *IEEE Transactions on Nuclear Science*, vol. 66–1, 2019, pp. 104–110.
- [200] Virtanen, A. “The use of particle accelerators for space projects”, *Journal of Physics: Conference Series*, vol. 41–1, 2006, pp. 101.
- [201] Vlagkoulis, V.; Sari, A.; Antonopoulos, G.; Psarakis, M.; Tavoularis, A.; Furano, G.; Boatella-Polo, C.; Poivey, C.; Ferlet-Cavrois, V.; Kastriotou, M.; Martinez, P. F.; Alía, R. G. “Configuration Memory Scrubbing of SRAM-Based FPGAs Using a Mixed 2-D Coding Technique”, *IEEE Transactions on Nuclear Science*, vol. 69–4, 2022, pp. 871–882.
- [202] Vlagkoulis, V.; Sari, A.; Vrachnis, J.; Antonopoulos, G.; Segkos, N.; Psarakis, M.; Tavoularis, A.; Furano, G.; Boatella Polo, C.; Poivey, C.; Ferlet-Cavrois, V.; Kastriotou, M.; Fernandez Martinez, P.; Alia, R. G.; Voss, K.-O.; Schuy, C. “Single Event Effects Characterization of the Programmable Logic of Xilinx Zynq-7000 FPGA Using Very/Ultra High-Energy Heavy Ions”, *IEEE Transactions on Nuclear Science*, vol. 68–1, 2021, pp. 36–45.
- [203] Wang, H.; Chu, J.; Wei, J.; Shi, J.; Sun, H.; Han, J.; Qian, R. “A single event upset hardened flip-flop design utilizing layout technique”, *Microelectronics Reliability*, vol. 102, 2019, pp. 113496.
- [204] Wang, H.-B.; Wang, Y.-S.; Cui, J.-L.; Wang, S.-L.; Liang, T.-J.; Mei, B.; Liu, X.-F.; Qian, R. “A Low-Overhead FFT Design With Higher SEU Resilience Implemented in FPGA”, *IEEE Transactions on Nuclear Science*, vol. 67–5, 2020, pp. 805–810.

- [205] Wang, H.-B.; Wang, Y.-S.; Xiao, J.-H.; Wang, S.-L.; Liang, T.-J. “Impact of Single-Event Upsets on Convolutional Neural Networks in Xilinx Zynq FPGAs”, *IEEE Transactions on Nuclear Science*, vol. 68–4, 2021, pp. 394–401.
- [206] Wang, J.; Prinzie, J.; Coronetti, A.; Thys, S.; Alia, R. G.; Leroux, P. “Study of SEU Sensitivity of SRAM-Based Radiation Monitors in 65-nm CMOS”, *IEEE Transactions on Nuclear Science*, vol. 68–5, 2021, pp. 913–920.
- [207] Wang, L.; Shu, L.; Liu, J.; Zhao, Y.; Li, Y.; Wang, D.; Li, T.; Sui, C. “Analysis of Clock Single-Event Transients in VLSI Through Built-In Scan Chains”, *IEEE Transactions on Nuclear Science*, vol. 66–6, 2019, pp. 875–879.
- [208] Wang, P.; Sternberg, A. L.; Kozub, J. A.; Zhang, E. X.; Dodds, N. A.; Jordan, S. L.; Fleetwood, D. M.; Reed, R. A.; Schrimpf, R. D. “Analysis of TPA Pulsed-Laser-Induced Single-Event Latchup Sensitive-Area”, *IEEE Transactions on Nuclear Science*, vol. 65–1, 2018, pp. 502–509.
- [209] Wang, X.; Ding, L.; Luo, Y.; Chen, W.; Zhang, F.; Guo, X. “A Statistical Method for MCU Extraction Without the Physical-to-Logical Address Mapping”, *IEEE Transactions on Nuclear Science*, vol. 67–7, 2020, pp. 1443–1451.
- [210] Wang, Z.; Chen, W.; Yao, Z.; Zhang, F.; Luo, Y.; Tang, X.; Guo, X.; Ding, L.; Peng, C. “Proton-induced single-event effects on 28nm Kintex-7 FPGA”, *Microelectronics Reliability*, vol. 107, 2020, pp. 113594.
- [211] Weste, N.; Harris, D. “CMOS VLSI Design: A Circuits and Systems Perspective”. Addison Wesley, 2011, 838p.p.
- [212] Weulersse, C.; Houssany, S.; Guibbaud, N.; Segura-Ruiz, J.; Beaucour, J.; Miller, F.; Mazurek, M. “Contribution of Thermal Neutrons to Soft Error Rate”, *IEEE Transactions on Nuclear Science*, vol. 65–8, 2018, pp. 1851–1857.
- [213] WikiChip 14nm. “14 nm Lithography Process”. Source: https://en.wikichip.org/wiki/14_nm_lithography_process, 2024-07-29.
- [214] WikiChip 22nm. “22 nm Lithography Process”. Source: https://en.wikichip.org/wiki/22_nm_lithography_process, 2024-07-29.
- [215] WikiChip 32nm. “32 nm Lithography Process”. Source: https://en.wikichip.org/wiki/32_nm_lithography_process, 2024-07-29.
- [216] WikiChip 65nm. “65 nm Lithography Process”. Source: https://en.wikichip.org/wiki/65_nm_lithography_process, 2024-07-29.
- [217] WikiChip 7nm. “7 nm Lithography Process”. Source: https://en.wikichip.org/wiki/7_nm_lithography_process, 2024-07-29.

- [218] Wikipedia. “Electrical Mobility”. 2024-07-06, Source: https://en.wikipedia.org/wiki/Electron_mobility, nd.
- [219] Wilson, A. E.; Larsen, S.; Wilson, C.; Thurlow, C.; Wirthlin, M. “Neutron Radiation Testing of a TMR VexRiscv Soft Processor on SRAM-Based FPGAs”, *IEEE Transactions on Nuclear Science*, vol. 68–5, 2021, pp. 1054–1060.
- [220] Wu, Z.; Chen, S.; Chen, J.; Huang, P. “Impacts of Proton Radiation on Heavy-Ion-Induced Single-Event Transients in 65-nm CMOS Technology”, *IEEE Transactions on Nuclear Science*, vol. 66–1, 2019, pp. 177–183.
- [221] Wu, Z.; Chi, Y.; Chen, J.; Huang, P.; Liang, B.; Zhang, X. “Sub-10 MeV proton-induced single-event transients in 65nm CMOS inverter chains”, *Microelectronics Reliability*, vol. 125, 2021, pp. 114366.
- [222] Xiao, T. P.; Bennett, C. H.; Agarwal, S.; Hughart, D. R.; Barnaby, H. J.; Puchner, H.; Talin, A. A.; Marinella, M. J. “Single-Event Effects Induced by Heavy Ions in SONOS Charge Trapping Memory Arrays”, *IEEE Transactions on Nuclear Science*, vol. 69–3, 2022, pp. 406–413.
- [223] Xiao-qiang, G.; Liang-zhi, C.; Wei, C.; Wen, Z.; Feng-qí, Z.; Xun, W.; Li-li, D.; Yin-hong, L.; Gang, G. “SET characterization of 130nm flash-based FPGA device”, *Microelectronics Reliability*, vol. 127, 2021, pp. 114369.
- [224] Yang, W.; Du, X.; He, C.; Shi, S.; Cai, L.; Hui, N.; Guo, G.; Huang, C. “Microbeam Heavy-Ion Single-Event Effect on Xilinx 28-nm System on Chip”, *IEEE Transactions on Nuclear Science*, vol. 65–1, 2018, pp. 545–549.
- [225] Yaqing, C.; Pengcheng, H.; Qian, S.; Bin, L.; Zhenyu, Z. “Characterization of Single-Event Upsets Induced by High-LET Heavy Ions in 16-nm Bulk FinFET SRAMs”, *IEEE Transactions on Nuclear Science*, vol. 69–5, 2022, pp. 1176–1181.
- [226] Yu, J.; Cai, C.; Ning, B.; Gao, S.; Liu, T.; Xu, L.; Shen, M.; Yu, J. “Design and verification of multiple SEU mitigated circuits on SRAM-based FPGA system”, *Microelectronics Reliability*, vol. 126, 2021, pp. 114340.
- [227] Yuan, H.; Guo, Y.; Chen, J.; Chi, Y.; Chen, X.; Liang, B. “28nm Fault-Tolerant Hardening-by-Design Frequency Divider for Reducing Soft Errors in Clock and Data Recovery”, *IEEE Access*, vol. 7, 2019, pp. 47955–47961.
- [228] Zerarka, M.; Crepel, O. “Radiation robustness of normally-off GaN/HEMT power transistors (COTS)”, *Microelectronics Reliability*, vol. 88-90, 2018, pp. 984–991.

- [229] Zhang, H.; Jiang, H.; Fan, X.; Kauppila, J. S.; Chatterjee, I.; Bhuva, B. L.; Massengill, L. W. "Effects of Total-Ionizing-Dose Irradiation on Single-Event Response for Flip-Flop Designs at a 14-/16-nm Bulk FinFET Technology Node", *IEEE Transactions on Nuclear Science*, vol. 65–8, 2018, pp. 1928–1934.
- [230] Zhang, W.; Li, T. "Microarchitecture soft error vulnerability characterization and mitigation under 3D integration technology". In: IEEE/ACM International Symposium on Microarchitecture (MICRO), 2008, pp. 435–446.
- [231] Zhao, W.; He, C.; Chen, W.; Chen, R.; Cong, P.; Zhang, F.; Wang, Z.; Shen, C.; Zheng, L.; Guo, X.; Ding, L. "Single-event multiple transients in guard-ring hardened inverter chains of different layout designs", *Microelectronics Reliability*, vol. 87, 2018, pp. 151–157.



Pontifícia Universidade Católica do Rio Grande do Sul
Pró-Reitoria de Pesquisa e Pós-Graduação
Av. Ipiranga, 6681 – Prédio 1 – Térreo
Porto Alegre – RS – Brasil
Fone: (51) 3320-3513
E-mail: propesq@pucrs.br
Site: www.pucrs.br